DEVELOPMENT OF A BIO-INDUCTIVE VASCULAR GRAFT BY COMPOSITING A FAST-RESORBING ELASTOMER WITH A SLOW-RESORBING POLYMER

by

Robert Andrew Allen

B.S. in Bioengineering, University of Pittsburgh, 2009

Submitted to the Graduate Faculty of

The Swanson School of Engineering in partial fulfillment

of the requirements for the degree of

Ph.D. in Bioengineering

University of Pittsburgh

2015

UNIVERSITY OF PITTSBURGH

SWANSON SCHOOL OF ENGINEERING

This dissertation was presented

by

Robert Andrew Allen

It was defended on

June 24, 2015

and approved by

Sanjeev G. Shroff, PhD, Distinguished Professor and Gerald McGinnis Chair, Departments of Bioengineering and Medicine

David A. Vorp, PhD, Associate Dean for Research and William Kepler Whiteford Professor, Departments of Bioengineering and Surgery, and Center for Vascular Remodeling and Regeneration

Bryan W Tillman, MD, PhD, Assistant Professor, Department of Vascular Surgery

Richard J. Bodnar, PhD, Research Assistant Professor, Department of Pathology, Vascular Medicine Institute, and Center for Vascular Remodeling and Regeneration

Jeffrey S. Isenberg, MD, MPH, Associate Professor, Department of Medicine, Division of Pulmonary, Allergy, and Critical Care Medicine, and Vascular Medicine Institute

Dissertation Director: Yadong Wang, PhD, William Kepler Whiteford Professor, Departments of Bioengineering, Chemical Engineering, and Surgery

DEVELOPMENT OF A BIO-INDUCTIVE VASCULAR GRAFT BY COMPOSITING A FAST-RESORBING ELASTOMER WITH A SLOW-RESORBING POLYMER

Robert A. Allen, PhD

University of Pittsburgh, 2015

Clinically used prosthetic vascular grafts fail frequently from thrombosis and anastomotic stenosis in small diameter applications. A bio-inductive vascular graft could improve performance by remodeling into an artery-like tissue after implantation, thereby approaching the mechanical and physiological function of healthy arteries. We hypothesized that a bio-inductive vascular graft must remodel rapidly to promote neoartery formation rather than a classical foreign body response. To test this hypothesis, we developed vascular grafts made from microporous foams of a fast-resorbing elastomer composited with a slower-resorbing polymer sheath for mechanical support. Composite grafts performed well (80% patency) as infrarenal abdominal aorta interposition grafts in rats, and within 90 days remodeled into neoarteries which approached native arteries in mechanical compliance and tissue architecture.

Following this encouraging proof-of-concept, the objective of this dissertation is to assess the potential of our vascular graft design to translate toward clinical application. To assess translational potential, we first assessed the long-term performance of the microporous foam composite design in rats at 1-year post-implantation. We found that the resultant neoarteries maintained 80% patency, contained the same amount of mature elastin as native arteries, and

possessed nerves resembling native perivascular nerves. To improve clinical feasibility of the design, we next sought to improve graft surgical handling and simplify the fabrication process, which we achieved by developing a novel technique to fabricate grafts from electrospun PGS microfibers. We then implanted electrospun microfiber grafts in a mouse model to assess whether they retained the favorable long-term performance observed in microporous PGS foam grafts. Electrospun grafts achieved 100% patency up to 1 year post-implant, but all grafts dilated within that time. Remodeled electrospun grafts retained polymer residues at 1 year, thereby demonstrating slower resorption than the original foam design, likely due to reduced pore size. An elastin-rich neotissue containing contractile smooth muscle cells developed on the luminal surface of the graft within 3 months, but macrophages persisted at 1 year, and calcification occurred in all neoarteries at late term. Taken together, these results suggest that a PGS-based vascular graft can achieve excellent long-term performance, but efforts to improve translational potential must preserve fast in-host remodeling.

TABLE OF CONTENTS

LIST OF TABLES

LIST OF FIGURES

PREFACE

This dissertation summarizes years of challenging but rewarding translational research spanning the wet laboratories and animal facilities of multiple research teams, departments, and institutions. I am grateful for the assistance, instruction, and personal guidance of the many mentors and collaborators who helped me to complete this work. First and foremost, I acknowledge my dissertation advisor Dr. Yadong Wang for providing me the opportunity to work on such an impactful project, and for empowering me to learn and grow through his mentorship and support. Thank you for teaching me to dream big, challenge dated paradigms, and make bold decisions in the face of uncertainty. I acknowledge all my colleagues at the Biomaterials Foundry for training, assisting, and inspiring me in this project and many others. In particular, I thank Dr. Keewon Lee for training me in scaffold fabrication, tissue engineering techniques, and mechanical testing. I acknowledge Dr. Jin Gao for his teachings in cell culture and polymer synthesis. I commend Dr. Wei Wu for pioneering the first successful fast-remodeling bio-inductive vascular graft in our laboratory. His seminal work serves as the foundation for this dissertation study. I thank Dr. Eric Jeffries for training me in electrospinning, and for developing the versatile technique for fabricating PGS microfibers which became an essential tool in my dissertation work. Lastly, I acknowledge the excellent team of graduate and undergraduate students who supported my work with their own. Thank you to Chelsea Stowell, Jennifer Zhuang, Anna Lehman, and Lisa Volpatti for their invaluable effort and insight. This

project was not possible without you, and I am proud to leave the future of this project in your capable hands.

Our collaborators at the University of Pittsburgh and its partner institutions have been an incredible help. I emphatically thank Dr. Masahiro Yoshida for implanting our first vascular graft prototypes into a challenging animal model. We greatly appreciate your patience and persistence, which led to key findings that informed the next generation designs. I gratefully acknowledge our collaborators at the Vascular Medicine Institute for lending us their world-class expertise in artery characterization. In particular, I thank Dr. Jeffrey Isenberg, Dr. Mingyi Yao, Dr. Hunter Champion, Timothy Bachman, and Jeffrey Baust. Dr. Isenberg has my additional thanks for providing mentorship that extended beyond the vascular graft project. For their assistance with non-invasive ultrasound monitoring of our vascular grafts, I graciously thank Dr. Kang Kim, Dr. Debaditya Dutta, and Dr. Daewoo Park. I thank Dr. Anne Robertson, Dr. Paolo Zunino, and their team (Dr. Arturo Valentin, Xinjie Duan, and Piyusha Gade) for assisting with graft mechanical testing, multiphoton imaging, and mathematical modeling of the host response to our implants. Our collaborators at the Center for Biologic Imaging deserve many thanks for empowering us to clearly visualize subtle but important changes in our neoarteries over time. In particular, I acknowledge Dr. Donna Stolz, Callen Wallace, and Jonathan Franks for their invaluable assistance in whole mount immunofluorescent staining and scanning electron microscopy. Importantly, I thank Dr. Sanjeev Shroff for his long-standing mentorship, which spanned my many years of undergraduate and graduate study at the Department of Bioengineering at the University of Pittsburgh. Your guidance has been essential to my progress in academic research, didactic coursework, and professional development.

Collaborations outside of the University of Pittsburgh have also been essential to this work. I extend deep gratitude to Dr. Christopher Breuer, Dr. Jay Humphrey, and their research teams at the Research Institute at Nationwide Children's Hospital and Yale University. In particular, I thank Ramak Khosravi, Cameron Best, Dr. Yong Ung Lee, and Dr. Tai Yi. Your extensive experience, keen insight, and hard work have helped us to understand the performance and remodeling potential of our latest designs. I am honored and humbled to learn and work alongside such a distinguished group whose expertise spans benchtop fabrication, *in vivo* testing, mechanical characterization, *in silico* simulation, and clinical application. I am proud that my work will contribute to your ambitious efforts to rationally design the ideal vascular graft, and I wish your teams the best of luck in achieving that impactful goal.

For their essential guidance in this dissertation, I gratefully acknowledge the members of my dissertation committee - Dr. David Vorp, Dr. Bryan Tillman, Dr. Jeffrey Isenberg, Dr. Richard Bodnar, Dr. Sanjeev Shroff, and Dr. Yadong Wang. Thank you for steering this project in a productive and impactful direction, and for challenging me to answer questions critical to understanding and improving the remodeling potential of our vascular graft design.

Lastly, I thank my family and friends, whose unconditional support kept me strong through the challenges of this work. I extend a loving thank you to my parents Brian and Eleanor and my siblings Maryann and Jonny for their moral support and understanding throughout the process. Thank you for constantly offering to help me with anything and everything, for adapting to my limited availability, and for always being proud of me. I extend a sincere and loving thank you to my significant other Dr. Caitlin Czajka. Thank you for supporting me through good times and bad, for teaching me to balance ambition with prudence, and for inspiring me with your brilliance. Thanks also to my hometown and college friends for helping

me to laugh and unwind in times of stress, and to celebrate in times of achievement (including the completion of this dissertation). To my fellow graduate students at the University of Pittsburgh's Department of Bioengineering, I extend an especially heart-felt thank-you. It's been an absolute pleasure learning and growing with you, and my time here would not have been nearly as enjoyable without you. Lastly, I thank my grandfather, the late Dr. Arthur Allen. My pursuit of this PhD was in many ways a following in your footsteps. Thank you for showing me the joys of science, teaching, and life-long learning. Your legacy of intellectual curiosity lives on in this dissertation, and continues to live on in me.

1.0 INTRODUCTION

The mission to construct a functional blood vessel substitute has captivated the scientific community for the past three decades. This field has historically drawn such strong and persistent interest for two main reasons: (1) the potential for large clinical impact, and (2) the technical challenge of building a tissue with such demanding mechanical and biological performance requirements. Because of its potential impact on both medicine and science, such a blood vessel substitute has been considered a “holy grail” of cardiovascular research [1].

Importantly, solving (2) does not necessarily achieve (1). For a vascular conduit to potentially help patients, its likeness to a living blood vessel is not alone sufficient. Production costs, lead time, surgical handling, and long-term performance (to name a few) must be within the realm of clinical feasibility for the implant to have a chance of reaching patients. This dissertation describes the development of a bio-inductive vascular graft with such considerations in mind. Thus to understand the rationale behind our approach, one must understand both the clinical significance and technical challenges of a bio-inductive vascular graft. To this end, the introductory chapter will begin by outlining the clinical importance of vascular grafts. The chapter will then review progress in the field of tissue engineered and bio-inductive vascular substitutes, and conclude the review with an introduction to our laboratory’s own approach. Lastly, this chapter will introduce the objective and specific aims of this dissertation.

1.1 CLINICAL SIGNIFICANCE

Vascular grafts are conduits which restore or reroute blood flow. Vascular grafts treat a number of clinical conditions of high incidence, impacting approximately 600,000 patients per year in the United States [2-4]. The two types of vascular grafts most commonly used clinically are autografts and prosthetic grafts. Autografts are autologous blood vessels harvested from the patient and transplanted ectopically. Autografts have superior patency to prosthetic grafts in most applications [5, 6]. Prosthetic grafts are made from permanent synthetic materials, most commonly ePTFE (Goretex) or PET (Dacron). Allografts and homografts are also considered prosthetic grafts, but are used sparingly in clinic and will not be reviewed in this section. The term "vascular graft" is often used clinically to describe prosthetic grafts only, but for simplicity this dissertation will define a vascular graft as any conduit which restores or reroutes blood flow. Prosthetic grafts have inferior patency to autografts in small diameter (< 6 mm) applications, but are used frequently in large diameter settings where performance is more comparable [7]. The most common application of vascular grafts is for arterial bypass, in which the graft reroutes blood flow around a narrowed artery to restore perfusion to ischemic tissue distal to the affected artery. Narrowing in arteries is often caused by atherosclerosis or complications of diabetes. Arterial bypass of the coronary arteries, known as *CABG* (coronary artery bypass grafting), is the most common bypass procedure with nearly 400,000 cases per year in the United States [2]. CABG procedures critically impact patient health, as the graft restores blood flow to the myocardium to treat life-threatening ischemic heart disease. Autografts are the standard of care for CABG procedures, with the internal mammary artery demonstrating the best clinical performance [8]. Prosthetic grafts are unsuitable for CABG procedures due to the small diameter

of coronary arteries. Clinical use of prosthetic grafts for CABG yields poor patency rates due to thrombosis and intimal hyperplasia [9].

Arterial bypass for the lower extremities, known as peripheral artery bypass, is performed in 100,000 patients per year in the United States [3] and has substantial healthcare impact, as it prevents limb loss and other ischemia-induced morbidities. Autografts, most commonly the greater saphenous vein, are preferred in peripheral artery bypass, but prosthetic grafts are used when autografting is not possible due to previous harvest, vascular disease in the vessel to be autografted, or when the length of the occlusion to be bypassed is too large [10]. Prosthetic grafts demonstrate inferior patency to autografts in below-the-knee peripheral bypass [11], yet are used in up to 20% of cases due to insufficient available length of saphenous vein for autografting [10]. Peripheral prosthetic vascular grafts fail by thrombosis and neointimal hyperplasia at the anastomoses [12].

Vascular grafts also direct blood flow for purposes other than reperfusion. Hemodialysis grafts link a patient's artery directly to a vein to achieve flow rates sufficiently rapid for hemodialysis, a procedure in which a patient's blood is detoxified outside of the body then returned. The preferred method of connecting the patient's artery to vein is by surgically creating an arteriovenous fistula, but prosthetic hemodialysis grafts are required when patients lack a healthy, suitably sized vein. Each year over 35,000 patients in the United States receive an ePTFE prosthetic hemodialysis graft [4, 13]. The clinical need to improve prosthetic hemodialysis graft performance is especially large, as 50% of grafts fail within 1 year due to stenosis, thrombosis, and infection [4].

Vascular grafts also treat a number of lower incidence conditions, but these have a major impact on the health of those affected. EC TCPC (Extra cardiac total cavopulmonary connections) are vascular grafts used to treat pediatric patients with single ventricle anomalies, a grouping of congenital heart defects which affect 8,000 patients in the US [2] and cause 70% mortality if left untreated [14]. EC TCPCs passively connect the vena cava directly to the pulmonary circulation reroute deoxygenated blood directly into the pulmonary artery, thereby preventing premature re-entry of deoxygenated blood into the systemic circulation. Autografts are preferred but rarely available. Consequently, ePTFE prosthetic grafts are the standard of care for EC TCPC [15]. These grafts fail frequently from thrombosis and lack growth potential, necessitating additional surgery when the patient outgrows the vascular graft [14]. Vascular grafts are also used to replace or reconstruct vessels damaged in traumatic injury [16, 17]. Saphenous vein grafts are preferred, as prosthetic grafts fail frequently from thrombosis and infection [16, 17]. Vascular grafts also connect transplanted tissues to implant site vasculature when native vessel stumps are too short. The small diameter of these native vessels necessitate vein grafts rather than prosthetic grafts to achieve adequate patency [18].

The opportunity to improve clinical outcomes for vascular grafting is substantial, as there are disadvantages to the use of both autografts and prosthetic grafts. Prosthetic grafts failures can be attributed to the persistence of long-lasting synthetic materials, which cause thrombosis, promote intimal hyperplasia at the native anastomoses due to compliance mismatch [19], and harbor late-term infection [20]. Autografts are limited in supply, and their harvest causes donor site morbidity and requires additional surgical manipulation. Additionally, despite often being the standard of care, vein autografts fail from thrombosis and intimal hyperplasia due to harvest-induced endothelial injury and adverse remodeling in response to arterial pressure [21].

To address the disadvantages of both prosthetic grafts and autografts, many groups including our own laboratory have sought to develop a vascular graft whose final state is a living, artery-like tissue. These grafts have the potential to outperform prosthetic vascular grafts by emulating arterial physiology and avoiding long-lasting materials. In pediatric patients, such grafts could theoretically grow with the patient, thereby circumventing the need for revision surgeries [14]. Ideally, if they can match autograft performance, such grafts could be used in their place, thereby circumventing harvest surgery and donor site morbidity. The next section will review such efforts to develop the ideal vascular graft, then introduce our own laboratory's approach which serves as the basis for the work described in this dissertation.

1.2 BIO-INDUCTIVE AND TISSUE ENGINEERED GRAFTS

Attempts to improve the patency of prosthetic grafts have shown limited success. These efforts employ surgical modifications, alternate non-resorbable materials, surface functionalization, endothelial cell seeding, and localized drug delivery ([12] for review). Today a range of clinically available prosthetic grafts employ some of these strategies, including heparin or carbon surface modification to reduce thrombogenicity, impregnation with antimicrobials, and use of compliant materials [12]. Though these approaches show promise, to date no prosthetic graft has demonstrated equivalent performance to autografts in small diameter applications.

In the absence of a prosthetic graft matching autograft performance, research groups across the world have sought to develop a vascular graft whose final state is a living artery-like vessel. Such a graft would be the ideal vascular substitute, as living arteries are optimally designed by nature to conduct blood flow under physiologic conditions. To resist thrombosis,

native arteries present a confluent layer of endothelial cells as the blood-contacting surface, which actively prevent thrombosis and platelet adhesion by presenting heparin sulfate, tissue plasminogen activator (tPA), thrombomodulin, prostacyclin, and nitric oxide. [22] Elastin-rich elastic laminae impart physiologic mechanical compliance in arteries, which prevents the hemodynamic disruptions responsible for neointimal hyperplasia in compliance mismatched vascular grafts [19].

To realize a living artery-like conduit, the research community has employed both tissue engineering and bio-inductive approaches. Tissue engineering techniques seek to develop a living artery-like conduit outside of the body, typically by growing and conditioning cell-rich tissue constructs in bioreactors *in vitro*. In contrast, bio-inductive approaches employ resorbable conduits as temporary scaffolding meant for the host's cells to infiltrate and remodel into a living artery *in situ*. This section will review progress in each type of approach, then introduce our own laboratory's fast-remodeling bio-inductive strategy to set the foundation for the work described in this dissertation.

1.2.1 Tissue engineered vascular grafts

Tissue engineering techniques seek to develop a living artery-like conduit outside of the body. Tissue engineered vascular grafts (TEVG) comprised substantially of vessel-like tissue are attractive because they could potentially require little host remodeling to assume vessel properties and physiologic function. The field of vascular tissue engineering began in 1986 when Weinberg and Bell produced a living tubular tissue *in vitro* from vascular smooth muscle cells, endothelial cells, and fibroblasts in a collagen gel. [23] Since then, researchers have examined the effectiveness of various materials, cells, and culture conditions for *in vitro* TEVG production.

Collagen gel-based TEVG have been strengthened through natural crosslinking [24], biochemical stimulation [25], mechanical stimulation [26-28], and reinforcement with other materials [29-31]. He and Matsuda reinforced collagen gel TEVGs with polyurethane sleeves that remained patent in dog carotid arteries for up to 6 months [32]. Fibrin gel-based TEVGs were pioneered by Grassl et al. [33], and have been similarly strengthened [34-41]. Swartz et al. implanted fibrin TEVGs made from smooth muscle and endothelial cells into sheep jugular veins with 100% patency at up to 15 weeks [40]. Koch et al. implanted PLA-reinforced fibrin TEVGs into sheep carotid arteries with 100% patency at up to 6 months, though stenosis was seen in one explant [42]. Tranquillo's group developed implantable fibrin TEVGs from human fibroblasts using pulsatile flow mechanical conditioning for 7-9 weeks [38], and recently demonstrated that similarly constructed TEVGs could be devitalized for off-the-shelf use. Devitalized grafts matched native artery compliance, and demonstrated complication-free remodeling into elastin-rich neoarteries in 24 weeks as ovine femoral interposition grafts [43]. Preseeding devitalized grafts with blood outgrowth endothelial cells substantially reduced neoartery wall thickness, likely due to accelerated deposition of basement membrane [44]. Esterified hyaluronic acid (HYAFF-11) [45] and silk fibroin [46-48] have also showed promise for developing TEVGs *in vitro*. Decellularized blood vessels have also been substantially recellularized *in vitro*. Yang et al. demonstrated that bioreactor conditioning of dog carotid arteries recellularized with arterial cells produced TEVGs with 100% patency at up to 6 months as canine carotid grafts [49]. Neff et al. used a similar approach to produce sheep carotid grafts that responded to vasomotor agents [50].

Niklason et al. developed the first highly cellular TEVG *in vitro* based on a degradable synthetic material. This work combined a PGA mesh with smooth muscle and endothelial cells *in vitro* under mechanical and biochemical stimulation to produce TEVGs that remained patent

in pigs for up to 24 days [51]. Niklason's group recently adapted this strategy to produce devitalized TEVGs with off-the-shelf availability by decellularizing the TEVGs after 10 weeks of bioreactor culture. Devitalized grafts made from porcine cells had 100% patency at 30 days as pig carotid bypass grafts [52], and grafts made from human cells had 88% patency for up to 6 months as baboon arteriovenous shunts and 83% patency for dog carotid and coronary bypasses [53]. Using human cells, Humacyte's devitalized TEVG is now being clinically trialed in the US as above-knee femoro-popliteal bypass grafts [54] and hemodialysis grafts [55, 56]. Zund's group showed that TEVGs coated with poly-4-hydroxybutrate, seeded with myofibroblasts, and matured in a pulsatile bioreactor yielded 100% patency at 2 years post-implant as sheep pulmonary artery grafts [57]. Long-term follow-up at 4.5 years demonstrated complete material resorption without major complication, and suggests that seeded cells were replaced by host cells [58].

Cell seeding with short-term culture can improve the patency of resorbable vascular grafts without the long lead times and production costs of traditional tissue engineering. This approach is typically still considered "tissue engineering," but should be distinguished from efforts to produce mature vessel-like tissues *in vitro*. Many groups have seeded grafts with endothelial cells and/or smooth muscle cells to improve graft patency [59-65]. A wide range of stem and progenitor cells have also been shown to improve graft patency and remodeling ([66] for review). Breuer and Shin'oka's groups demonstrated that bone marrow mononuclear cells improve the patency of degradable polyester grafts in both small and large animal models [67-69]. These grafts have been used clinically with good patency as EC-TCPC conduits [70], and are currently in Phase I clinical trials in the US [71, 72]. Hashi et al. showed that human mesenchymal stem cells can improve the patency of PLA grafts in rat common carotid arteries

[73]. Vorp's group demonstrated that muscle derived stem cells [74] and pericytes [75] improve the patency of PEUU grafts in rat abdominal aortas. These grafts used a novel rotational vacuum seeding technique to improve the number and distribution of seeded cells [76]. Zhou et al used endothelial progenitor cells to improve the patency of decellularized canine carotid arteries when used as dog carotid grafts [77]. In a sheep model, Tillman et al. demonstrated translational feasibility of using decellularized arteries seeded with endothelial cells for hemodialysis access. Grafts demonstrated healing potential after needle puncture, as host cells infiltrated puncture sites [78]. For clinical translation of strategies which employ autologous stem cells, the likely potency of each patient's cells should be carefully considered. In elderly patients, adipose-derived mesenchymal stem cells demonstrated inferior ability to promote smooth muscle cell migration or differentiate into smooth muscle *in vitro* [79].

"Self-assembled" TEVGs are developed entirely from cells and the matrix they produce. These TEVGs have the potential to assume especially artery-like structure and function *in vitro* because their assembly avoids the interference of foreign materials with neotissue formation. Autologous self-assembled TEVGs might elicit less inflammation than other tissue engineered strategies, as they are completely void of foreign material. The first self-assembled TEVG was developed by L'Heureux et al. in 1998 by rolling sheets of smooth muscle and fibroblasts into a tube to produce implantable grafts [80]. Refining this approach to use only human fibroblasts [81] led to the development of autologous self-assembled hemodialysis grafts that performed well in clinical trials [82]. Recently, this approach has employed devitalization of the TEVGs so they are available off-the-shelf [83]. Allogeneic devitalized TEVGs performed well in 3 patients at up to 11 months as hemodialysis grafts, with no evidence of dilation or immune reaction [84]. Another promising self-assembly approach is bioprinting, in which cells are deposited by a

printer into three-dimensional structures [85]. This technology is still in its early stage but has already made TEVGs with tunable geometries [86]. Another approach related to self-assembly is the “Sparks Mandril” approach in which a tubular fibrous tissue for vascular grafting is generated by implanting a mandrel subcutaneously and then isolating the fibrous capsule. This method was pioneered in part by Schilling et al., who implanted them as dog abdominal aorta grafts with excellent patency at 3 years post-implant [87]. Sparks used a similar strategy and began implanting human patients with variable results [88, 89]. This approach was adapted by Campbell’s group, who implanted silastic tubing in the peritoneal cavity of animals and used the granulation tissue as vascular grafts. These grafts demonstrated 65% patency in rat arteries and 70% patency in rabbit arteries at 4 months [90]. Adaptation to dog femoral grafts yielded 83% patency at 6.5 months and demonstrated constructive graft remodeling [91].

1.2.2 Bio-inductive vascular grafts

Much research has sought to develop a bio-inductive small diameter vascular graft that can regenerate a host blood vessel *in situ*. By harnessing the host’s own neotissue generating capacity, bio-inductive grafts combine the off-the-shelf availability of prosthetic grafts with the patency and growth potential of autografted vessels. They also have a substantial advantage over tissue engineered grafts in production cost by circumventing the need for cell culture and bioreactor maturation. Bio-inductive vascular grafts were first investigated in the late 1970’s and 1980’s. Early work employed acellular grafts made fast-resorbing polyesters and polyurethanes. Poly(glycolic acid) (PGA) based grafts implanted as short aorta grafts in pigs experienced near-complete material resorption between 40 and 90 days, and remodeled into neoarteries with artery-like tissue architecture, albeit elastin was less organized than the native elastic lamina

[92]. Testing of longer, large diameter aorta bypass grafts revealed that grafts up to 15 cm long could remodel into neoarteries without rupture, though longer grafts failed by rupture within 22 days [93]. The first small diameter PGA grafts were implanted by Greisler and colleagues in 1982 as rabbit aorta interpositions. These grafts remodeled into neoarteries over a similar time course, but elastin deposition was minimal, and both dilation and intimal hyperplasia were observed at 11% and 13% incidence, respectively [94, 95]. Slower-degrading polydioxanone grafts resorbed within 6 months and reduced rates of aneurysmal dilatation, but also reduced the rate of tissue ingrowth [96]. Concurrent to research in fast-resorbing polyester grafts, fast-resorbing polyurethanes with physiologic compliance were investigated for their capacity to generate neoarteries while avoiding compliance mismatch. Initial testing of polyurethane grafts as pig aorta grafts showed complete material resorption within 4 months, and grafts and remodeled into neoarteries with organized elastic fibers [97]. Curiously, a similar polyurethane graft demonstrated high propensity for thrombosis, requiring aspirin or high-lipid diet to recover patency [98].

Despite the early promise of faster-resorbing bio-inductive grafts, most subsequent work employed slower resorbing materials, likely to assure mechanical stability for the duration of the remodeling process. These materials included degradable polyesters [92-96, 99-101] or decellularized extracellular matrix [102-105]. Since then, some bio-inductive grafts have shown promise *in vivo*. Huynh et al. implanted acellular collagen-based grafts as rabbit carotid bypasses that demonstrated constructive graft remodeling and 100% patency at 90 days [106]. Yokota et al. implanted composites of polyglycolic acid (PGA) and poly-L-lactic acid (PLA) in dog carotid arteries with 100% patency at up to 12 months and vessel-like tissue covering the graft lumen [107]. PLA has also been functionalized with hirudin to reduce thrombogenicity, leading to

improved patency in rat carotid arteries [108]. Recent work by Shinoka's group demonstrated that nanofibrous PLA grafts demonstrate favorable patency as mouse abdominal aorta grafts, with neoartery-like tissue formation in the luminal side of the graft [109]. Increasing PLA graft pore size reduced calcification and improved neotissue formation in elastin and smooth muscle content [110]. Soletti et al. developed rat aorta grafts from poly(ester urethane)urea (PEUU) coated with phospholipid to improve hemocompatibility, yielding 92% patency at 8 weeks and patent grafts at up to 24 weeks [111]. Schima's group developed microfibrous grafts made biodegradable thermoplastic polyurethane (TPU), and achieved superior patency to ePTFE grafts as rat abdominal aorta interpositions at 1 year post-implantation, with no sign of neointimal hyperplasia and moderate resorption of graft material [112].

Recently, several research teams including our own have revisited the concept of fast-remodeling, cell-free bio-inductive vascular grafts. Cortivo's group demonstrated that nonporous conduits made from esterified hyaluronic acid remodel rapidly into neoarteries containing elastin fibers in rats [113, 114] and pigs [115], though patency in the porcine model was limited by thrombosis and intimal hyperplasia. Breuer's group demonstrated in 2015 that combining PLCL-sealed PGA grafts with localized delivery of an inhibitor for TGF Beta receptor can achieve the same neovessel patency as cell-seeded grafts [116]. Fast-remodeling bio-inductive grafts have also reached the clinic. In 2015 European medical device company Xeltis AG began a phase I clinical trial testing a proprietary fast-resorbing graft as EC-TCPCs in pediatric patients with single ventricle anomalies [117].

1.2.3 Fast-remodeling composite of PGS and PCL

Our laboratory developed our own bio-inductive vascular graft in 2012 [118]. We chose a bio-inductive approach rather than tissue engineering for the advantages in production time and costs, which improve the graft's potential for clinical translation (**Figure 1**). In determining the design, we observed from literature that neoarteries with the most likeness to native arteries were formed from either fast-resorbing bio-inductive grafts or tissue engineered grafts comprised primarily of fast-resorbing materials. Consequently, we hypothesized that for a bio-inductive vascular graft to promote neoartery formation rather than fibrosis and prolongued inflammation, the graft material must resorb rapidly. We chose PGS as the material to comprise the bulk of the graft because of its rapid resorption rate *in vivo* [119], its artery-like mechanical properties [120], and its ability to promote substantial elastin production from seeded smooth muscle cells in bioreactor conditions *in vitro* [121].

The final graft design was a composite consisting of a fast-resorbing microporous PGS core and a sheath of slower resorbing PCL nanofibers (**Figure 2**). **Table 1** reports structural specifications of these grafts. The purpose of the microporous PGS core was to enable rapid cell-infiltration, transduce mechanical forces to cells, and resorb quickly to make way for neoartery tissue formation. The nanofibrous PCL sheath served multiple functions: (1) to impart the mechanical strength required for the graft to hold suture; (2) to render the graft leak-proof; and (3) to protect the early-stage neoartery from dilating as the PGS core degrades. The PGS core was fabricated using a solvent casting particulate leaching (SCPL) technique which yields seamless microporous tubular scaffolds [122]. The fibrous PCL sheath was applied by electrospinning PCL directly onto the PGS core. To distinguish these grafts from others described in the dissertation, we abbreviate these design as SCPL PGS-PCL.

To evaluate the patency and remodeling potential of these constructs, we implanted SCPL PGS-PCL grafts as abdominal aorta interposition grafts in rats. Grafts patency was 80%, and patent grafts remodeled rapidly and extensively into neoarteries which were nearly free of foreign material by 3 months post-implant. (**Figure 3**) Neoarteries demonstrated native or supra-native mechanical compliance in the physiologic pressure range (11 ± 2.2% vs. 6.7 ± 2.3%; **Figure 4**) and artery-like tissue architecture at in both cell organization (**Figure 5**) and matrix organization (**Figure 6**). Notably, neoarteries contained 77% of the mass of mature elastin present in native arteries, and an equivalent amount of collagen (**Figure 6b**). Neoarteries resisted dilation, as neoartery inner diameter was comparable to age-matched controls at 90 days (**Figure 5c**) Taken together, these results support the central hypothesis that rapid remodeling guides *in situ* generation of functional neoarteries rather than fibrotic encapsulation. Further, the favorable graft performance and near-absence of residual material suggests the potential for long-term neoartery stability. In light of this encouraging proof of concept, the work described in this dissertation aims to further assess the translational potential of a fast-remodeling bio-inductive vascular graft made from compositing PGS with a slower-resorbing material.

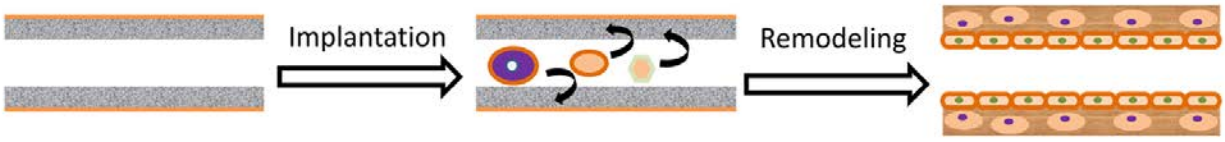

Figure 1. Schematic of in-host remodeling of SCPL PGS-PCL bio-inductive graft.
Direct implantation of a cell-free PGS-PCL composite graft (left), and the proposed remodeling process of the graft into a biological neo-artery. Image from [118].

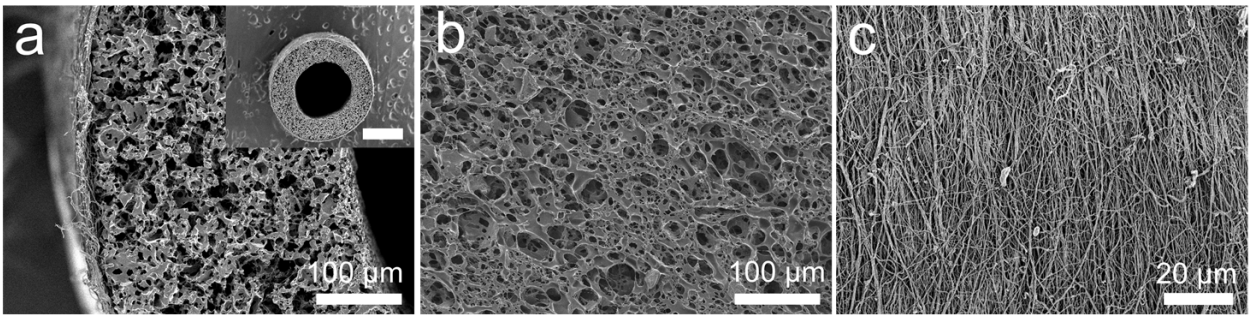

Figure 2. Structure of SCPL PGS-PCL composite grafts.
SEM images show surface topology of microporous composite grafts. (a) Transverse cross section of graft wall shows PCL sheath (left edge) and microporous SCPL PGS core (bulk). Luminal surface is the rightmost edge, scale bar 100 µm. Inset: low magnification of graft, scale bar 500 µm. (b) Luminal surface of the PGS core, scale bar 100 µm. (c) Abluminal surface of the PCL sheath, scale bar 20 µm. Image from [118].

Table 1. Geometric specifications of SCPL PGS-PCL bio-inductive vascular grafts

Pore size (µm)	21.2 ± 0.79
Porosity (%)	81.06 ± 0.97
Pore interconnectivity (%)	99.99 ± 0.00027
Inner diameter (µm)	723 ± 1.33
Wall thickness (µm)	295 ± 5.52
Sheath thickness (µm)	15.7 ± 6.11

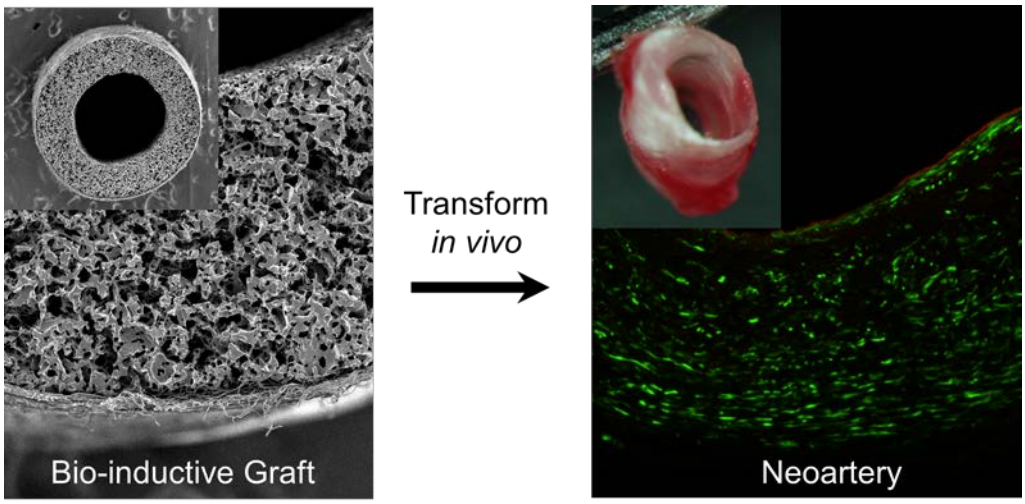

Figure 3. Neoartery formation from SCPL PGS-PCL bio-inductive graft.
Cell-free bio-inductive grafts remodel *in situ* into a neoarteries within 3 months of implantation as rat abdominal aorta interposition grafts. *Left*: SEM micrograph of SCPL PGS-PCL composite graft. Inet: Low magnification. *Right:* Neoartery at 3 months post-implant. α-SMA immunostaining (green) indicates smooth muscle cells or myofibroblasts. vWF immunostaining (red) suggests a confluent endothelial lining. Right inset: dissecting microscope image of neoartery. Image adapted from [118].

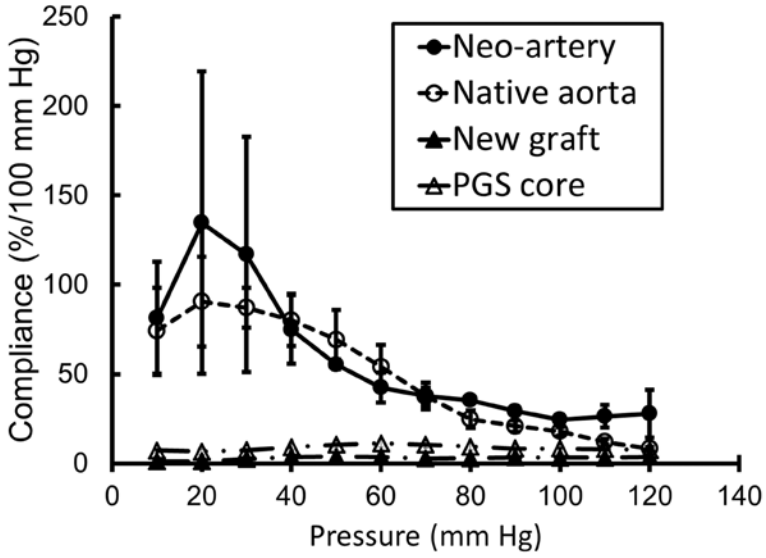

Figure 4. Neoarteries demonstrate native or supra-native compliance.
Compliance as a function of luminal pressure, tested *ex-vivo*. "New grafts" represents unimplanted composite grafts. "PGS core" represents new SCPL PGS grafts without the PCL sheath. Error bars represent standard error of the mean. Standard errors for new grafts and the PGS core are very small and barely visible at the plotted scale. n = 3 for neo-arteries and n = 4 for native aortas. Image adapted from [118].

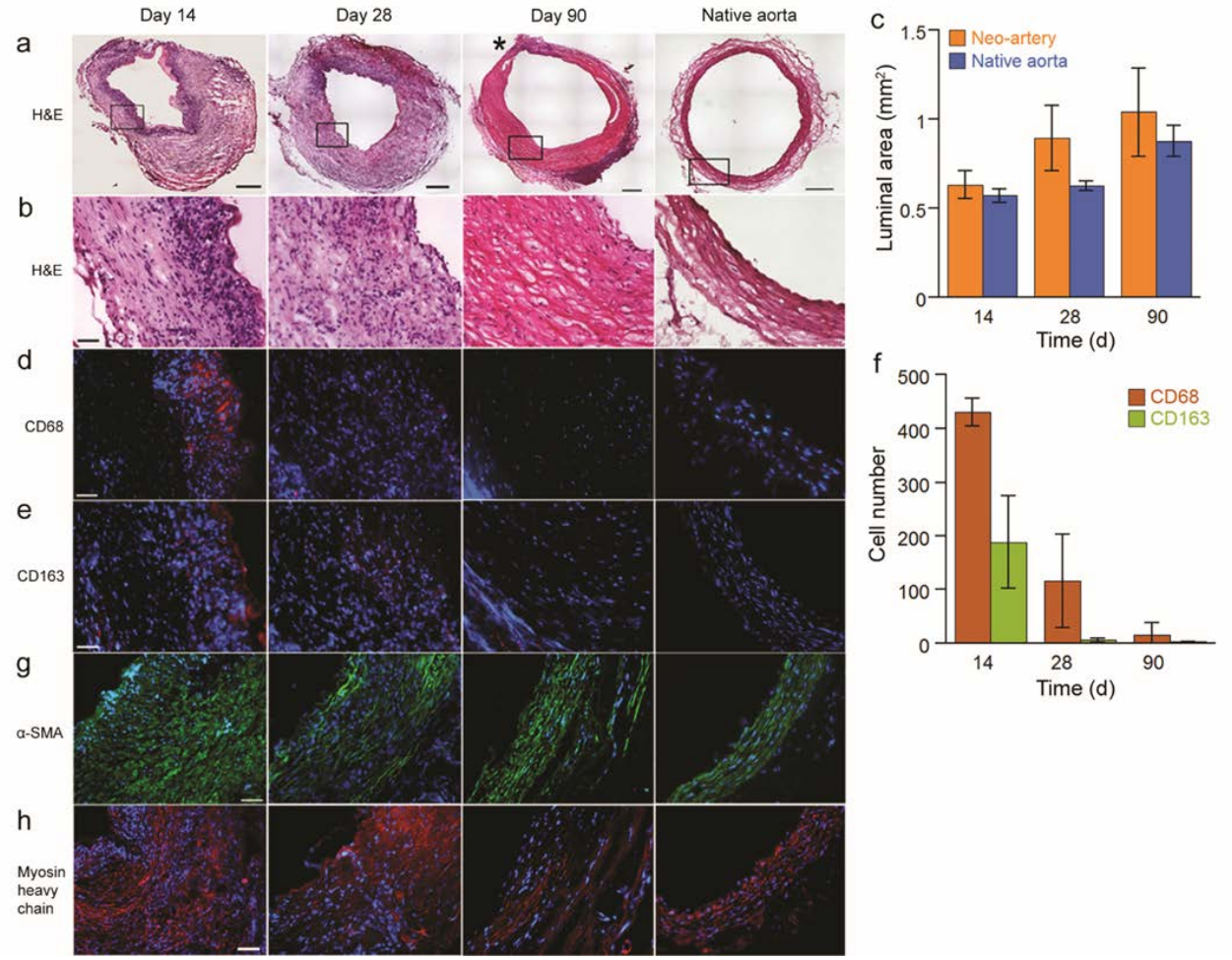

Figure 5. Cellular organization of neoarteries

(**a**) H&E staining of the grafts during the transition into a neo-artery. An area of the neo-artery wall containing inflammatory cells is marked by (*). The top of the 14-day sample was trimmed to remove the adjoining vein. Image merged from a panel of 100x micrographs, scale bar 250 µm. (**b**) Magnified view of the vessel wall shows ECM content and alignment, scale bar 50 µm. (**c**) Luminal area of remodeling grafts to assess stenosis and aneurysm formation. There is no statistical difference between the two groups. (**d**) Changes in number and organization of macrophages (CD68, red). (**e**) Distribution of M2 macrophages (CD163, red). (**f**) Number of CD68 and CD163 positive cells quantifies total macrophage number and the proportion of M2 macrophages. (**g**) Changes of smooth muscle cell (α-SMA, green) organization over time. (**h**) Distribution of contractile smooth muscle cells (myosin heavy chain, red). All the immuofluorescent micrographs were counterstained for nuclei by DAPI (blue), scale bar 50 µm. Data represent mean ± standard deviation for **c** and **f.** Image adapted from [118].

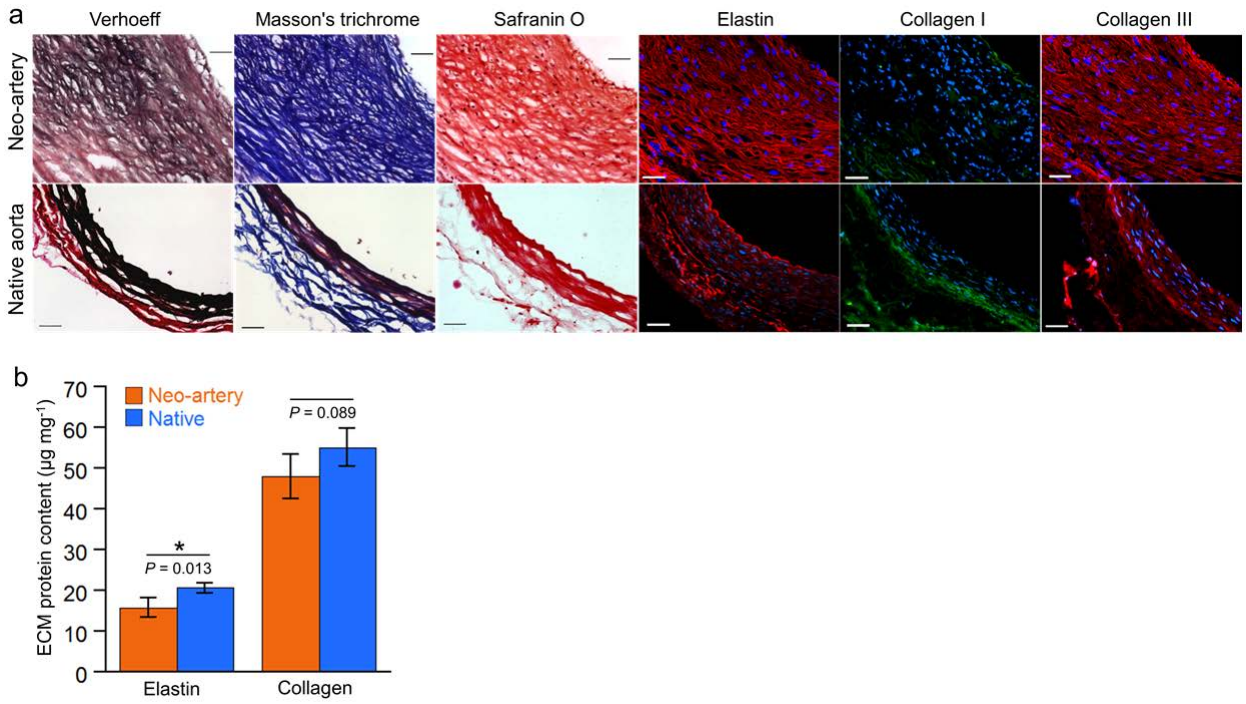

Figure 6. Extracellular matrix organization of neoarteries
ECM organization and quantification at 90 days. (**a**) Verhoeff's, Masson's trichrome, and safranin O staining show elastin (black), collagen (blue), and glycosaminoglycansin (red). Immunofluorescent staining shows distribution of elastin (red), collagen I (green), and collagen III (red). Top: day 90 explant, bottom: native aorta. (**b**) Quantification of elastin (n = 4) and total collagen (n = 4). Data represent mean ± standard deviation**.**

1.3 OBJECTIVES AND SPECIFIC AIMS

The long-term objective of our laboratory's research is to develop a bio-inductive vascular graft with the improved performance compared to prosthetic vascular grafts, and for which use in a clinical setting is feasible. The objective of this dissertation is to assess the translational potential of a fast-remodeling, cell-free vascular graft based on fast-degrading elastomer PGS. Driving the pursuit of this objective is our central hypothesis, which is consistent with that which we used in our previous graft design. We hypothesized that for a bio-inductive vascular graft to promote neoartery formation rather than fibrotic encapsulation, the graft material must resorb rapidly. The rationale is that rapid clearance of graft material minimizes the interference of foreign material with in-host tissue formation and long term homeostasis.

For a new technology to translate to the clinic, it must demonstrate both desirable clinical performance and feasibility of application in a clinical setting. Our laboratory's recently reported bio-inductive vascular graft seems well poised for potential clinical translation, as it demonstrated encouraging short-term performance, and its cell-free design suggests clinical feasibility in production costs and lead time. However, long term performance remains unknown, and grafts require gentle surgical handling, limiting their ease of use in a clinical setting. Thus, to further evaluate the graft's translational potential, the work described in this dissertation pursues the following three aims:

Aim 1 - *Long-term performance testing of original design.* The objective of this aim is to assess the long-term *in vivo* stability of composite grafts made from microporous SCPL PGS and PCL fibers (SCPL PGS-PCL). We hypothesized that at late-term, neoarteries will maintain

homeostasis without complication, as material residues are largely absent at 3 months and the neotissue is elastin-rich and compliant. To test this hypothesis, we implanted composite grafts into rats as abdominal aorta interpositions, and incubated for 1 year. At term, we characterized neoarteries extensively both *in vivo* and *ex vivo*, and compared with age-matched unoperated controls.

Aim 2 – *Improve the translational potential of the design.* The objective of this aim is to improve the feasibility of applying PGS-based bio-inductive vascular grafts in a clinical setting. We hypothesized that fabricating the PGS core from microfibers will improve surgical handling and simplify fabrication. To realize improved translational feasibility, we developed a novel method for fabricating PGS microfibers involving electrospinning a range of polymer blends, then constructed novel microfibrous grafts. We then compared these grafts to SCPL PGS in fabrication time and labor, strength *in vitro*, and likelihood of successful *in vivo* implantation.

Aim 3 - *Performance testing of the improved design.* The objective of this aim is to assess the *in vivo* performance and remodeling potential of the most promising electrospun graft designs developed in Aim 2. We hypothesized that electrospun PGS PCL composites (Espun PGS-PCL^{Sheath}) would retain the fast-remodeling behavior of the original microporous design in spite of reduced pore size, as even nonporous PGS resorbs rapidly *in vivo*, and nonporous bio-inductive grafts have previously remodeled into neoarteries. To evaluate graft performance *in vivo*, we joined a multi-institutional collaboration to implant microfibrous vascular grafts as mouse abdominal aorta interpositions, and evaluated at up to 1 year post-implant.

2.0 LONG-TERM PERFORMANCE OF SCPL PGS-PCL COMPOSITES

The demonstration of short-term patency is necessary but insufficient for a new vascular graft to improve clinical outcomes. Long-term performance must also be favorable, as the ideal vascular graft should conduct blood flow for the remaining lifetime of the patient. This chapter presents our investigation of the long-term performance of microporous SCPL PGS-PCL composite vascular grafts.

2.1 INTRODUCTION

Prosthetic vascular grafts are prone to a range of long-term complications, many of which require percutaneous or surgical intervention. Neointimal hyperplasia is the most common underlying cause of late-term graft occlusive failure [123]. Neointimal hyperplasia describes the narrowing of a vessel lumen due to cells migrating into and proliferating within the vascular intima. In prosthetic vascular grafts, neointimal hyperplasia occurs in the native vessel at the site of anastomosis with the prosthetic graft. Anastomotic occlusion due to neointimal hyperplasia reduces patency to as low as 54% at 4 yrs in below-the-knee bypass using prosthetic grafts [124]. Late thrombosis in prosthetic grafts most commonly occurs secondary to vessel narrowing due to neointimal hyperplasia, and is often the mechanism of final graft occlusion. Infection is another serious late-term complication, with incidence ranging from 1 to 6 % ([125] for review).

Infection rates are substantially higher in applications more susceptible to infection, such as hemodialysis (~20%) [126] and wartime vascular trauma reconstruction (up to 48% in ePTFE grafts) [17]. Infection typically requires either graft replacement or salvage techniques, both of which are surgical interventions.

The persistence of foreign material drives pathologies which substantially contribute to these late term failure modes. Foreign material contributes to compliance mismatch, a major driver of neointimal hyperplasia, when the graft material is stiffer than native arteries. Compliance mismatch is thought to drive neointimal hyperplasia by hemodynamic disruptions including turbulent flow and shear stress alteration [12, 120], although the exact mechanism of promoting cell migration and proliferation in the intimal layer remains controversial [127]. The hemodynamic disruptions caused by compliance mismatch also promote thrombosis [123]. Foreign material may exacerbate neointimal hyperplasia and thrombosis by paracrine effects from the chronic inflammation associated with long-lasting material, which promote migratory phenotypes in SMCs associated with neointimal hyperplasia, and activate endothelial cells toward a pro-coagulatory state [128]. Long-lasting materials also limit the potential for prosthetic vascular grafts to develop a thrombosis-resistant endothelium, as endothelial cells can only migrate 2 cm onto foreign material from adjacent arteries in humans, thereby leaving the majority of vascular graft length without a confluent endothelium [129]. Infection risk is also substantially exacerbated by long-lasting materials, which are known to serve as a nidus for microbial colonization and subsequent biofilm formation [130].

A fast-remodeling bio-inductive graft could avoid these late-term failures by minimizing the duration of the host's exposure to foreign materials. However, an additional late term risk in fast-remodeling grafts is aneurysmal dilatation, which can occur if the loss of graft strength due

to degradation exceeds the rate at which developing neotissue can bear load. Aneurysmal dilatation is seen in rarely-used homografts and heterografts, and can cause catastrophic failure by rupture, as well as thrombosis and/or embolism due to endothelial disruption associated with aneurysm pathology [131]. A fast-remodeling bio-inductive vascular graft must avoid aneurysmal dilatation as well as traditional late-term failure modes to improve graft performance compared to prosthetic conduits.

In this chapter, we examined the long-term *in vivo* stability of microporous composite fast-remodeling grafts. This evaluation is essential for understanding the design's potential for translation, as vascular grafts must conduct blood flow for the remainder of the patient's lifetime. We hypothesized that at late-term, neoarteries will maintain homeostasis without complication, as material residues are largely absent at 3 months and the neotissue is elastin-rich and compliant. To test this hypothesis, we implanted composite grafts into rats as abdominal aorta interpositions, and incubated for 1 year. At term, we characterized neoarteries extensively both *in vivo* and *ex vivo*, and compared with age-matched unoperated controls.

2.2 METHODS

2.2.1 Fabrication of composite vascular grafts

SCPL PGS-PCL grafts were fabricated as previously described [118]. Briefly, PGS prepolymer was synthesized in house [132]. The PGS core of the composite graft was fabricated by casting a PGS prepolymer solution into a fused salt template within a tubular mold. To cross-link the PGS prepolymer, constructs were heat cured at 150 °C under vacuum for 24 h to produce a PGS-salt

template. To fabricate the PCL sheath, PCL (Mn 80 kDa; Aldrich, St. Louis, MO) was dissolved in 2,2,2-trifluoroethanol at 14% weight/volume and electrospun onto a rotating PGS-salt template at 20 RPM. Salt was removed from PGS-PCL-salt composites by immersing them in deionized water. Composite grafts were lyophilized (Labconco Freezone 4.5, Kansas City, MO) and stored in a desiccator at ambient temperature until use. Grafts were sterilized with ethylene oxide prior to implant.

2.2.2 Implantation

Rats were cared for in compliance with protocols approved by the Institutional Animal Care and Use Committee (IACUC) of the University of Pittsburgh following NIH guidelines for the care and use of laboratory animals (NIH publication No. 85–23 rev. 1985). We used male Lewis rats (body weight: 200–250 g, n = 5, Charles River Laboratories, Boston, MA) for experiments. We performed interpositional implantation in rat abdominal aortas as follows. Rats were anesthetized by isoflurane inhalation (5% for induction, then 2-3% for maintenance). A midline abdominal incision was made to expose the abdominal aorta. The aorta was separated from the inferior vena cava, the infrarenal abdominal aorta was cross-clamped, and then a 4-mm segment was transected. The SCPL PGS-PCL graft (8-10 mm long) was placed in the gap and connected to the native aorta by end-to-end anastomosis with 9-0 suture. Rats received no anticoagulation or antiplatelet treatment preoperatively or postoperatively. After implantation, grafts resorbed and transformed into “neoarteries” (regenerated arteries). At one year post-implant, neoarteries were characterized in situ, then rats were sacrificed to explant grafts for ex-vivo analysis (n = 5).

2.2.3 In vivo dynamic mechanical compliance

In a non-survival surgery, rats were anesthetized with isoflurane inhalation (5% for induction, then 2-3% for maintenance), then ventilated by the insertion of a tracheal cannula attached to a rodent ventilator (Harvard Apparatus, South Natick, MA) set to 90 breaths/min with a tidal volume of 8 ml/kg body weight. The chest was opened with a midline incision and then a four-electrode pressure-volume catheter (Scisence Inc., London, Ontario, Canada) was placed through the left ventricular apex and fed into the aortic arch. aortic pressure and neoartery inner diameter were measured simultaneously to determine the dynamic mechanical compliance of neoarteries. Aortic pressure was measured using the same pressure-volume catheter used in arterial impedance measurement. To measure neoartery inner diameter, hair was removed from the abdominal skin, then the abdominal aorta was imaged transcutaneously using a 21 MHz ultrasound linear probe (MS 250) connected to a high frequency small animal imaging system (Vevo2100, Visualsonics, Canada) in B-scan mode. The change in inner diameter of neoarteries due to blood pressure was measured from B-scan images. Dynamic mechanical compliance was calculated from Equation 1:

$$C = ((D_{inner}(P_{Systole}) - D_{inner}(P_{Diastole})) / (D_{inner}(P_{Diastole})) \times 100) / (P_{Systole} - P_{Diastole}) \quad (1)$$

where D_{inner} represents inner diameter, $P_{Systole}$ represents aortic pressure at systole, and $P_{Diastole}$ represents aortic pressure at diastole.

2.2.4 Characterization of neoartery vasoactive properties

The following were obtained from Sigma-Aldrich, St. Louis, MO: L-phenylephrine hydrochloride, norepinephrine, acetylcholine chloride, sodium nitroprusside dihydrate, serotonin, and forskolin. Animals were humanely euthanized. Functional arterial myography assays were performed as previously published with several modifications. [133] The neoarteries or native aortas were dissected free, cleaned of surrounding connective tissue, and placed in standard Krebs buffer (composition in mM: NaCl, 118.4; KCl, 4.7; CaCl2, 2.5; MgSO4, 1.2; KH2PO4, 1.2; NaHCO3, 25; dextrose, 11.1; Na2Ca EDTA, 0.029; pH 7.4). Aorta segments (2 mm in length) were mounted in a dual wire myograph system (Multiple Myograph Model 610 M, DMT, Denmark). The rings were allowed to equilibrate in Krebs buffer with 95% O2 - 5% CO2 at 37 ºC at the optimized passive tension. Single dose challenges to phenylephrine (PE) and serotonin (5-HT) were performed. Rings were then preconstricted to serotonin (5-HT) and allowed to reach a steady-state plateau. Single dose challenges to acetylcholine (Ach) and forskolin were then determined. In other experiments log-dose response curves of preconstricted rings to the NO prodrug sodium nitroprusside (SNP) were obtained. Concentration-response curves were plotted as percentage of relaxation using all points on the concentration-response curve by nonlinear regression curve fitting using GraphPad Prism 5.0 (GraphPad Software, San Diego, CA). Data represents results from 12 individual neoartery ring assays, derived from explants from 3 animals.

2.2.5 Histology and immunofluorescence

All microscope images presented are representative fields from at least three different animals. Neoartery images are all taken from the middle 4 mm of the remodeled graft. Explants were fixed in 2% paraformaldehyde (Electronic Microscopy Sciences, Hatfield, PA) for 2 h at room temperature, then frozen in Optimal Cutting Temperature Compound (OCT; Tissue-Tek, Torrance, CA) with liquid nitrogen and stored at -80°C until use. Sections were cut to 8 µm thickness using a cryomicrotome (HM525, Thermo Scientific, Waltham MA), mounted on glass slides, and stored at -80°C until staining. Slides were stained with hematoxalin and eosin (H&E), Picosirius red, and von Kossa according to standard protocols, and imaged using a Nikon Eclipse Ti inverted microscope with Nikon Elements software (Melville, NY). Slides stained with Picosirius red were illuminated with plane-polarized light and imaged using differential interference contrast (DIC). Immunofluorescent staining was performed as follows: slides were incubated in 5% normal goat serum (Sigma, St. Lois, MO) for 1 h at 37 °C, incubated with primary antibodies in 1% goat serum for 45 min at 37 °C, rinsed with Phosphate Buffered Saline (PBS; Mediatech, Manassas, VA), and incubated with secondary antibodies in 1% goat serum for 45 min at 37 °C. Primary antibodies are listed in **Table 2**. Secondary antibodies included goat anti-mouse or goat anti-rabbit AlexaFluor 594 (1:400; Invitrogen, Grand Island, NY). Slides were coverslipped in VectaShield Hard Set mounting medium with DAPI (Vector Laboratories, Burlingame, CA), which co-stains nuclei blue. Coverslipped slides were stored at 4°C protected from light until being imaged with a Nikon Eclipse Ti inverted microscope.

Table 2. Primary antibodies for immunofluorescence microscopy

Antigen	Host	Dilution	Manufacturer	Location	Product no.
α-smooth muscle actin (αSMA), FITC conjugated	Mouse	1:1000	Sigma	St. Louis, MO	F3777
von Willebrand Factor (vWF)	Rabbit	1:400	Abcam	Cambridge, MA	Ab6994
CD68	Mouse	1:250	Millipore	Billerica, MA	MAB1435
Elastin	Rabbit	1:100	Abcam	Cambridge, MA	Ab21610
Fibrillin-1	Rabbit	1:100	Santa-Cruz	Dallas, TX	Sc20084
Collagen III	Rabbit	1:100	Abcam	Cambridge, MA	Ab7778
Collagen I	Rabbit	1:40	Millipore	Billerica, MA	Ab745

2.2.6 *En face* immunofluorescence microscopy

Neoartery explants were cut into 1 to 2 mm long rings, then cut longitudinally into segments. Segments were fixed in 2% paraformaldehyde for 2 h at room temperature. Segments were then immunostained as whole mounts by blocking in 2% bovine serum albumin (BSA; EMD Chemicals, Gibbstown, NJ) with 0.1% Triton-X100 (Sigma) for 6 h at 4 °C, incubating in primary antibodies overnight at 4 °C, washing with 0.5% BSA for 5 h at 4 °C, incubating in secondary antibodies overnight at 4 °C, then rinsing again with 0.5% BSA. Segments were stained for either (1) endothelial cells, or (2) perivascular nerves. For endothelial cell staining, primary and secondary antibodies were mouse anti-rat CD31 (1:250; Millipore MAB1393) and goat anti-mouse AlexaFluor 594 (1:200; Invitrogen), respectively. For nerve staining, segments were co-stained with two primary antibodies: rabbit anti-rat protein gene product 9.5 (PGP 9.5;

1:250, Millipore Ab9724) and mouse anti-rat β-Tubulin (1:1000; Sigma T5293). Secondary antibodies were goat anti-rabbit AlexaFluor 594 (1:200; Invitrogen) and goat anti-mouse AlexaFluor 488 (1:200; Invitrogen), respectively. Dual staining was used to reduce effects of nonspecific staining which are amplified in whole mount imaging. To prepare stained whole mounts for imaging, segments were mounted in gelvatol on glass slides, flattened under a coverslip, and stored at 4 °C protected from light until imaging. Glass slides were imaged *en face* using an Olympus Fluoview 1000 confocal microscope (Center Valley, PA), and Z-stacked images were flattened using MetaMorph imaging software (Molecular Devices, Downingtown PA).

2.2.7 *En face* multiphoton microscopy

Neoartery explants were cut, fixed, and mounted as done for *en face* immunofluorescence, but without incubation in BSA or antibodies, and saline was used instead of gelvatol for mounting. Collagen and elastin autofluorescence within the neoartery wall was measured as previously described using an Olympus Fluoview FV1000-MPE Multiphoton microscope with a 1.12 NA 25x MPE water immersion objective [134]. Excitation was set to 870 nm, and the emission range was set to 400-500 nm and 525-575 nm for collagen and elastin, respectively. To image collagen and elastin close to the abluminal (outer) surface, explants were placed within the wells of hanging drop slides, coverslipped, and turned with the abluminal surface facing the objective. A schematic depicting each *en face* view is shown in **Figure 7.**

2.2.8 Elastin quantification

Neoartery explants were cut into ring segments as described for *en face* imaging. Each segment was minced finely, weighed to obtain wet weight, and then digested three times with 0.25 M oxalic acid at 95 °C for 1 h to extract mature insoluble elastin into the solution supernatant. Elastin content in each extract was measured using a Fastin Elastin assay (F2000; Biocolor, Carrickfergus, UK) according to manufacturer's instructions, then pooled and normalized to sample wet weight to yield the mass of insoluble elastin per tissue wet weight (μg/mg). Sample size: n = 3 for neoarteries and native aortas. All samples were tested in duplicate during the same assay run, except for one neoartery for which there was insufficient tissue to run in duplicate.

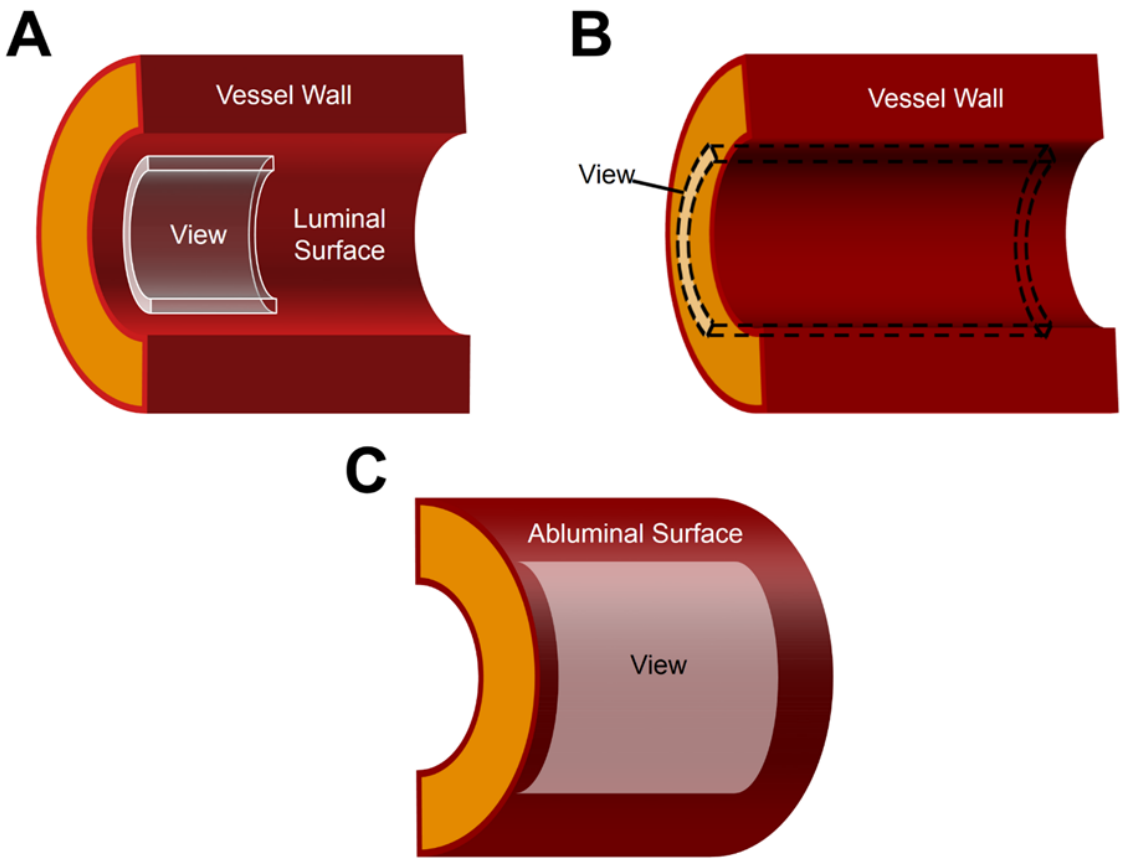

Figure 7. Schematic of *en face* multiphoton microscopy
En face imaging of collagen and elastin autofluorescence using multiphoton microscopy. **A.** View of the explanted "neoartery" (regenerated artery) near the luminal surface. The middle of each neoartery was cut into ring segments, then cut open into ring halves and flattened between a glass slide and a cover slip. Slides were imaged with the luminal surface facing the objective. Neoarteries were imaged within 10 μm of the luminal surface. **B.** View of the media-like layer of the neoartery. Explants were mounted as in **A**, then the viewing plane was focused within the vessel wall, at least 10 μm from the luminal surface. **C.** View of the adventitial surface of the neoartery. Mid-graft segments were cut into ring halves as in **A**, then placed in hanging drop glass slides which contain a cavity within the slide. Slides were coverslipped and imaged with the adventitial surface facing the objective. Image from [135].

2.2.9 Statistical Analysis

Comparisons between two groups were made with a two-tailed Student's t-test using IBM SPSS Statistics 19 software (Armonk, NY). Comparisons between three groups were made using a one-way analysis of variance test followed by Tukey's Honestly Significant Difference (HSD) post hoc test using GraphPad Software (LaJolla, CA).

2.3 RESULTS

2.3.1 SCPL PGS-PCL grafts remodel into "neoarteries" resembling native arteries

By one year post-implant, SCPL PGS-PCL grafts transformed into tissues grossly resembling native aortas (**Figure 8**) with similar tissue architecture and no visible graft material residues (**Figure 9**). "Neoarteries" (regenerated arteries) showed a confluent endothelium as demonstrated by complete coverage of the luminal surface with cells positive for von Willebrand Factor (vWF) and CD31 (**Figure 10**). Endothelial cells in neoarteries had cobblestone-like morphology and alignment in the direction of blood flow, as seen in native aortas (**Figure 10 B**). The middle layer of the neoartery vascular wall contains many smooth muscle-like cells with elongated nuclei which stain positively for α-SMA, resembling the native arterial medial layer (**Figure 10 A)**. Many α-SMA$^+$ cells are also positive for myosin heavy chain 11 (MHC-11), suggesting a mature, contractile phenotype (**Figure 10 C)**. Some α-SMA$^+$ cells are negative for MHC-11, suggesting they are myofibroblasts or smooth muscle cells of a synthetic phenotype. Regenerated arteries showed an adventitia-like layer outer layer of less dense, α-SMA-negative

tissue which stains positive for DAPI. Interestingly, neoarteries contain some cells which are negative for α-SMA and MHC-11 in the vascular media-like layer, including cells with elongated nuclei. In sparse, unrepresentative sections of neoarteries, the majority of cells in the media-like vascular layer are negative for smooth muscle markers (**Figure 11**). These cells have yet to be identified. Neoarteries also contain some α-SMA and MHC-11 positive cells adjacent to the endothelium which are not elongated in the circumferential direction (**Figure 10 and Figure 11**).

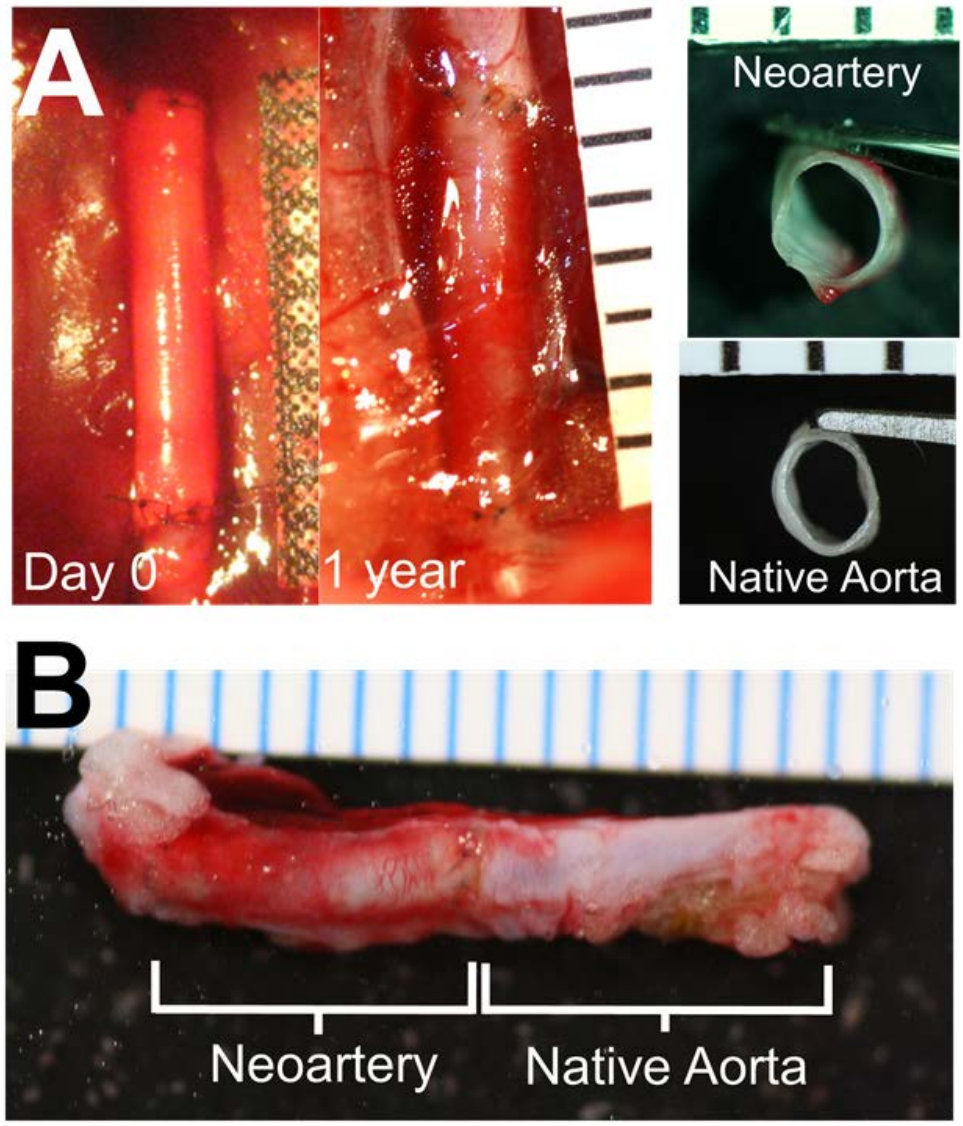

Figure 8. Gross morphology of neoarteries.
A. Left: transformation of SCPL PGS-PCL graft into neoartery in situ over the course of 1 year. Nondegradable sutures (black) mark the graft location. Right: Transverse view of explanted neoarteries resembles that of native aortas. **B.** Longitudinal view of explanted neoarteries resembles the adjacent native aorta. All ruler ticks are 1 mm. Image from [135].

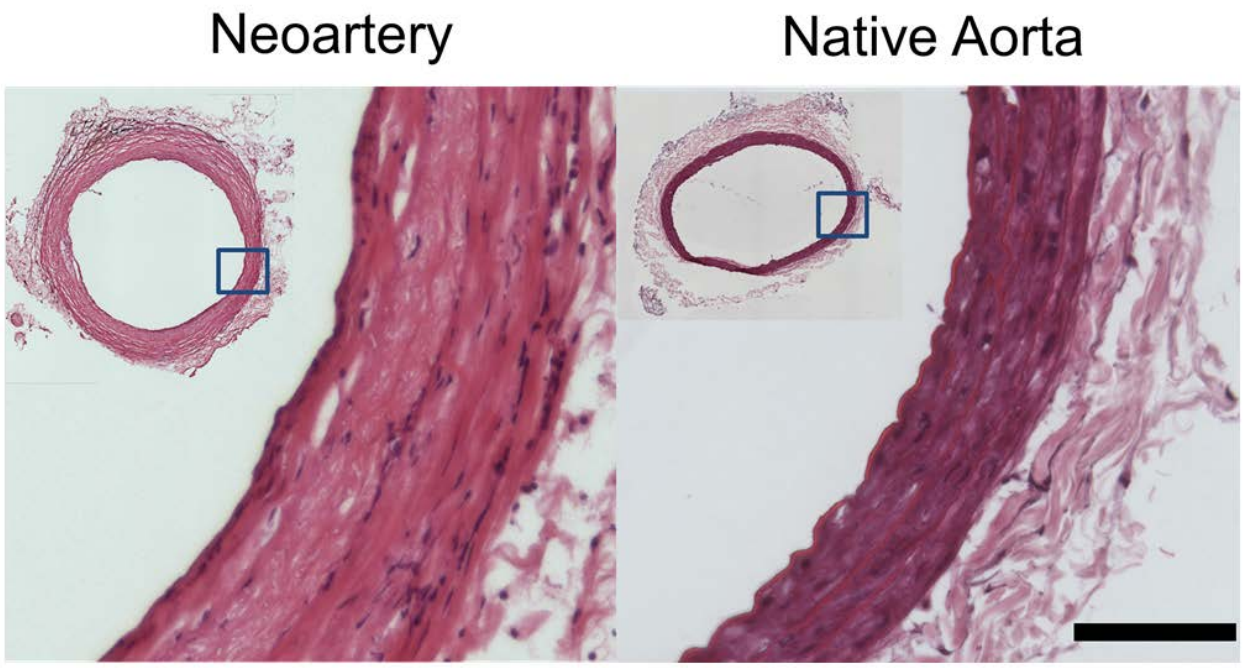

Figure 9. Hematoxylin and eosin staining of neoarteries
H&E stained transverse sections of the middle of neoarteries show similar tissue architecture with native aortas, with no sign of residual graft material. Scale bar 100 μm. Image from [135].

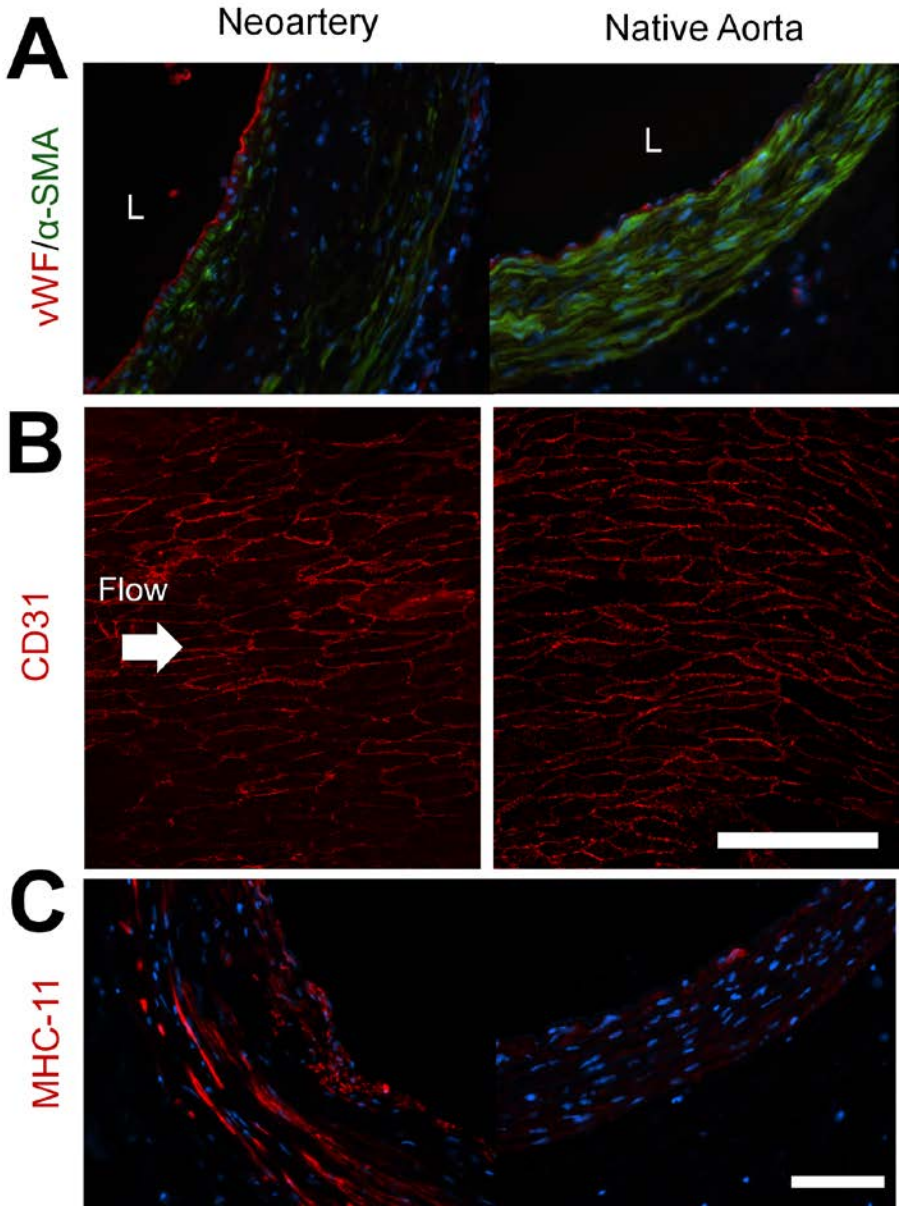

Figure 10. Vascular cell phenotypes within neoarteries.
A. Neoartery sections immunostained for von Willebrand factor (vwf, red) and alpha smooth muscle actin (α-SMA, green). The luminal surface of neoarteries is completely covered by vWF positive cells (red), suggesting a confluent endothelium. Neoarteries contain a media-like middle layer of the vascular wall rich in α-SMA positive cells with circumferentially elongated nuclei, similar to vascular smooth muscle found in native aortas. The outermost layer of neoarteries lacks α-SMA, resembling native adventitia. Some cells in the media-like layer are negative for α-SMA, and some cells adjacent to the endothelium are α-SMA positive but not circumferentially elongated. Scale bar 100 mm. L indicates vessel lumen. Nuclei stained with DAPI (blue). **B.** Immunostaining for smooth muscle myosin heavy chain 11 (MHC-11, red). Many elongated cells in the media-like layer are positive for MHC-11, suggesting a mature, contractile smooth muscle phenotype. The distribution of MHC-11 appears similar to that of α-SMA. MHC-11 positive cells in neoarteries stain brighter than those in native aortas at the same exposure. Scale bar 100 mm. L indicates vessel lumen. Nuclei stained with DAPI (blue). Image from [135].

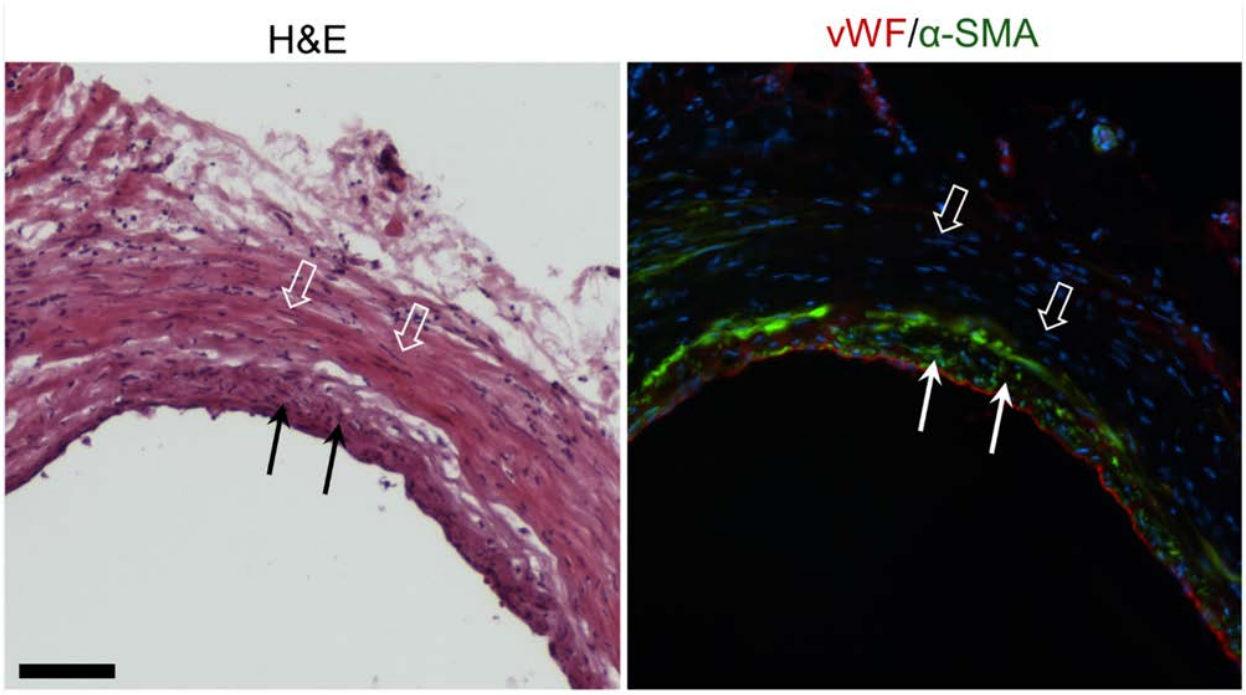

Figure 11. Some neoartery media cells negative SMC markers.
Unrepresentative transverse section of neoartery differs from native arteries in cell phenotypes. *Left:* H&E stained neoartery. *Right:* Serial neoartery section immunostained for vWF (red) and α-SMA (green). The majority of cells within the vessel wall are negative for α-SMA, including cells with elongated nuclei which look similar to smooth muscle cells in H&E stained sections (arrow outlines). Many cells adjacent to the endothelium are positive for α-SMA, but exhibit punctate morphology rather than alignment in the circumferential direction (solid arrows). Scale bar 100 µm. Image from [135].

2.3.2 Neoarteries resist common modes of late-term vascular graft failure

One-year patency was unchanged from the three-month patency of 80% [118], suggesting resistance to late-term failure. The only occluded SCPL PGS-PCL graft was likely closed by acute thrombosis, as the non-vascular tissue architecture at the mid-graft suggests little constructive remodeling occurred before occlusion, and the tissue occluding the graft lumen does not resemble neointimal hyperplasia (**Figure 12**). Patent grafts showed no statistically significant difference in inner diameter compared with native arteries, suggesting resistance to both dilation and narrowing by neointimal hyperplasia (**Figure 13 A**). Neoarteries showed no evidence of

mineralization or calcification, as they are negative for von Kossa staining (**Figure 13 B**). Macrophages are present only in the adventitia-like region of regenerated arteries at 1 year post-implant, likely associated with a small amount of remnant PCL (**Figure 13 C**).

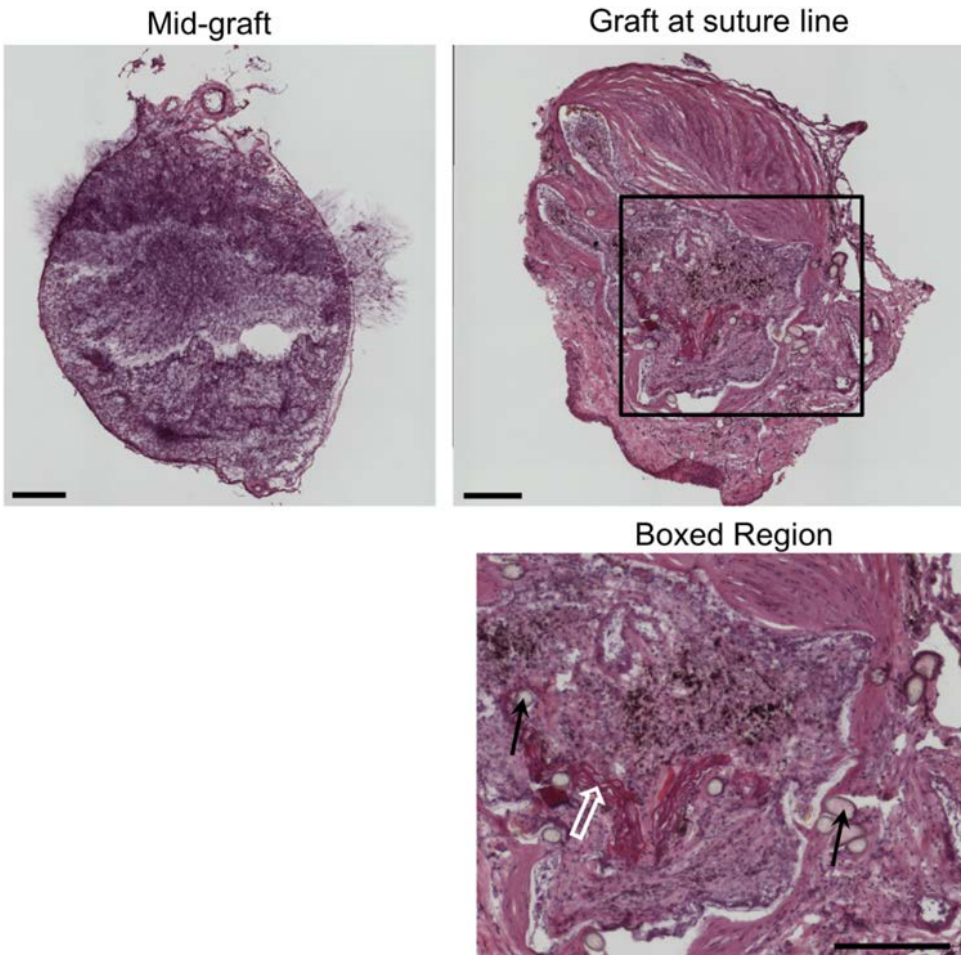

Figure 12. Occluded SCPL PGS-PCL graft at 1 year post-implant.
Occluded graft at 1 year post-implant. *Left:* H&E of transverse section of middle of occluded graft. Scale bar 250 µm. *Right*: Occluded graft at the suture line. *Bottom*: Boxed region of occluded graft at suture line. The non-vascular tissue architecture suggests occlusion soon after implantation, as little constructive remodeling occurred before occlusion. The tissue occluding the graft lumen is densely cellular but does not resemble neointimal hyperplasia, suggesting thrombosis as a likely cause of occlusion. White arrow outlines depict vascular media from the native aorta proximal to the graft. Black arrows denote suture. Scale bar 250 µm. Image from [135].

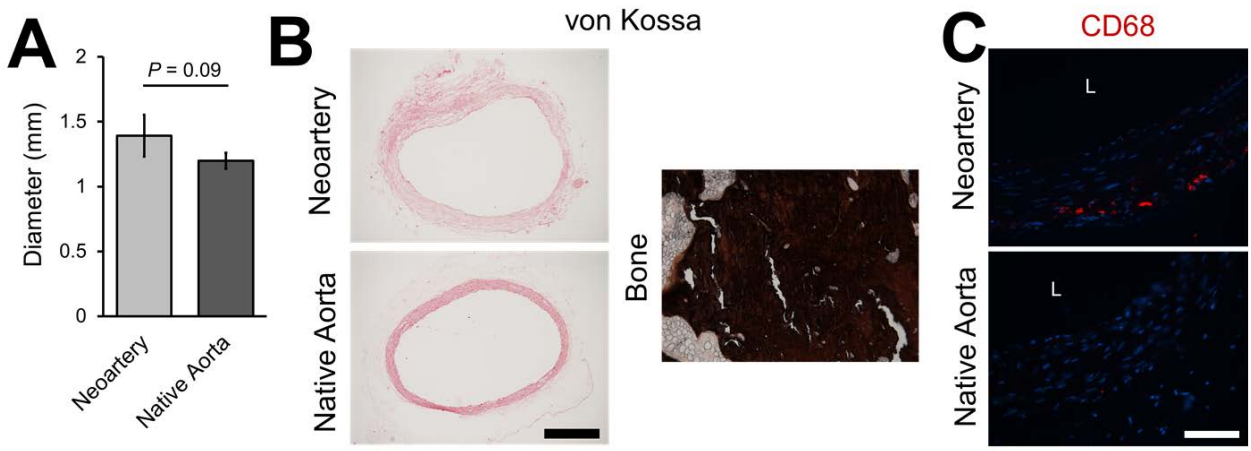

Figure 13. Neoarteries resist common modes of late-term graft failure.
A. Neoartery inner diameter is not significantly different from that of age-matched native aortas, suggesting resistance to dilation and neointimal hyperplasia. **B.** Neoarteries are negative for von Kossa staining (black indicates a positive stain), suggesting resistance to calcification. Bone (rabbit ulna) was stained with von Kossa as a positive control for calcified tissue. Scale bar 500 µm. **C.** Neoarteries contain cells positive for macrophage marker CD68, concentrated mostly in the outermost layer of the neoartery wall. Scale bar 100 µm. Image from [135].

2.3.3 Nerves in the perivascular space of neoarteries

We searched regenerated vessels for perivascular nerves to (1) investigate whether neoartery tone could be regulated by the nervous system, and (2) determine whether nerves can regenerate and traverse the implant site. We found nerves on the adventitial surface of neoarteries with similar morphology and distribution to those found in native arteries (**Figure 14**). Nerves were positive for protein gene product 9.5, a nerve-specific marker commonly used to identify perivascular nerves.

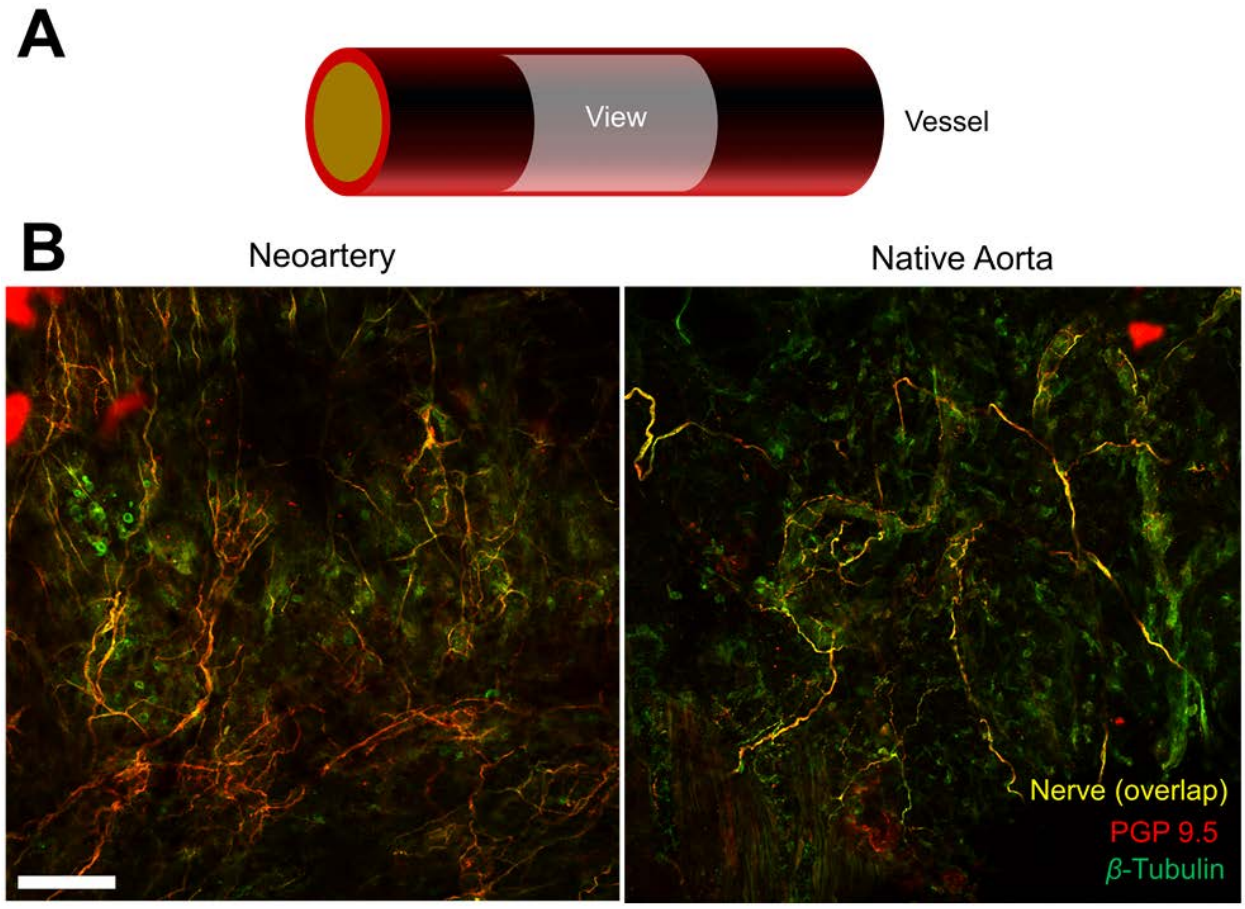

Figure 14. Perivascular nerves innervate neoarteries.
A. Schematic of *En Face* imaging of the adventitial surface of neoarteries. Neoarteries were cut open, immunostained for protein gene product 9.5 (PGP 9.5) and β-Tubulin, and imaged as whole mounts using confocal microscopy with z-stack flattening. **B.** Perivascular nerves cover the adventitial surface of neoarteries with similar morphology to those in native aortas. Nerves appear yellow from the overlap of nerve-specific marker PGP 9.5 and nerve non-specific marker β-Tubulin, which stains nerves brightly but is also expressed ubiquitously. The co-staining technique was used to reduce effects of nonspecific staining which are amplified in whole mount imaging. Scale bar 100 μm. Image from [135].

2.3.4 Neoartery extracellular matrix composition and mechanical properties

Proper matrix composition and structure is crucial for the long-term mechanical stability of arteries. Excitingly, we found that regenerated arteries contain the same quantity of cross-linked elastin as found in native arteries (P = 0.80; **Figure 15 A**). Furthermore, neoarteries contain

fibrillin-1, a crucial component of functional elastic fibers (**Figure 15 B**). However, elastin and fibrillin-1 are less uniformly distributed in the media-like layer of neoarteries than in native aortas. Regenerated arteries contain collagens III and I as well, both found in native aortas, but their organization also differs from native aortas (**Figure 16**)**.** These differences in matrix organization may be responsible for the apparent reduced dynamic mechanical compliance of neoarteries compared with native aortas (**Figure 16 C**). Although the difference was not statistically significant at the limited sample size (n = 4), the data appears to be trending toward significance.

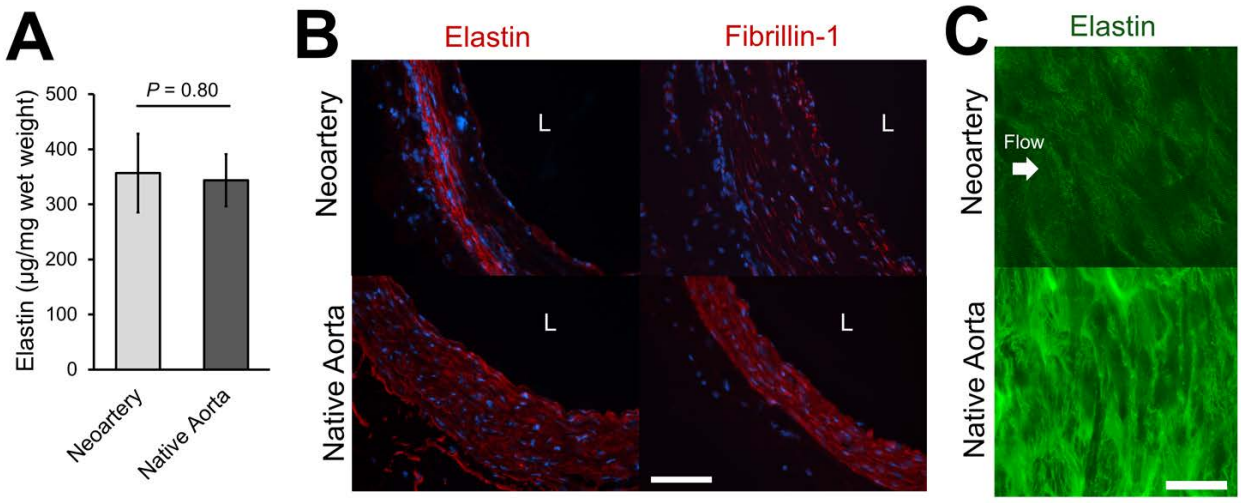

Figure 15. Elastin content and organization in neoarteries.
A. Elastin quantification using a Fastin Elastin assay showed that neoarteries contain the same amount of cross-linked elastin per tissue wet weight as native aortas. **B.** Transverse immunostained cross-sections show that neoarteries contain both elastin and fibrillin-1, though the distribution differs from that of native arteries. L indicates vessel lumen. Scale bar 100 µm **C.** *En Face* view of the middle layer of the neoartery wall shows elastin autofluorescence (false-colored as green). Elastin is aligned perpendicular to the direction of blood flow (arrow), similar to native arteries Scale bar 25 µm. Detailed depiction of *en face* view shown in **Figure 7.** Transverse immunostained cross-sections of neoarteries show the distribution of collagen III and collagen I throughout the neoartery wall. Neoartery collagen III appears ubiquitously distributed, whereas collagen III localizes to vascular media in native arteries. Collagen I is less bright in neoartery adventitia compared with adventitia in native aortas. L indicates vessel lumen. Scale bar 100 µm. Image from [135].

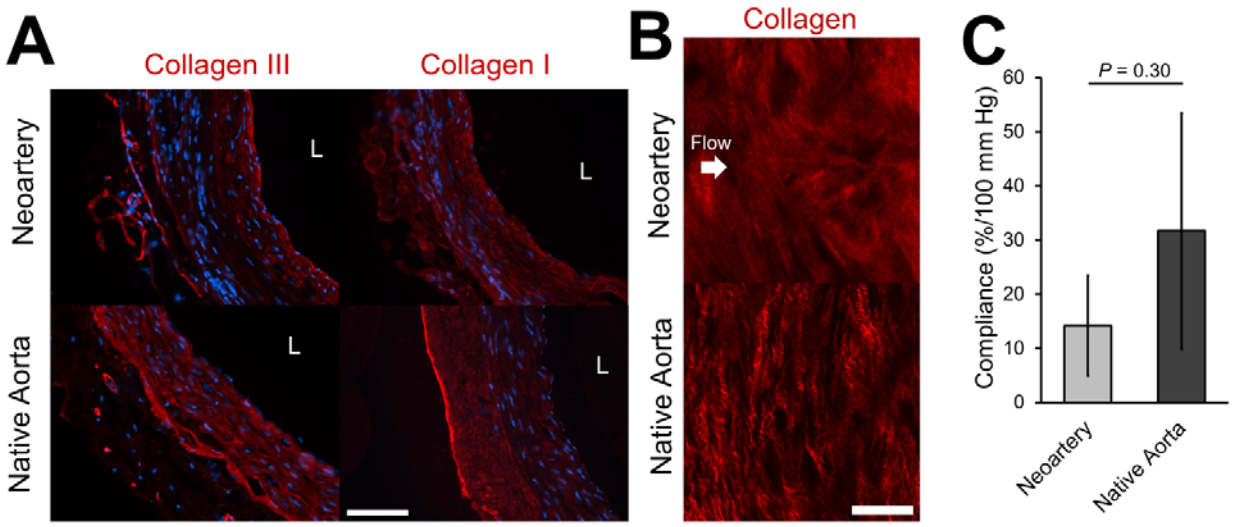

Figure 16. Collagen content and mechanical properties of neoarteries.
A. Transverse immunostained cross-sections of neoarteries show the distribution of collagen III and collagen I throughout the neoartery wall. Neoartery collagen III appears ubiquitously distributed, whereas collagen III localizes to vascular media in native arteries. Collagen I is less bright in neoartery adventitia compared with adventitia in native aortas. L indicates vessel lumen. Scale bar 100 µm. **B**. *En Face* view of the middle layer of the neoartery wall shows collagen autofluorescence (false-colored as red). Collagen in neoarteries shows some alignment perpendicular to the direction of blood flow (arrow), though it is less aligned and less crimped than collagen from native aortas. Scale bar 25 µm. Detailed depiction of *en face* view shown in **Figure 7**. **C**. *In vivo* dynamic mechanical compliance of neoarteries and native aortas. Neoarteries appear less compliant than native aortas, but the difference was not statistically significant in this limited data set (n = 4). Compliance was measured *in vivo* using ultrasound to record neoartery inner diameter and a manometer implanted in the aorta to record pressure. Compliance was taken as % change in diameter normalized to the difference between systolic and diastolic pressure. Image from [135].

2.3.5 *En face* comparison of elastin and collagen architecture

Elastin in neoarteries was arranged as a fine fibrous network, in contrast to the fenestrated lamellae seen in native aortas (**Figure 17 A, B**). Near the abluminal surface, elastin is largely absent in neoarteries, similar to native adventitial matrix (**Figure 17C**). Throughout the majority of the neoartery wall, collagen was aligned in the circumferential direction similar to native medial collagen (**Figure 18**). However, regenerated collagen lacked the crimped fibril morphology seen in native aortas and showed weaker fiber alignment. Interestingly, the axis of

collagen alignment changed near the luminal surface in some regions of neoarteries (**Figure 18,** *region 2*). Collagen near the albumen is crimped resembling native adventitial collagen, but crimp is still less than in native arteries, and neoartery collagen is aligned more strongly than that of the native adventitia (**Figure 18,** *right*).

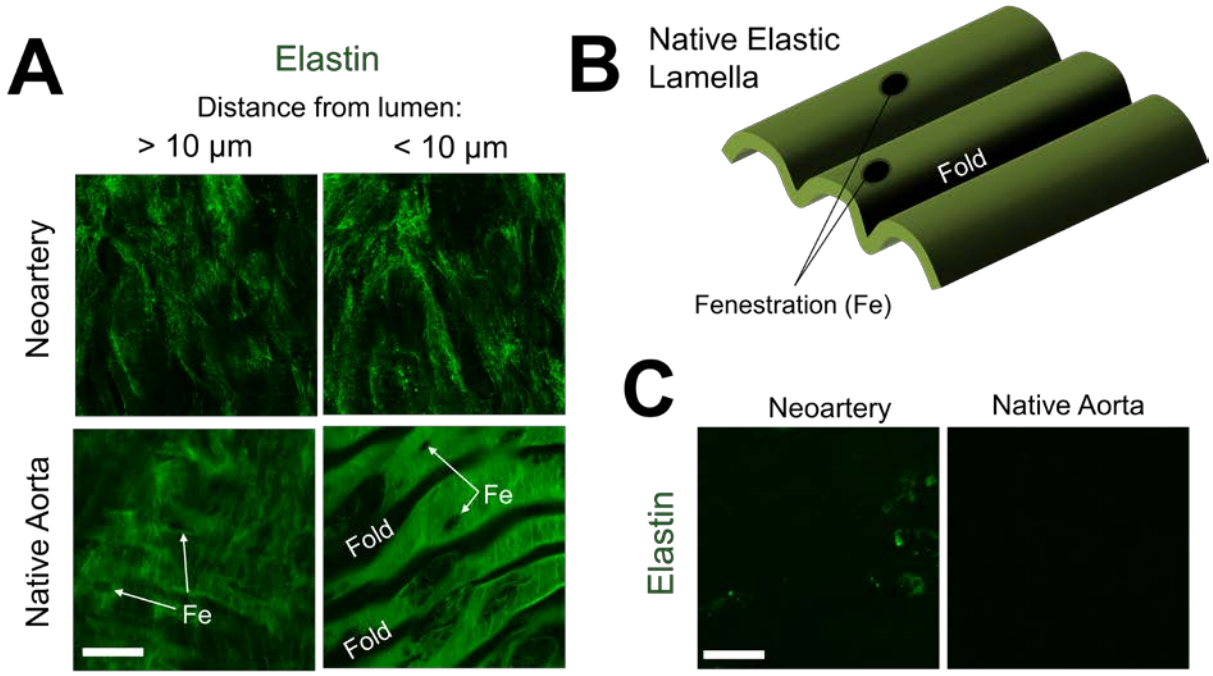

Figure 17. Elastin architecture in neoarteries and native aortas.
Detailed depiction of *en face* view shown in **Figure 7.** Scale bars 25 µm. **A.** Elastin architecture within the neoartery wall, imaged > 10 µm from the luminal surface (left), or within 10 µm of the lumen (right). Elastin is arranged as a fibrous network in neoarteries, in contrast to the fenestrated lamellae seen in native aortas. "Fe" indicates fenestrations in elastic lamellae in native aortas. "Fold" notes where the lamellae drop below the viewing plane. **B**. Schematic of the elastic lamella of native arteries. **C.** Elastin architecture near the abluminal surface of neoarteries. Neoarteries contain little elastin near the abluminal surface, similar to native aortas. Image from [135].

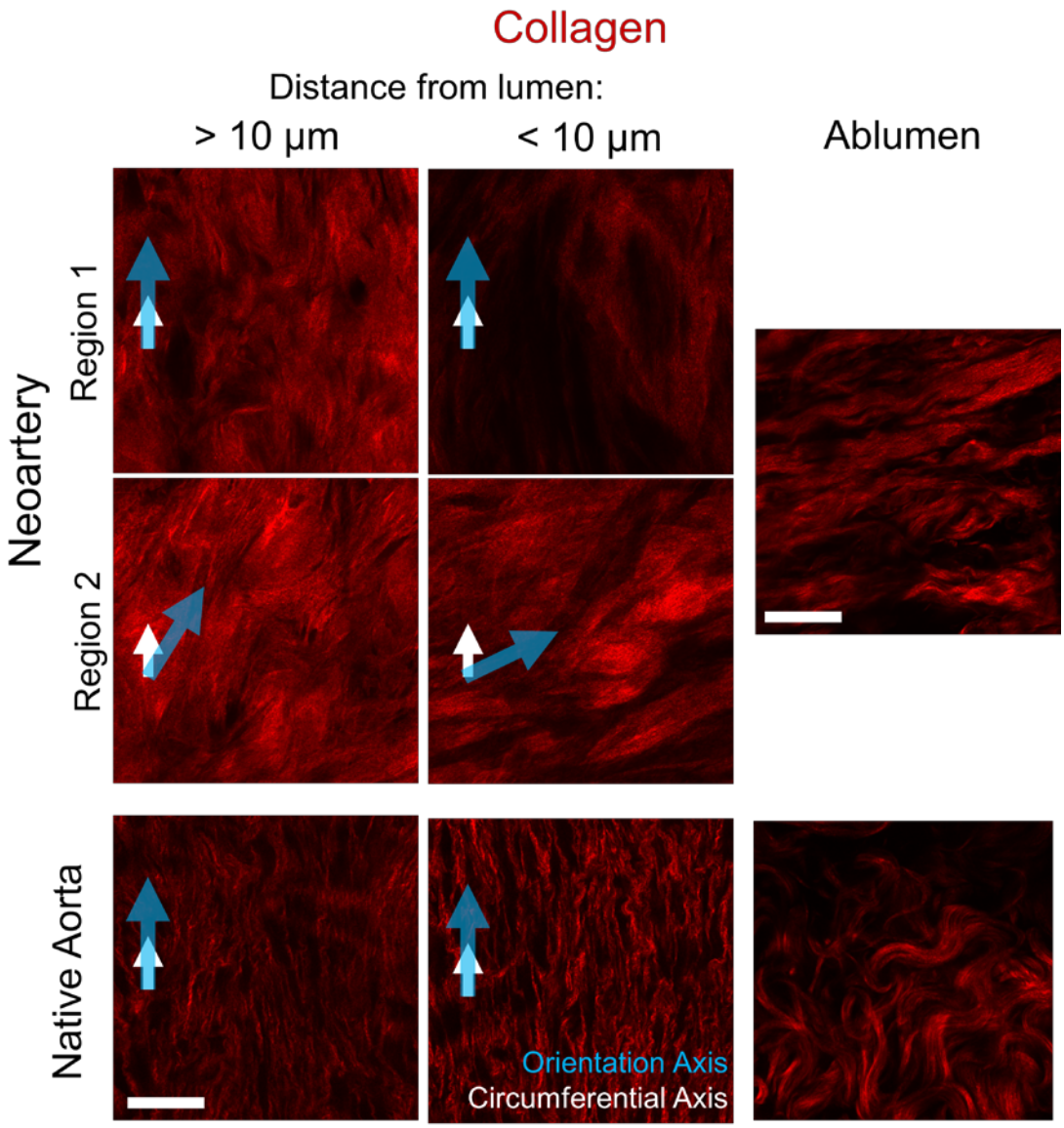

Figure 18. Collagen architecture in neoarteries and native aortas.
Detailed depiction of *en face* view shown in **Figure 7.** Scale bars 25 µm. Collagen architecture within the neoartery wall, viewed from the luminal side. Collagen is less aligned and less crimped than collagen seen in native aortas. Two regions from the same vessel segment (Region 1 and Region 2) are shown to demonstrate variation in collagen architecture within the same neoartery. Regions 1 and 2 represent different circumferential locations at the same longitudinal position near the middle of the regenerated vessel. In both regions, collagen at >10 mm from the luminal surface is oriented in the circumferential direction, as seen in the vascular media of native aortas. However, collagen at <10 mm from the lumen can either retain its orientation (Region 1) or substantially shift its orientation (Region 2), the latter contrasting with collagen near the intima of healthy native aortas. Arrows indicate the circumferential direction (white) and direction of orientation (blue). *Right:* Collagen and architecture near the abluminal surface of neoarteries is undulated resembling native adventitial collagen, but has higher undulation frequency than native arteries. Neoartery collagen alignment is stronger than that in native adventitia. Image from [135].

2.3.6 Neoartery response to physiologic vasodilators and vasoconstrictors

We used standard dual pin wire myography to determine whether neoarteries could respond to vasomotor signals. Neoarteries constricted in response to both the selective α1-adrenergic receptor agonist phenylephrine (PE) and the 5-hydroxytryptamine receptor activator serotonin (5-HT), though the magnitude of constriction was significantly less than that of native aortas (32.5 +/- 2.78 vs. 1616 +/- 836.6 mg and 42.2 +/- 25.8 vs. 3485 +/- 1161 mg for PE and 5-HT, respectively) (**Figure 19 A**). Regenerated vessels displayed vasodilation to the endothelial-specific activator acetylcholine (Ach) (**Figure 19 B**), suggesting the presence of signaling capability between endothelial cells and contractile smooth muscle. Percent relaxation in response to Ach was significantly larger than observed in native arteries. Neoarteries also dilated in response to endothelium-independent vasodilators including the andenylyl cyclase activator forskolin (**Figure 19 C**) and the direct soluble guanylyl cyclase (sGC) activator sodium nitroprusside (SNP) (**Figure 19 D**), though magnitude differed from native aortas. However, due to small sample size we cannot completely rule out the potential for passive relaxation to contribute to our observed results. Nonetheless, regenerated vessels showed no substantial dilation *in situ* at the time of explant, suggesting the absence of passive relaxation *in vivo*. Taken together these data demonstrate that the neoarteries are sensitive to several physiologically relevant activators and can translate these signals into vasoactivity, suggesting that some vascular cells within neoarteries express healthy phenotypes.

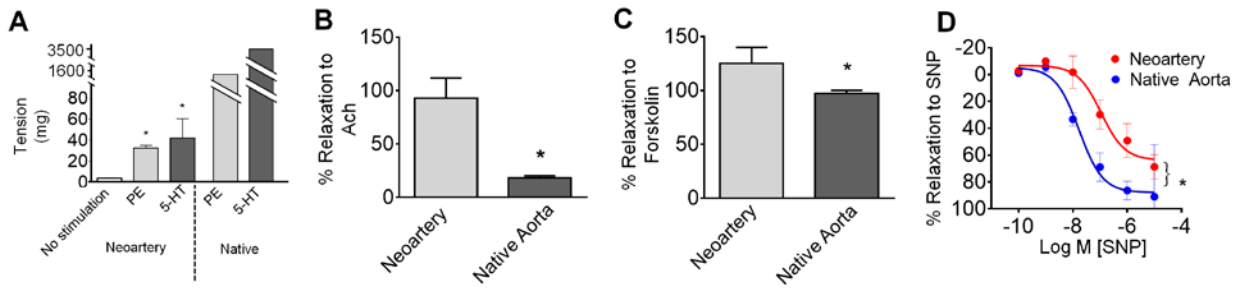

Figure 19. Response to vasodilators and vasoconstrictors.
Neoarteries display sensitivity to vasodilators and vasoconstrictors. **A.** Response to physiologic vasoconstrictors. Neoarteries were freshly harvested, mounted on a standard dual pin myograph, resting tension established, then assessed in their response to vasoconstrictors. Neoarteries demonstrated constriction in response to both the selective a1-adrenergic receptor agonist phenylephrine (PE) and the 5-hydroxytryptamine receptor activator serotonin (5-HT). However, the magnitude of constriction was substantially less than native arteries (32.5 ± 2.78 vs. 1616 ± 836.6 mg and 42.2 ± 25.8 vs. 3485 ± 1161 mg for PE and 5-HT, respectively). Results are the mean ± standard error of the mean of n = 12 rings from 3 animals per treatment group. *P > 0.05. **B**-**D**. Response to physiologic vasodilators. Neoarteries were mounted as described in A, preconstricted with serotonin, then assessed in their response to vasodilators. Results are the mean ± SEM of n = 12 rings from 3 animals per treatment group. *P < 0.05. **B.** Neoarteries relax in response to the endothelial-specific activator acetylcholine (Ach, 10 mM), suggesting signaling capability between endothelial cells and contractile smooth muscle. **C.** Neoarteries relax in response to the cAMP activator (NO independent) forskolin (10 mM). **D.** Neoarteries respond to the vascular smooth muscle cell specific activator sodium nitroprusside (SNP) in a dose-dependent manner.

2.4 DISCUSSION

An ideal vascular graft should conduct blood flow for the duration of a patient's lifetime. Consequently, long-term *in vivo* performance is an important indicator of a new vascular graft's clinical potential. A number of cell-free, bio-inductive vascular grafts have shown promising long-term results (> 3 months) in small animals. HYAFF-11 rat abdominal aorta grafts completely resorbed by 120 days and remodeled into artery-like tissues with elastic fibers [136]. Silk fibroin grafts showed good patency as rat abdominal aorta grafts, but some residual material and substantial inflammation were still present at 1 year post-implant [137]. PLA, PEUU, and PCL have also shown good long-term patency as rat abdominal aorta grafts, but graft resorption and cellular infiltration were limited due to slow material degradation [108, 111, 138].

Long-term assessments in large animals have shown variable results for acellular bio-inductive vascular grafts. Early work employing cell-free PGA graft yielded impressive long-term results in large animals. Bowald et al. showed that PGA-based grafts implanted as short aorta grafts in pigs remodeled into neoarteries with artery-like tissue architecture at up to 2 years post-implant [99]. Elastin was present in substantial quantity, although it was less organized than the native elastic lamina [92]. Greisler and colleagues investigated PGA-based grafts as well, and found that aorta grafts in rabbits formed similar neoarteries with moderate stability at up to 12 months, though elastin was largely absent, and dilation and neointimal hyperplasia occurred in some grafts. Slower-degrading polydioxanone grafts resorbed within 6 months and reduced rates of aneurysmal dilatation, but also reduced the rate of tissue ingrowth [96]. Fast-resorbing polyurethanes with physiologic compliance were investigated for their capacity to generate neoarteries while avoiding compliance mismatch. Initial testing of polyurethane grafts as pig aorta grafts yielded good patency and neoartery formation with organized elastic fibers at up to 6 months post-implant [97]. A similar polyurethane graft demonstrated high propensity for thrombosis, requiring aspirin to recover patency [98]. Canine carotid artery replacements made from small intestinal submucosa (SIS) showed similar patency to saphenous vein grafts at 1 year post-implant [104]. Composite grafts made from PGA, PLA, and collagen also performed well as canine carotid artery replacements for 1 year, but showed limited cell infiltration and graft resorption [107]. HYAFF-11 grafts in porcine carotid arteries showed complete graft resorption and remodeling into artery-like tissues with elastic fibers over the course of 5 months, though intimal hyperplasia and thrombosis was observed in some implants [139]. Decellularized tissue engineered blood vessels based on PGA showed good patency at 6 months as an arteriovenous shunt in baboons and at 1 year as a carotid artery replacement [53]. Devitalized tissue engineered

blood vessels made from fibrin and human dermal fibroblasts matched native artery compliance post-decellularization, and demonstrated complication-free remodeling into elastin-rich neoarteries in 24 weeks as ovine femoral interposition grafts [43].

Our design departs from the above by using a faster resorbing material which enables more rapid host remodeling. The vast majority of our SCPL PGS-PCL graft design is completely resorbed by 30 days post-implant, except for sparse PCL residues [118]. The advantage of this approach is that it minimizes the duration of host's response to foreign material, which may promote neointimal hyperplasia [128], calcification [138, 140], and tissue regression [138] in the late term. Indeed, we found that our grafts showed no sign of tissue regression, no significant narrowing from neointimal hyperplasia, and resisted calcification at 1 year post-implant. Grafts also resisted dilation and aneurysm, common failure modes for resorbable synthetic and collagen based vascular grafts. The only graft occlusion appeared to be thrombosis. The time of thrombosis is unknown, but it likely occurred during or shortly after surgery, as we did not use systemic heparinization during graft implantation. Systemic heparinization is standard practice for human surgery, and should substantially reduce the risk of thrombosis in SCPL PGS-PCL grafts.

In addition to displaying encouraging long-term patency, SCPL PGS-PCL grafts remodeled into neoarteries demonstrating close resemblance to native aortas at 1 year post-implant. This design regenerated nerves in perivascular tissue, and neoartery responsiveness to some vasomotor agents suggests these nerves may regulate vascular tone. Two other groups have also demonstrated vasomotor responsiveness in cell-free degradable vascular grafts [106, 141]. SCPL PGS-PCL grafts achieve full regeneration of the amount of mature elastin seen in native tissue. Coupled with the graft's stable inner diameter, this data demonstrates that neoarteries are

mechanically stable at late term despite complete or near-complete resorption of the original graft material.

Understanding the graft remodeling process will empower the research community to reproduce or improve this favorable long-term performance in future graft designs. While developing a comprehensive understanding is beyond the scope of this dissertation, the data collected to date allows for some speculation. The acute host response to the graft (0 to 48 h post-implant) can be speculated from findings in the wound healing, foreign body response, and angiogenesis literature. Acute response should begin with protein adsorption on the biomaterial and the deposition of a fibrin-rich a “provisional matrix” within the graft wall [142]. Platelets and a range of myeloid cells are likely included in the provisional matrix within graft pores. Other early-responding cells include neutrophils, mast cells, and lymphocytes [142, 143]. During the acute response, platelets, provisional matrix thrombolytic agents, and early responding inflammatory cells secrete a milieu of bio-active agents which recruit and activate multiple cell types. Two key multifunctional proteins released would include TGF-β and PDGF, which recruit macrophages [143] as well as smooth muscle cells [144] and myofibroblasts [145]. Myofibroblasts are contractile synthetic cells derived from multiple origins which contract tissue and secrete extracellular matrix [146]. Synthetic smooth muscle cells are a functionally similar cell population which are further described by a propensity to migrate and proliferate in blood vessels, but their distinction from myofibroblasts remains controversial [147]. These two cell types are the likely source of extracellular matrix including tropoelastin within the forming neoartery [34, 148]. These cells could originate from circulating fibrocytes [149], surrounding connective tissue, the adventitia of the adjacent vena cava, or the adjacent native aortic wall [129]. VEGF also likely plays a role in recruiting endothelial cells [150], and is secreted by M1

phenotype macrophages and hypoxic cells from the initial cell infiltrate [143]. In addition to their paracrine roles, phagocytic cells play a key role in degrading graft material by secreting acid, lipases, and reactive oxygen species [142]. Circulating stem and progenitor cells from the blood might be captured in the initial infiltrate, or may home to the implant site in response to chemotactic factors. These cells likely promote further cell recruitment, proliferation, and survival through paracrine signaling [151], and protect recruited cells from oxidative stress [152]. They may also differentiate into vascular cells [153], but the frequency of differentiation *in situ* and duration of their retention remains controversial [154].

The net result of these interrelated processes is a highly cellular proto-neoartery at 14 days post-implant (**Figure 5**). These proto-neoarteries are abundant in both alpha-SMA^{+} myofibroblasts and/or synthetic smooth muscle cells, as well as contractile smooth muscle cells positive for myosin heavy chain. The relative contribution of these cells from the blood, native adjacent arteries, and surrounding connective tissue is unknown in our system and beyond the scope of this dissertation. However, a study of a similar bio-inductive vascular graft implanted in the venous circulation suggests that in short interpositional grafts in rodent models, the principal source of neovessel cells is the adjacent native vessel [154]. Regardless of origin, the synthetic smooth muscle cells and myofibroblasts likely continue to produce matrix and remodel the matrix past the 3 month time point, as wall thickness and matrix organization differs at each time point up to 1 year.

Neoarteries at 14 days post-implant contain macrophages of both the classically activated M1 phenotype (CD68^{+} CD163^{-}) and alternatively activated M2 phenotype (CD68^{+} CD163^{+}) (**Figure 5**). Both phenotypes likely play constructive roles in the formation of the neoartery. M1 macrophages degrade graft material, recruit more macrophages by secreting monocyte

chemoattractant protein-1 (MCP-1) [142], and secrete VEGF [155] to recruit endothelial cells [156]. M2 macrophages secrete PDGF-BB [155] which recruits smooth muscle cells and mural cells [144, 157], as well as TGF-β [142] which promotes synthetic phenotypes in smooth muscle and myofibroblasts, thereby promoting matrix production [145]. However, both macrophage types also exhibit tissue destabilizing behaviors; M1 macrophages produce reactive oxygen species and release pro-inflammatory cytokines such as IL-1β, IL-6, and TNF-α [143], while the TGF-β released by M2 macrophages can promote vessel stenosis by promoting smooth muscle cell migration into the neointimal and subsequent proliferation [158]. M1 macrophages are generally considered to be more tissue-destabilizing, and much biocompatibility literature suggests that M1 macrophages should be quickly replaced with M2 macrophages to avoid a classical foreign body response [159]. However, recent work has challenged this theory. Hibino et al. found that bio-inductive venous grafts containing more M1 macrophages than M2 demonstrated reduced rates of stenosis [158]. Similarly, Sussman et al. found that implants which shift infiltrating macrophages toward an M1 phenotype showed less fibrosis and more vascularization [160]. Our findings corroborate the findings of the latter two groups, as the macrophage population in our grafts increased in the ratio of M1 to M2 phenotypes between 14 and 90 days, and we saw constructive neoartery formation rather than excessive matrix deposition and prolonged inflammation. Macrophage phenotype was not measured at 1 year post-implant, but such a measurement could further inform our understanding of the graft remodeling process. Taken together, these results suggest that in a remodeling bio-inductive vascular graft, M1 macrophages may be desirable at up to 90 days post-implant, and possibly beyond.

Despite substantial constructive remodeling, neoarteries still differ from native arteries even at 1 year post-implant. Neoartery collagen fibers are less crimped than those of native aortas in the unloaded state, suggesting they may provide a larger contribution to neoartery stiffness than collagen does in native aortas at physiologic pressures. Indeed, the compliance of neoarteries trends toward significantly less than that of native aortas, which is expected for a vessel whose collagen bears tensile loads at lower pressures. Encouragingly, neoarteries did not significantly dilate despite their engagement of collagen at physiologic pressures, suggesting that neoartery elastin bears sufficient load to prevent collagen creep.

Macrophages remain present in the adventitia at 1 year, likely due to trace amounts of residual PCL, as PCL nanofibers can persist longer than 18 months in vascular grafts [138]. Neoarteries showed no evidence of late-term failure, suggesting the macrophages are not adversely affecting graft performance. The role of these macrophages in tissue homeostasis depends on their phenotype, which was not examined at the 1 year time point. M1 and M2 macrophages facilitate tissue remodeling, and both phenotypes exhibit behaviors which could adversely affect neoartery homeostasis. Encouragingly, we saw no sign of either calcification or vessel narrowing from neointimal hyperplasia, suggesting that macrophage levels are likely below the threshold for complicating tissue homeostasis.

Neoarteries at 1 year post-implant still contain some α-SMA^{+} cells which are likely myofibroblasts or smooth muscle cells with synthetic phenotypes, neither of which are present in large numbers in healthy native arteries. The presence of both cell types indicates that neoarteries could continue to change in matrix content and cellular organization even at 1 year post-implant. However, it is also possible that the neoartery has reached homeostasis despite the presence of synthetic cells, as apoptosis and matrix degradation could match rates of proliferation and matrix

production. The neoartery wall appears to have shrunk in thickness between 3 months and 1 year post-implant, so it is unknown whether such homeostasis is reached at 1 year. Synthetic smooth muscle cells could cause vessel narrowing by migrating into the neointima and proliferating as seen in neointimal hyperplasia [147], but we saw no significant narrowing of the lumen at 1 year post-implant. Still, neointimal hyperplasia may remain a risk at even later time points.

The magnitude of the neoartery's response to vasoconstrictors is smaller than that of native arteries, which could be explained by neoarteries containing less contractile smooth muscle than native arteries. Indeed, some elongated cells in neoarteries do not express smooth muscle markers, and some MHC^{+} smooth muscle-like cells are not elongated in the circumferential direction. Endothelium-dependent vasodilation in response to acetylcholine was larger in neoarteries than in native aortas, which may also be explained by differences in cellular distribution; neoarteries likely contain a similar number of endothelial cells to native arteries, yet have less smooth muscle, suggesting an increased ratio of endothelial to smooth muscle cells compared to native aortas. Since acetylcholine-induced relaxation relies on endothelial cells to transduce the signal to smooth muscle cells, the relative strength of the relaxation signal should be proportional to that cell ratio, which is higher in neoarteries. While neoarteries do not precisely mimic native vasoresponsiveness, response to vasomotor agents serves minimal physiologic function in the aorta or any arteries for which vascular grafts are used as bypasses or replacements. Thus the reduced capacity of neoarteries to change their tone should not impair their long term performance as conduits for blood flow. Rather than assessing neoartery function, myography serves to assess the overall health of arterial cellular and structural components. In this context, the observed vasoresponsiveness of neoarteries suggests that they contain some

contractile smooth muscle cells and some endothelial cells capable of transducing vasomotor signals to the smooth muscle.

The disparity between neoarteries and native arteries is expected, as graft remodeling differs from natural artery development. In the embryo, primitive blood vessels remodel into arteries largely in response to changing hemodynamic forces over the course of development [161]. In contrast, these grafts are immediately exposed to adult hemodynamics. In this context, it is remarkable that cells in the neoarteries synthesized ECM proteins with composition resembling native aortas. While neoarteries differ from native arteries, these differences might not be clinically significant, as neoarteries matched native arteries mechanically and demonstrated good long-term performance *in vivo*.

We initially hypothesized that 1-year neoarteries would retain similar cell phenotypes and tissue architecture compared with neoarteries observed at 3 months [118]. The rationale was that neoarteries seemed to have reached homeostasis at that time, as material residues are largely absent at 3 months and the neotissue is elastin-rich and compliant. Surprisingly, the present study demonstrates that between 3 months and 1 year, neoarteries increase in elastin content, decrease in wall thickness, and achieve responsiveness to physiologic vasoconstrictors and vasodilators. These results indicate that in-host remodeling of neoarteries continues between 3 months and 1 year post-implant in healthy rodents. Encouragingly, we saw no evidence of aneurysmal dilatation or other late term pathologies, suggesting that short SCPL PGS-PCL grafts in a healthy host are mechanically and biologically stable by 3 months despite continued remodeling. The persistence of likely synthetic αSMA^{+} $MHC\text{-}11^{-}$ cells at 1 year post-implant suggests that neoarteries may continue to remodel even after 1 year, and thus should be observed at later time points to fully appreciate their long-term stability.

The remodeling process occurring in this chapter's SCPL PGS-PCL composite grafts compares favorably with that seen in many other bio-inductive grafts, but is not entirely unique to this design. Other fast-resorbing bio-inductive grafts have demonstrated the eventual formation of an elastin-rich neoartery [92, 93, 97, 98, 110, 114, 136, 139]. This is consistent with our central hypothesis, which postulates that rapid resorption of graft material is the key requirement for constructive neotissue formation rather than the excessive matrix deposition and prolonged inflammation seen in slow-resorbing or nondegradable vascular grafts. The rationale for this hypothesis is that rapid material clearance minimizes the duration of the inflammatory response, thereby reducing the duration of local promotion of dense matrix production, cell recruitment, and release of toxic macrophage-derived oxidants and pro-inflammatory cytokines.

Other characteristics of the SCPL PGS-PCL graft may have also modulated the host response, but likely to a lesser extent. The close mechanical matching between PGS and native arteries likely promoted elastin production as has been previously demonstrated *in vitro* [121], but elastin-rich neoarteries can still be formed in stiffer bio-inductive grafts made from fast-resorbing poly(glycolic acid) [92, 93] and poly(lactic acids) [110]. Favorable biocompatibility of PGS degradation products might also promote constructive neotissue formation, as PGS degradation produces a less acidic local environment than poly(glycolic acid) and poly(lactic acid)-based materials [162]; but again, neoarteries can still form from such polymers. The distribution of proteins adsorbed to the graft upon implantation is undoubtedly important in modulating the initial host response, but it was not investigated in this study.

The importance of pore size in bio-inductive vascular grafts remains controversial. While some reports identify pore size as critical determinant of neotissue formation and inflammation [110, 160, 163], others have achieved elastin-rich neoartery formation using completely

nonporous but fast-resorbing implants [113, 114, 139]. The role of pore size in a PGS-based bio-inductive vascular graft is unknown, but Chapter 4 provides some insight, as the graft design used in that investigation has substantially smaller pores than SCPL PGS-PCL grafts.

2.5 LIMITATIONS AND FUTURE WORK

Future work will address this study's limitations. Without cell seeding, it may be challenging for bio-inductive grafts to endothelialize in humans. The rat model we used does not test graft endothelialization to a clinical standard, as rats have superior endothelialization capacity to large animals and humans [129, 164]. Large animal studies will provide better indication of this design's clinical potential. The host must replace the graft with artery-like tissue quickly enough to prevent dilation, but many patients have reduced healing potential due to old age and disease. Localized delivery of bioactive reagents may be necessary to accelerate both endothelialization and graft remodeling to prevent graft failure. A thicker slow-resorbing sheath could also protect from mechanical failure, but may promote neointimal hyperplasia by increasing compliance mismatch and generating chronic inflammation. Conversely, macrophages persisting in the neoartery at 1 year post-implant might be avoided if the graft sheath was made from a material that resorbs faster than PCL, thereby reducing the sheath's residence time *in vivo*. Such modification would come at an increased risk for mechanical failure if patients cannot generate neotissue quickly enough to bear load. Quantifying total collagen content and staining for additional collagen types and subtypes could improve our understanding of neoartery health and mechanical stability. Further study is needed to determine whether passive relaxation contributed to vasodilation observed in neoarteries during myography.

Mechanisms of graft remodeling need to be studied to inform strategies to further accelerate graft remodeling. The contribution of myeloid cells could be determined by implanting grafts in chimeric rodents whose marrow cells express green fluorescent protein (GFP) or other reporters. The contribution of cells from the adjacent aorta could be tested by anastomosing to the graft an aorta segment from a male syngeneic donor, and then implanting the composite into a female animal. This model enables infiltrating cells from the donor vessel to be tracked using fluorescence in situ hybridization (FISH) for the Y chromosome [154]. Monitoring the phenotype of these tracked cells will shed substantial light on the remodeling process. Assessing cell phenotypes during the acute periods of graft remodeling (e.g. the first few days) will be necessary to characterize the initial cellular infiltrate, which likely plays a major role in dictating the ultimate fate of the neoartery. Conversely, further characterizing cells at late term can inform speculations on neoartery long-term stability. Staining for markers of proliferation (Ki-67) and apoptosis (Caspase 3) would reveal what cell turnover occurs at 1 year post-implant.

Local protein delivery could be a powerful tool with which to accelerate and improve graft remodeling. Our laboratory has previously developed a novel delivery system which can locally releases a range of heparin-binding proteins [165]. Localized release of PDGF-BB could accelerate the recruitment of matrix-producing smooth muscle cells and myofibroblasts to the bio-inductive graft [144, 157], and TGF-β could further promote matrix production including tropoelastin [145]. Local release of VEGF [156] or FGF-2 [166, 167] could accelerate endothelial cell recruitment for lining the graft lumen or forming vaso vasorum. Local delivery of monocyte chemoattractant protein 1 (MCP-1) could enhance early recruitment of macrophages, which has been previously shown to accelerate neotissue formation in bio-

inductive grafts in the venous circulation [69]. Releasing SDF-1α from grafts could recruit circulating mesenchymal stem/progenitor cells from the blood, which may promote neotissue formation via paracrine effects [151], oxidant scavenging [152], and differentiation into vascular cells [153]. Our laboratory recently demonstrated that modifying SCPL PGS grafts to release SDF-1α enhances their recruitment of mesenchymal progenitor cells from a flow loop *in vitro* [168].

2.6 CONCLUSIONS

This study demonstrates that a fast-resorbing, cell-free bio-inductive vascular graft can remodel *in situ* into tissues with favorable long-term stability and likeness to healthy arteries. It also shows that a neoartery can sustainably bear physiologic loading conditions despite continued constructive remodeling for months after graft material is resorbed. Taken together, these results suggest that this design is a promising strategy for improving the performance of vascular grafts used in small arteries. Additionally, fast-remodeling elastic implants may be applicable to other regenerative applications, including wound dressings and soft tissue repair.

3.0 IMPROVING TRANSLATIONAL POTENTIAL IN BIO-INDUCTIVE GRAFTS

Favorable long-term performance is a key requirement for a bio-inductive vascular graft to have translational potential, but it is not the sole requirement. Surgical handling, fabrication yield, and manufacturing feasibility are also required for potential clinical use. In chapter 3, we report our progress on improving these qualities in our bio-inductive graft design.

3.1 INTRODUCTION

A new technology must satisfy many criteria to reach the clinic. Surgical handling must be excellent to minimize implantation-related complications and meet the usability requirements of clinicians. Fabrication must also be amenable to clinical translation. Manufacturing costs must be low to maintain the margins required for a sustainable medical product. The manufacturing process must also yield reproducible outcomes to ensure the level of quality required for regulatory approval. Low costs, fast production, and reproducible outcomes also benefit early stage academic research employing laboratory-scale fabrication methods. Time-consuming fabrication methods hamper research progress. Large variability in graft properties amplify the variability of *in vivo* results, which can increase the number of animals required to find significant trends. Thus for a bio-inductive vascular graft to translate, it must demonstrate

excellent surgical handling and be fabricated in manner that is fast, lo2 w-cost, reproducible, and amenable to large-scale manufacturing.

The SCPL PGS-PCL grafts described in Chapter 2 do not yet meet the requirements for translation. Many limitations in translational potential can be traced to the current fabrication technique used. The foam-like microporous structure of SCPL PGS is produced using a technique known as solvent casting particulate leaching (SCPL). In SCPL, a polymer or prepolymer solution is cast into a template of fused porogen particles. The polymer is cross-linked if necessary, then the porogen template is dissolved to leave interconnected pores in its place (**Figure 20**). At the time of our investigation, macroporous PGS scaffolds were limited to SCPL fabrication. Alternative methods such as thermally induced phase separation (TIPS) or 3D printing are impractical due to the low glass transition temperature of PGS prepolymer, which causes the polymer to flow and fibers fuse into a nonporous sheet [169].

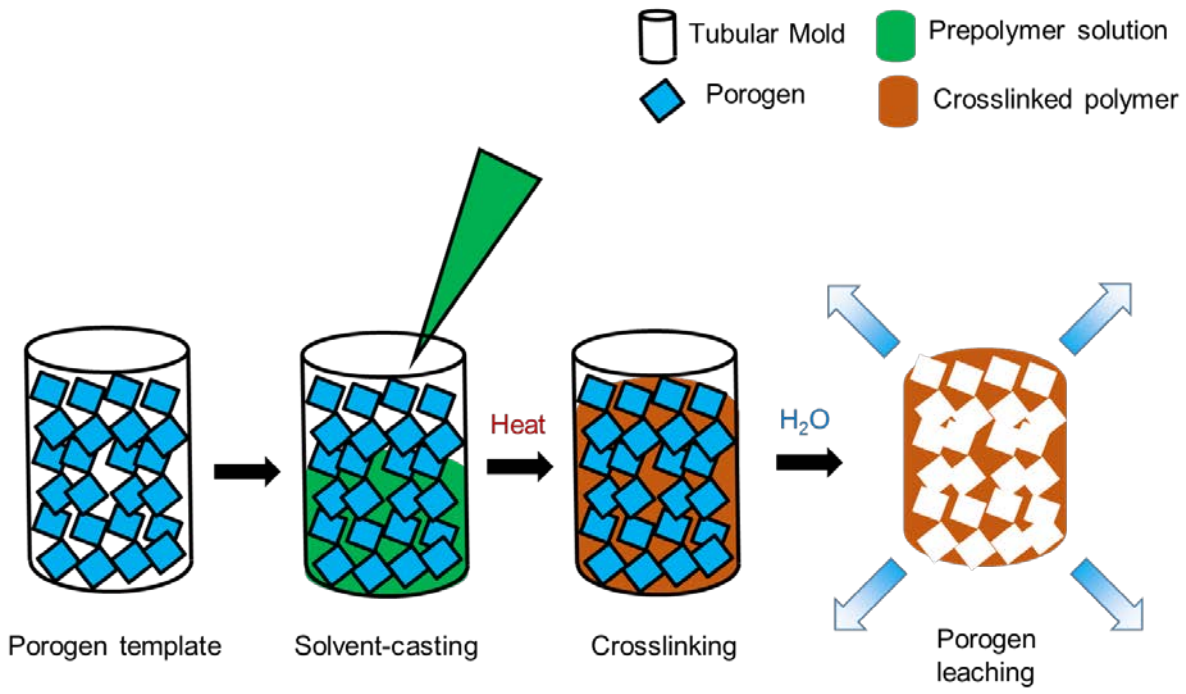

Figure 20. Solvent casting particulate leaching (SCPL)
Schematic depicting the SCPL process. From left to right: *Porogen template* is formed by packing water soluble particles (porogen) into a mold. Porogen fusion (not pictured) may be performed to attach adjacent porogens to one another. Fusion improves interconnectivity of pores realized at the end of the process. *Solvent casting* adds the prepolymer solution to the porogen template, filling the space between porogen particles. *Crosslinking* uses heat or other means to change the prepolymer into crosslinked polymer. *Porogen leaching* uses rinses in water to remove water soluble porogen, leaving pores in its place. The result is a porous, foam-like polymer scaffold (right).

Microporous vascular grafts based on SCPL PGS foams are impractical for clinical applications requiring suture anchoring and/or tensile loading conditions, as they are prone to failure by tearing. Consequently, successful implantation requires gentle surgical handling characteristic of reconstructive microsurgery, which is impractical to apply to human vascular surgery for two reasons: (1) vascular surgery imparts substantial tensile loads on grafts during implantation, with the magnitude of load varying greatly between cases; and (2) vascular surgeons typically lack microsurgery training. Even in a laboratory setting, SCPL PGS-PCL grafts are challenging to implant. In our experience, these grafts fail most frequently by tearing during suturing of the second anastomosis, which requires additional surgery time to excise and

replace the graft. The level of surgical training required to consistently implant SCPL PGS-PCL grafts is substantial. While our team member with microsurgical training could implant with 100% success after a brief surgery learning curve, our pediatric surgeon collaborator tore all of the SCPL PGS-PCL grafts during attempted implantation.

The process of SCPL fabrication is also impractical for clinical translation. There is no known manufacturing equivalent for SCPL fabrication. Developing a novel large-scale manufacturing process for SCPL would be challenging. Per batch of 5 usable SCPL PGS grafts, fabrication requires skilled manual labor for 9 out of 19 steps, totaling 14.5 hours of skilled manual labor and nearly 200 hours lead time. Low reproducibility is another limitation, as within-batch variability is unacceptably high for mass production. The yield of grafts acceptable for implant is as low as 25% for an experienced operator, necessitating large batch sizes and the corresponding increase in manual labor required. The most common defects are thin, tortuous gaps in the graft which have the same effect as a physical tear. These gaps occur due to caking of porogen particles during the formation of the porogen template. The incidence of gap defects is a function of scaffold thickness and length, making it nearly impossible to fabricate defect-free long and thick-walled grafts, which are required for large animal studies.

Electrospinning fabrication is an attractive alternative to SCPL. Electrospinning is a process which uses electrical forces to draw a polymer solution into mirco- or nano-scale fibers ([170] for review). Electrospinning has several notable advantages over SCPL: (1) electrospun polymer constructs are typically stronger than their SCPL counterparts [171]; (2) Electrospinning is a semi-automatable process, thereby reducing fabrication time and the duration of skilled labor required; and (3) Electrospinning is substantially more reproducible than SCPL, dramatically increasing yield and improving quality toward potentially meeting regulatory standards.

Electrospinning thermosets like PGS is challenging [172] for two reasons: (1) the insolubility of crosslinked PGS in organic solvents necessitates the use of the uncrosslinked PGS prepolymer (pPGS); and (2) pPGS has a glass transition temperature (Tg) below room temperature causing the polymer to flow and fibers fuse into a nonporous sheet. This fusion is exacerbated by the high temperature needed for thermal crosslinking [169]. Overcoming these challenges could enable PGS-based vascular grafts or other implants to realize the improvements in translational potential associated with electrospinning fabrication.

To improve the translational potential of fast-remodeling bio-inductive vascular grafts, we sought to develop a novel fabrication method which yields strong grafts in a simple, rapid, low-cost, and reproducible manner. We hypothesized that fabricating the PGS core from electrospun microfibers will improve surgical handling, fabrication yield, and manufacturing feasibility. To overcome the challenges of electrospinning PGS, we blended PGS prepolymer with a range of other polymers (termed "carrier polymers") to enable microfiber formation, then constructed novel microfibrous grafts and characterized their handling *in vitro* and *in vivo*. Herein we report novel patent-pending [173] fabrication strategies including retaining or removing the carrier polymer from cross-linked PGS fibers, as well as cross-linking with either heat or chemical cross-linkers. (**Figure 21**). We used data from pilot implantation studies to guide our experimental approach. Consequently, not every graft design was fully characterized. **Table 3** summarizes the development and characterization of each graft design tested. To distinguish these grafts from other designs described in this dissertation, we abbreviate them as "Espun PGS."

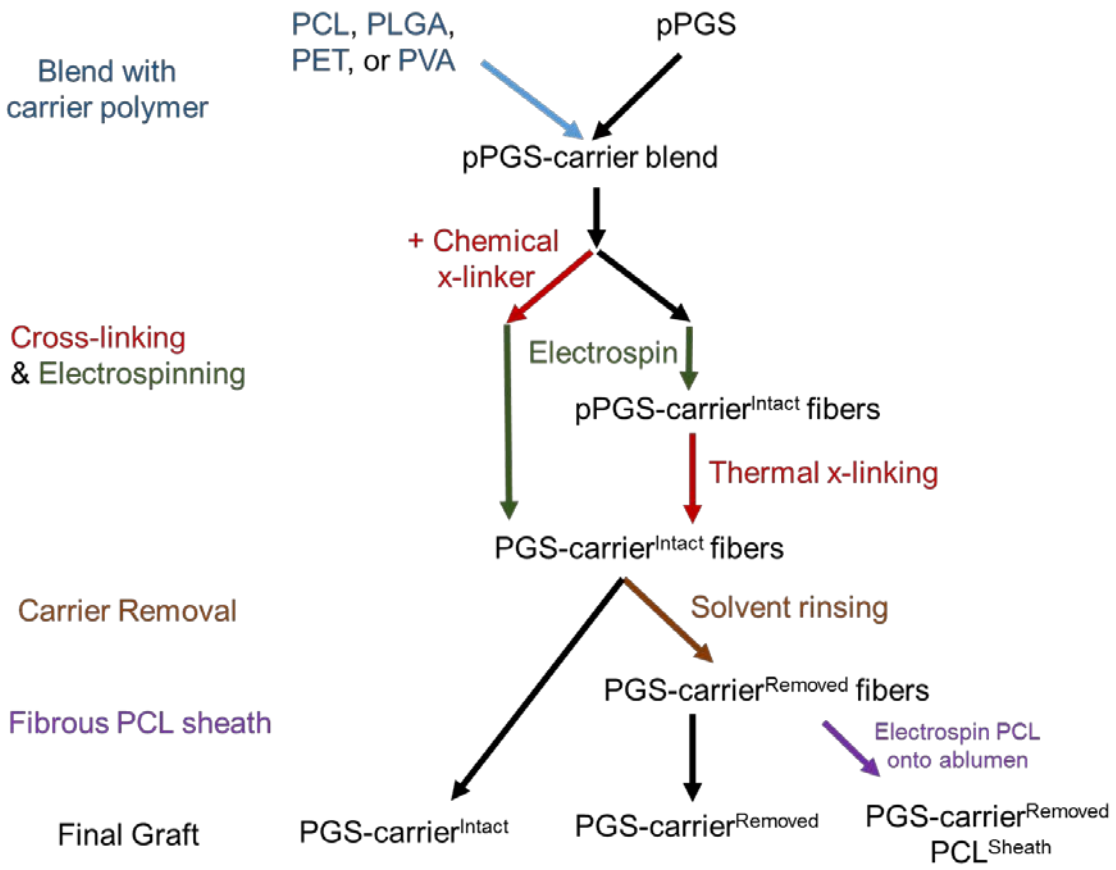

Figure 21. Fabrication strategies for Espun PGS-based implants
Schematic runs from top to bottom. *Blend with carrier polymer* – PGS prepolymer (pPGS) must be blended with a carrier polymer to be electrospun using standard equipment. We investigated polycaprolactone (PCL), poly(lactic-co-glycolic acid) (PLGA), poly(ethylene terepthelate) (PET), and poly(vinyl alcohol) PVA as carrier polymers. *Cross-linking and electrospinning* - pPGS must be cross-linked (x-linked) into PGS to attain the favorable biocompatibility associated with PGS. pPGS could be cross-linked prior to electrospinning using chemical cross-linker lysine triisocyanate (left path), or after electrospinning using thermal crosslinking (right path). Only carrier polymers with high melting points (PVA and PET) could maintain a microfibrous structure through thermal cross-linking. The result of this step is microfibers of cross-linked PGS blended with carrier polymer (PGS-carrier^{Intact}). *Carrier Removal* – We investigated removing the carrier polymer by rinsing with solvents which dissolve the carrier (orange). Water and ethanol washes were used for removing PVA. Tetrahydrofuran (THF) and HFIP were used to remove PLGA and PET, respectively. PGS does not dissolve in these solvents due to its cross-links. The result of this step is microfibers of cross-linked PGS in which the majority of carrier polymer is removed (PGS-carrier^{Removed}) *Fibrous PCL sheath* – We applied a fibrous PCL sheath onto select grafts by electrospinning directly onto the abluminal surface of salt-hardened, PGS-only grafts. Salt hardening (not pictured) is described in methods. In total, our fabrication methods produced microfibrous PGS-PCL composite grafts (right; PGS-carrier^{Removed} PCL^{Sheath}), microfibrous PGS grafts (middle; PGS-carrier^{Removed}), and microfibrous blended grafts of PGS and a carrier polymer (left; PGS-carrier^{Intact}).

Table 3. Development and characterization of Espun PGS graft designs.

Carrier Polymer	Microfiber Formation	Cross-linking	Carrier Removal	Apply PCL sheath	Mechanical Testing	Implantation
PCL	Y	N	N	N	N	N
PLGA	Y	Y	Y and N*	Y and N**	Y	Y
PET	Y	Y	Y	N	N	N
PVA	Y	Y	Y	Y	Y	Y

*****PGS-PLGA blended grafts were either purified of PLGA (Y), or retained PLGA (N).
**PGS-PLGA blended grafts were implanted without PCL sheaths. PGS-only grafts (purified of PLGA) were sheathed with PCL in some cases.

3.2 METHODS

3.2.1 Materials

PGS prepolymer (pPGS) was synthesized in house as described in **2.2.1.** Polycaprolactone (PCL) was obtained from Sigma-Aldrich, PCL (Mn 80 kDa; Aldrich, St. Louis, MO). Poly(lactic co-glycolic acid) PLGA was obtained from Lakeshore Biomaterials (L:G ratio 75:25, Mw 105 kDa; Birmingham, AL). Poly(ethylene terepthelate) (PET) was generously provided by the University of Toledo (Inherent viscosity = 0.80). Poly(vinyl alcohol) (PVA) was generously provided by Soarus LLC (Arlington Heights, IL). 1,1,1,3,3,3-hexafluoroisopropanol (HFIP) was purchased from Oakwood Products Inc. (West Columbia, SC). 2,2,2-trifluoroethanol (TFE) was purchased from Acros Organics (Belgium).

3.2.2 Electrospinning fabrication and cross-linking

Nomenclature. All electrospun microfibrous grafts are abbreviated as "Espun (p)PGS-Carrier^{Superscript} (PCL^{sheath})", where parentheses indicate that the abbreviation may be omitted. The "p" indicates prepolymer (if that is the final form of PGS); "carrier" indicates either PCL, PET, PLGA, or PVA; "superscript" describes whether the carrier polymer is left intact or has been removed; and "PCL^{Sheath}" describes whether or not the graft includes a microfibrous PCL sheath. For example, Espun PGS-PLGA^{Removed} PCL^{Sheath} would indicate a graft made from electrospun, cross-linked PGS fibers blended with PLGA, in which the PLGA was subsequently removed, and an electrospun PCL sheath was placed around the graft.

Espun pPGS-PCL^{Intact} sheets. To fabricate sheets of Espun pPGS-PCL^{Intact} microfibers, pPGS was mixed with PCL at a mass ratio of 2:1 pPGS:PCL, then dissolved in tetrahydrofuran (THF) at a total polymer concentration of 33% (w/v). The pPGS-PCL blend solution was infused into an electrospinning setup consisting of a 22 gauge syringe needle spinerette (cathode) and an aluminum plate coated in aluminum foil as the collector (anode). The solution was infused through the spinerette at 10 μL/h. Voltage sources were used to set the cathode and anode voltages to +12.5 kV and -12.5 kV, respectively. The distance between the spinerette and the collector was set to 26 cm.

Espun PGS-PLGA^{Intact} Grafts. To fabricate tubes of crosslinked PGS blended with PLGA fibers (Espun PGS-PLGA), pPGS was mixed with PLGA at a range of mass ratios, then dissolved in THF. 300 mM of Lithium Bromide (LiBr) was added to each blend to enhance solution conductivity. To optimize the mass ratio of pPGS:PLGA, mass ratios of 8:2, 7.5:2.5, and 7:3 were compared in their capacity to resist fusion between formed fibers. The optimized mass ratio was determined to be 7:3, and this ratio was used in all subsequent experiments. To

crosslink the pPGS into PGS, lysine triisocyanate (LTI) was added to the solution at 29 mol% with respect to PGS monomer. LTI was applied under nitrogen gas in a dry box immediately prior to electrospinning. The electrospinning solution was then infused into an electrospinning setup consisting of a 22 gauge syringe needle spinerette (cathode), and an aluminum plate (anode), and a mandrel placed between the two (collector) (**Figure 22**). Microfibers initially deposit onto the anode, then draw from the anode onto the rotating mandrel. The solution was infused through the spinerette at 12.5 μL/min. Voltage sources were used to set the cathode and anode voltages to +11 kV and -11 kV, respectively. The distance between the spinerette and the anode was set to 17.5 cm. The distance between the rotating mandrel and the aluminum plate was constantly adapted manually to maximize fiber collection efficiency. The rotating mandrel was comprised of water soluble glucose, formed by melting glucose in a custom mold, to enable release of microfibers by dissolution of the rod in deionized water. The mandrel outer diameter was typically 1.2 cm, and it was rotated at 350 RPM.

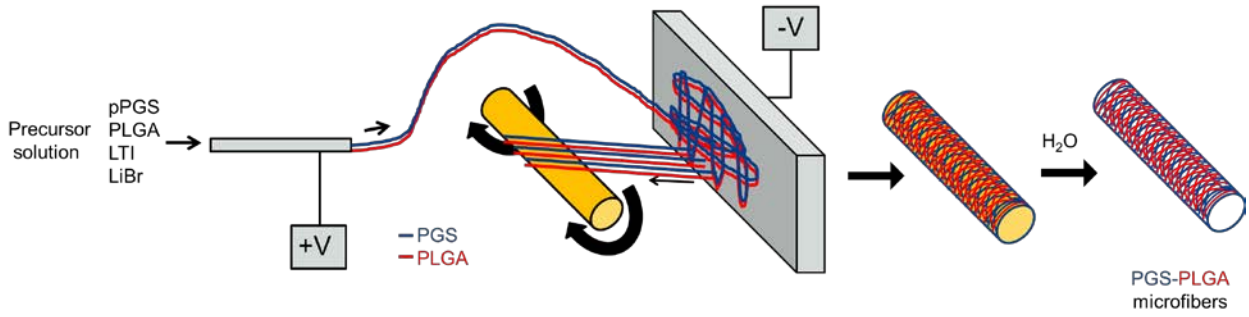

Figure 22. Fabricating Espun PGS-PLGA^{Intact} microfiber tubes
A precursor solution containing PGS prepolymer (pPGS), PLGA, chemical cross-linker lysine triisocyanate (LTI), and LiBr is infused into an electrospinning chamber. PGS-PLGA microfibers first travel from the needle cathode (+V) to deposit onto the aluminum plate anode (-V). Microfibers then draw from the aluminum plate anode onto a rotating glucose mandrel. Soaking in water (right) dissolves the mandrel to leave only a microfibrous tube made from a blend of PGS and PLGA (Espun PGS-PLGA^{Intact}) microfibers.

Espun PGS-PET^{Intact} sheets. To fabricate sheets of Espun pPGS-PET microfibers, pPGS was mixed with PET at a mass ratio of 2:1 pPGS:PET, then dissolved in 1,1,1,3,3,3-hexafluoroisopropanol (HFIP) at a total polymer concentration of 23% (w/v). The pPGS-PET blend solution was infused into an electrospinning setup consisting of a 22 gauge syringe needle spinerette (cathode), a stainless steel razor blade as the anode, and a rotating aluminum mandrel as the collector (Similar to **Figure 22**, except for mandrel composition and anode shape. Fibers sheets are isolated from the mandrel using a razor blade and pulling with forceps, rather than soaking in water). The solution was infused through the spinerette at 19 μL/min. Voltage sources were used to set the cathode and anode voltages to +7.5 kV and -7 kV, respectively. The distance between the spinerette and the collector was set to 27 cm. The distance between the rotating mandrel and the aluminum plate was 13.3 cm. The mandrel outer diameter was 2.54 cm, and it was rotated at 210 RPM. Sheets of pPGS-PET microfibers were thermally crosslinked to form PGS-PET microfibers by heating under vacuum in incremental steps to minimize the potential

for melting and fiber fusion; Fibers were initially heated at 70 °C, then the temperature was increased 10 °C every 7-12 hours, terminating after heating at 120 °C.

Espun PGS-PVA^{Intact} grafts. Initial blends using PVA to form Espun PGS-PVA sheets were developed by Eric Jeffries, a colleague in our laboratory. The following methods are published in [169] and described in patent application [173]. Briefly, A 16% w/v solution was prepared by mixing pPGS and PVA at 55:45 mass ratio and dissolving in HFIP overnight. This solution was pumped at 29 μL/min through a 22 gauge needle serving as the spinneret. Positive and negative 9 kV were applied to the spinneret and another needle positioned 60 cm from the spinneret, respectively. Electrospun fibers were collected on a rotating aluminum mandrel (100 rpm) placed between the needles at a 30 cm distance from the spinneret. No voltage was placed on the mandrel. Fibrous sheets were removed from the collector and crosslinked in a preheated vacuum oven under high temperature (120–150 °C) and vacuum (60 mmHg). We investigated crosslinking at 120 °C for 24 h (C1), 48 h (C2), 72 h (C3), and 96 h (C4). As a means to achieve a high degree of crosslinking with less processing time, we also explored 120 °C for 24 h followed by 150 °C for 24 h (C5).

Fabrication of tubes of Espun PGS-PVA fibers for rodent-sized grafts (**Figure 23**) is reported in this dissertation for the first time as follows: to form pPGS-PVA microfibers, the solution was pumped at 29 uL/min through a 22 gauge needle serving as the spinneret. Positive and negative 12 kV were applied to the spinneret and another needle serving as the anode, positioned 55 cm from the spinneret, respectively. pPGS-PVA microfibers initially deposited onto a plastic rod held at an elevated position between the spinneret and the anode and were subsequently drawn onto a hyaluronic acid-coated stainless steel mandrel (Inner diameter 0.78 mm) located 30 cm from the spinerette and 25 cm from the anode. The mandrel was rotated at

100 and 300 RPM, alternating every 100 uL of solution spun, in order to collect a combination of loosely-wound and tightly-wound fibers. No voltage or grounding was applied to either the rod or the mandrel. To crosslink the pPGS into PGS, fiber-coated mandrels were heated under vacuum (-60 mm Hg) at 120 °C for 24 h, then 150°C for an additional 24 h.

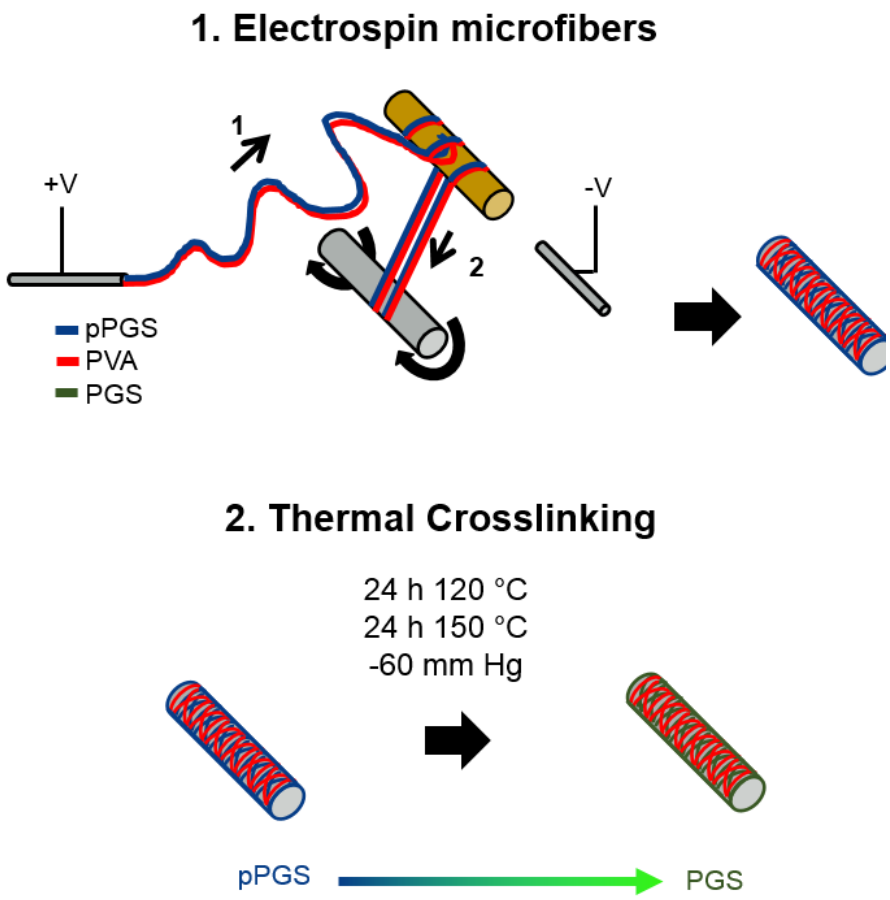

Figure 23. Fabricating Espun PGS-PVA^{Intact} microfiber tubes
1. Electrospinning microfibers. A polymer solution containing pPGS (blue) and PVA (red) is infused through a spinerette needle cathode. The solution forms a polymer jet which deposits onto a plastic rod (1), then is drawn onto a rotating stainless steel mandrel (2). The result is a mandrel coated with microfibers of a pPGS-PVA blend (right).
2. Thermal Crosslinking. Microfiber coated mandrels are thermally crosslinked to convert pPGS (blue) into into PGS (green). The result is a microfibrous tube of PGS blended with PVA (Espun PGS-PVA^{Intact}).

3.2.3 Scanning Electron Microscopy

Microfibers were prepared for scanning electron microscopy (SEM) as previously described [169]. Samples were adhered onto aluminum stubs with conductive carbon tape. Mounted samples were sputter coated with gold–palladium to a 3.5 nm thickness. Imaging was performed using a JSM-6330F SEM (JEOL, Tokyo, Japan) in collaboration with the Center for Biologic Imaging at the University of Pittsburgh.

3.2.4 Purification of Espun PGS grafts, and removal of carrier polymer

*Removal of impurities of Espun PGS-PLGA^{Intact} fiber*s. PGS-PLGA blends were washed in deionized water to quench unreacted LTI, leach LiBr, and dissolve the glucose mandrel. Water washing included three 1-hour washes with agitation, followed by a fourth wash overnight.

Removal of carrier polymers. Carrier polymer and impurities are purified by solvent washes, as shown in **Figure 24**. The solvent regimen depends on the carrier polymer.

Espun PGS-PLGA^{Removed} Grafts. To remove PLGA and unreacted pPGS and oligomers, blends were washed in THF. THF washing included four washes of at least 4-hours duration with agitation. We then employed a rinsing strategy with THF, ethanol, and deionized water to successively swell and shrink the grafts in an effort to free deeply trapped impurities from between polymer chains (**Figure 25**).

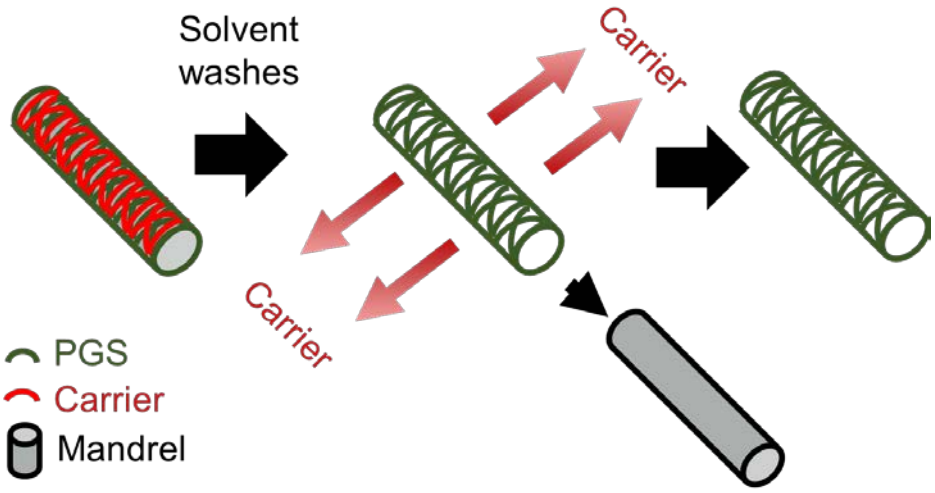

Figure 24. Removal of carrier and impurities in Espun PGS-Carrier^{Removed} grafts
Tubular constructs of cross-linked PGS (green) blended with carrier polymer (red), with or without a mandrel affixed to the lumen (gray rod), are purified of carrier and impurities using washes in solvents. Solvents dissolve the carrier, but do not dissolve PGS because it is cross-linked. In the case of PGS-PVA blends, the solvent washes are a series of water and ethanol rinses. Water rinsing also dissolves the hyaluronic acid coating on the mandrel, thereby delaminating the PGS tube from the mandrel and enabling facile removal. The same process applies for purifying microfibrous sheets of PGS-carrier blends (not pictured).

Espun PGS-PET^{Removed} Grafts. PGS-PET blends were washed in HFIP to dissolve PET and unreacted pPGS and oligomers. There were no chemical cross-linkers to quench or salts to remove. Microfiber blends were soaked in HFIP for three days, with fresh changes of HFIP at least once per day. HFIP was then removed by washing with a graded series of ethanol solutions dissolved in HFIP (25%, 50%, and 75% ethanol dissolved in HFIP, followed by 100% ethanol. Each wash was at least 1 hr) followed by a graded series of ethanol solutions dissolved in water (75%, 50%, and 25% ethanol dissolved in deionized water, followed by 100% deionized water. Each wash lasts at least 1 hour).

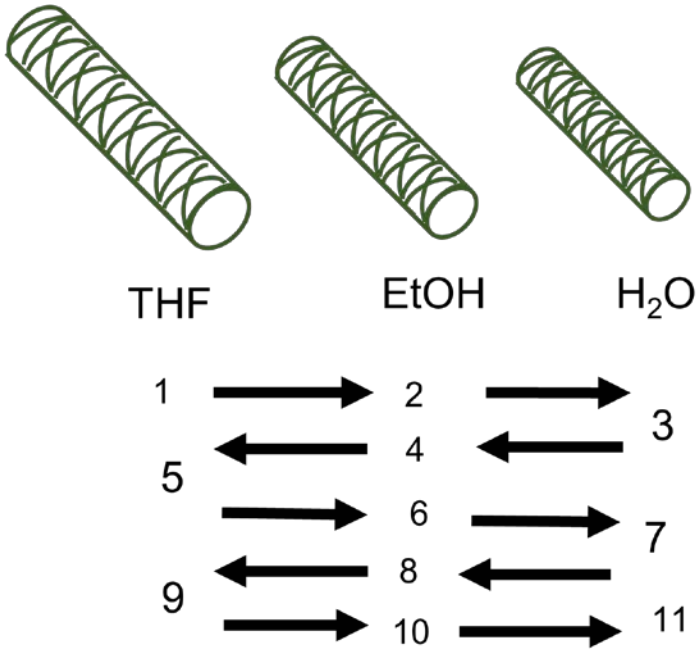

Figure 25. Swelling purification for Espun PGS-PLGA^{Removed} grafts
Espun PGS-PLGA^{Removed} microfibers (green) begin the process with the majority of PLGA already purified from four THF wash. The process pictured above shrinks and re-swells the blend in an effort to free deeply trapped impurities from between polymer chains. Blends begin at step 1 with the final wash of the initial THF washes. The tube is washed for 4 hours with agitation, then the THF is decanted and substituted with ethanol (EtOH) in step 2 for another 4 hours with agitation. The process continues with a transfer to deionized water (H_2O) in step 3. The process then reverses in order to swell the microfibers again. The process terminates in deionized water at step 11.

Espun PGS-PVA^{Removed} Grafts. Microfibrous PGS tubes were purified and isolated as follows: (1) To remove PVA, the fiber-coated mandrels were subsequently washed 3 changes of deionized water (1 h each), followed by a fourth wash overnight with agitation. The deionized water washes also dissolved the hyaluronic acid coating from the mandrels, enabling the microfiber tube to be easily isolated from the mandrel (**Figure 26**). (2) To remove unreacted monomers and oligomers, microfibrous PGS cores were washed in a graded series of ethanol solutions (25%, 50%, 70%, 100%) for 1 h each, then left in 100% ethanol overnight. The washes were then performed again in reverse order to remove residual ethanol, ending with overnight washing in DI H2O. Note that some residual PVA remains present within the PGS core following purification [169].

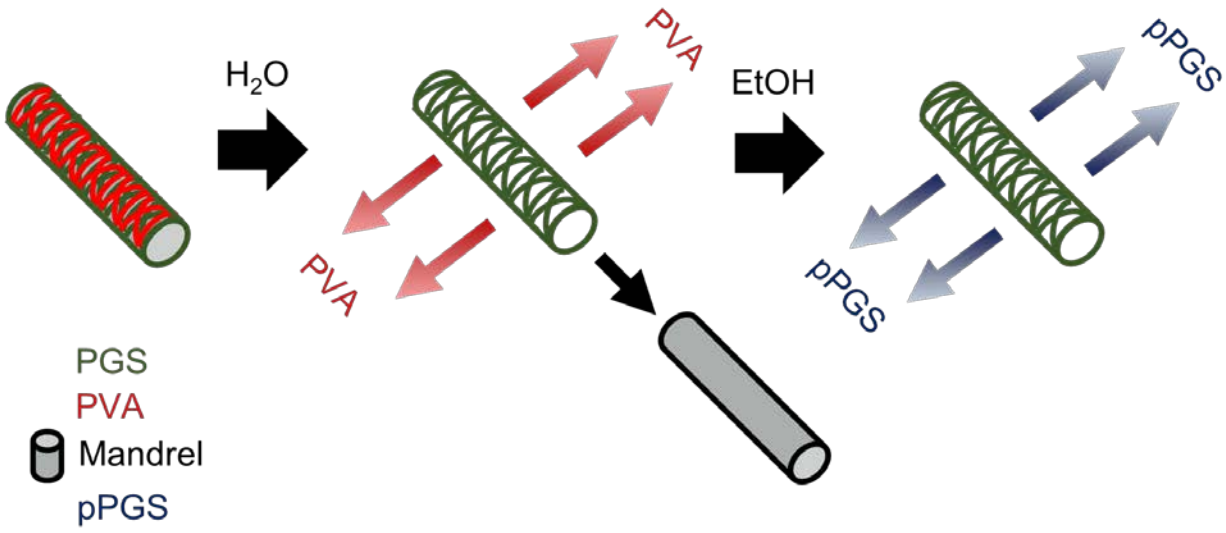

Figure 26. Removal of carrier and impurities for Espun PGS-PVA^{Removed} grafts
Tubular constructs of cross-linked PGS (green) blended with PVA (red) affixed to a hyaluronic acid-coated mandrel (gray rod) are purified of carrier and impurities using water (H_2O) and ethanol (EtOH) washes. Water washing removes PVA and dissolves the hyaluronic acid coating on the mandrel, thereby delaminating the PGS tube from the mandrel and enabling facile removal. Ethanol washing removes unreacted PGS prepolymer (pPGS; blue) and oligomers. Ethanol is subsequently removed using a graded series of ethanol washes of increasing water content (not pictured).

3.2.5 Application of fibrous PCL sheath

We applied PCL sheaths to PGS-only fiber tubes as previously described [118], with some modification (**Figure 27**). To improve the PGS core's resistance to compression during sheath application, PGS cores were hardened by freeze-drying in a 30% w/v NaCl solution using a lyophilizer (Labconco Freezone 4.5, Kansas City, MO), thereby filling pores with NaCl crystals (**Figure 28**). Hardened PGS tubes were mounted onto uncoated stainless steel mandrels (0.78 mm inner diameter) for PCL sheath application. The PCL electrospinning solution was prepared by dissolving PCL at 14 % w/v in a 5:1 solution of TFE:H_2O. To form PCL fibers, the PCL solution was pumped at 29 uL/min through a 22 gauge needle serving as the spinneret. Positive and negative 12 kV were applied to the spinneret and an aluminum plate serving as the anode, positioned 55 cm from the spinneret, respectively. PCL fibers initially collected onto the aluminum plate, and were subsequently drawn onto the hardened PGS core template held at 1 to 3 cm from the plate.

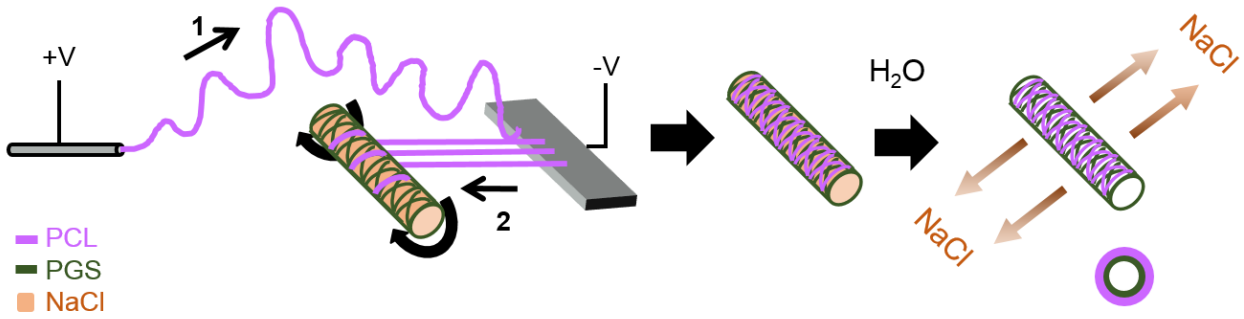

Figure 27. Application of PCL sheath to Espun PGS grafts
A PCL solution (pink) is infused through a spinerette needle cathode. The solution forms a polymer jet at the tip of the spinerette, which initially deposits onto an aluminum plate anode (1), then is drawn onto the rotating PGS tube (green), which is temporarily hardened with salt (NaCl; orange) (2). Electrospinning yields an NaCl-hardened PGS microfibrous tube sheathed with PCL fibers. NaCl is removed by rinsing in water. The result (right) is a composite graft consisting of an Espun PGS microfiber core (green) and a PCL fiber sheath (pink).

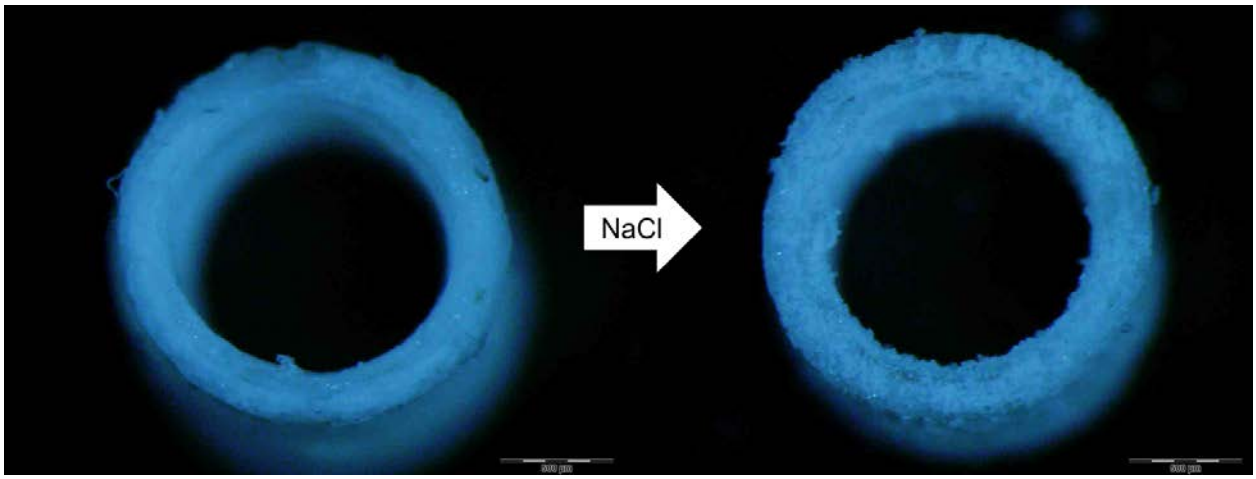

Figure 28. Salt-hardening of Espun PGS grafts
Espun PGS grafts are hardened with NaCl crystals in preparation for PCL sheath application. Dissecting microscope image of grafts before (left) and after (right) applying NaCl. NaCl was applied by soaking grafts in a 35% (w/v) NaCl solution, then freezing and lyophilizing to remove water. Scale bar 500 µm.

3.2.6 Porosity and pore size measurement

Porosity and pore size were measured for Espun PGS-PVA^{Removed} PCL^{sheath} grafts. Porosity of the PGS core was measured gravimetrically using equation (2):

$$\phi = 1 - \frac{\rho_{bulk}}{\rho_{par}} \quad (2)$$

where Φ represents porosity, ρ_{bulk} represents the bulk density of the portion of graft wall comprising PGS core, and ρ_{par} represents the density of a nonporous particle of PGS, taken from literature as 1.1 g cm^{-3} [174]. ρ_{bulk} was calculated by dividing the mass of the PGS core by the PGS core volume. PGS core mass and volume were calculated by finding the mass and volume of the graft wall (using a microbalance and dissecting microscope), then subtracting the estimated mass and volume of the PCL sheath.

Pore size and fiber diameter were measured from SEM images of graft cross-sections using Image J software (NIH, Bethesda, MD). To prepare graft cross-sections for SEM, grafts were hydrated by soaking in deionized water, then cut into ring-shaped sections using surgical microscissors. Graft rings were freeze-dried, then adhered onto aluminum stubs with conductive carbon tape before sputter coating with gold-palladium to a 3.5 nm thickness. Samples were imaged using a JSM-6330F SEM (JEOL, Tokyo, Japan). Pore size and fiber diameter measurements were sampled along a representative radial line drawn on 4 SEM fields per graft, then data was pooled between all measured grafts (n = 3). Pore size was estimated by treating each pore as an ellipse, calculating pore area from the conjugate diameters, then reporting the diameter of a circular pore with the same area.

3.2.7 *In vitro* degradation of PGS core

In vitro degradation was measured for Espun PGS-PVA^{Removed} grafts. Hydrolytic degradation of PGS cores was measured by mass loss *in vitro* under basic conditions. To produce 3 mm diameter PGS disks, microfibrous PGS cores were slit along the long axis, stretched flat, and then cut with a 3 mm diameter hole punch. For comparison, we also tested previously reported PGS foam cores made from SCPL PGS. Foam cores were fabricated as previously described [118], then formed into disks with the same hole punch.

For each disk, dry weight was recorded, then disks were placed in 1.5 mL Eppendorf tubes containing 1 mL of pH 11.75 buffer. Eppendorf tubes were incubated on a heated rocking plate (Thermal Rocker, ThermoFisher Scientific, Waltham, MA) set to 37 °C and set at rocking setting #1. Disks were retrieved at 12, 24, and 36 h. Retrieved disks were rinsed 3x with deionized water, then freeze-dried and weighed to determine final dry weight. The relative mass remaining was determined at each time point by dividing the final dry weight by the initial dry weight prior to incubation.

3.2.8 Mechanical Testing

Suture retention. Suture pull-out strength was measured in microfibrous grafts by uniaxial tensile testing in a MTS Insight (Eden Prairie, MN). For Espun PGS-PLGA^{Intact} microfiber grafts, 2 mm-long segments were clamped onto tensile grips with a 0.5 mm sized bite. A 7-0 prolene suture was run through the graft at 0.75 mm from the free end. The suture size was chosen to keep the method consistent with that used by other research groups in the field of vascular tissue engineering [38]. The free ends of the suture were clamped into another tensile grip. The second

grip then pulled the suture at a displacement rate of 0.2 mm/s. The force at which grafts yielded or failed was taken to be the suture pull-out strength. Espun microfiber grafts were tested against SCPL PGS-PCL composites used in Aim 1 (Graft dimensions listed in **Table 1**).

Espun PGS-PVA^{Removed} grafts, suture pull-out strength was measured as described in [169]. This test protocol normalizes suture retention strength to cross-sectional area and uses a larger suture than the method described above. We chose this testing regimen for consistency with that used for soft tissue repair applications [175]. Fully washed samples were cut into dog bone shaped test specimens using a customized punch with outer dimensions (28.75 mm (l) × 4.75 mm (w)) and a narrow region (8.25 mm (l) × 1.5 mm (w)). Sample thickness was measured by dial calipers. Samples were clamped onto tensile grips, then hydrated in deionized water immediately prior to suture retention testing. Suture retention strength was measured by inserting a 4-0 suture 2 mm from the edge of the long axis of 5 mm × 20 mm samples and strained to rupture. Suture retention strength was calculated as maximum load/(suture diameter × sample thickness) in N/mm^2. PGS-only sheets were tested against SCPL PGS sheets, both without compositing with PCL. These tests were designed, performed and interpreted by Eric Jeffries, a doctoral student and colleague in the laboratory.

Ring segment tensile testing. For Espun PGS-PLGA^{Intact} and PGS-PLGA^{Removed} grafts, uniaxial loading of ring-shaped segments was tested as previously described [118]. To obtain stress-strain curves, we cut grafts into 2 mm long segments. We fixed segments to two identical hooks connected to the load cell and the bottom plate of machine. To strain segments we applied uniaxial tensile force at 0.01 mm s^{-1}. For preconditioning, segments cycled between 10 and 40 % ring strain until yielding reproducible stress-strain curves. We then performed strain to failure

and calculated wall stress, circumferential strain, and elastic modulus as previously described [121, 122]. Microfiber grafts were tested against native rat aortas and SCPL PGS-PCL grafts.

We also performed longitudinal axis testing on Espun PGS-PLGA^{Intact} to compare long-axis tensile strength with SCPL PGS-PCL grafts. 5-mm long graft segments were clamped into tensile grips with a bite size of 1-2 mm and strained at 0.2 mm/s. The force at which grafts yielded or failed was taken as the long-axis tensile strength.

For Espun PGS-PVA^{Removed} sheets, uniaxial tensile loading was performed as described in [169]. Microfiber sheets were placed on tensile grips and then hydrated in diH2O immediately before stretching to failure at 25 mm/min. Multi-cycle testing from 10% to 100% strain for 100 cycles at 100 mm/min was performed on hydrated samples to evaluate elastic recovery. Microfibers were compared against SCPL PGS sheets and nonporous films of PGS.

3.2.9 Implantation

Graft sterilization and heparin adsorption. All grafts were sterilized by room temperature ethylene oxide (EtO) gas with at least 24 hours of additional aeration time. Grafts were washed in sterile saline overnight to quench any remaining EtO residues. To improve hemocompatibility, grafts in *Methods A-C* (see below) were soaked overnight in a heparin solution of 400 U/mL. Grafts in *Method D* were not soaked with heparin.

Implantation. The implantation technique evolved over the course of the study. The techniques used are summarized in **Table 4**, and described below.

Method A (grafts 1-15). Grafts were implanted without the use of systemic heparin as previously described [118]. Grafts were implanted as interpositional implantation in rat abdominal aorta as follows: Rats were induced with 5% isofluorane gas, then maintained

anesthetized at 1.5-3% isofluorane gas. Rats received pre-operative ketoprofen and ampicillin for analgesic and antibiotic, respectively. A midline abdominal incision exposed the abdominal aorta in rats anesthetized by isoflurane inhalation. To implant the graft we separated the aorta from the inferior vena cava, cross-clamped the infrarenal abdominal aorta, transected a 0-4 mm segment, and inserted the composite graft (5-10 mm in length) in the gap. End to end anastomosis connected grafts to the native aorta with interrupted 9-0 nylon suture. Animals received no postoperative anti-coagulation or anti-platelet treatment.

Method B (grafts 16-25). Grafts were implanted similarly to in method A, but with the use of systemic heparinization. Prior to aorta cross-clamping, rats received an intravenous injection of 50 IU/kg heparin in a tributary vein to the vena cava. Prior to the final anastamotic stitch, the proximal aorta was briefly unclamped to prime the graft with blood and flush air out of the graft. The proximal aorta was then re-clamped for the final anastamotic stitch. After anastomosis, the aorta was unclamped. Leaks at either anastomosis were repaired with additional interrupted suture, or by topical application of surgicel absorbable hemostat. Surgicel was removed prior to closure.

Method C (grafts 25-32). Grafts were implanted using systemic heparinization and further precautions to prevent thrombosis. After midline incision, the rat's abdominal organs were temporarily translocated onto sterile gauze which was periodically soaked in warm saline. After aorta exposure, heparinization, and cross-clamping as described in *method B*, the native aorta was transected between the clamps. The resulting aorta stumps were flushed with heparinized saline (saline containing a small amount of heparin solution) to prevent thrombus formation. Prior to the final anastamotic stitch, the graft was filled with heparinized saline using a syringe, thereby removing air from the graft lumen. After anastomosis, the aorta was

unclamped, and hemostasis was achieved as described in *method B*. Organs were translocated back into the abdomen prior to closure.

Method D (grafts 33-42) Implantations performed by Christopher Breuer's laboratory at the Research Institute of Nationwide Children's Hospital. These implants were performed without heparinization by operators with microsurgery training and extensive experience in the mouse infrarenal abdominal aorta model. Nine nanofiber PGS scaffolds were implanted as infrarenal aortic interposition grafts using standard aseptic microsurgical technique as previously described. The mice were administered an intraperitoneal injection of pre-anesthesia analgesic (ketoprofen, 10mg/kg), anesthetized with ketamine (100 mg/kg) and xylazine (10 mg/kg), and opened with a midline incision. The abdominal organs were eviscerated and a 3.0 mm portion of the infrarenal aorta was identified, isolated, crossclamped, and divided. Scaffolds were then implanted as interposition grafts using a running 10-0 nylon suture for the end-to-end proximal and distal anastomoses. All animals received routine postoperative care and were maintained for the duration of the study without any anti-coagulation or anti-platelet therapy. All animals received humane care in compliance with the National Institutes of Health (NIH) Guide for the Care and Use of Laboratory Animals. The Institutional Animal Care and Use Committee of The Research Institute at Nationwide Children's Hospital approved and monitored the use of animals and all animal procedures described in this study. 8-12 week old C57BL/6 female mice (n = 9) were purchased from Jackson Laboratories (Bar Harbor, ME, USA).

Table 4. Implantation methods used for pilot *in vivo* assessments

Implant no.	Implant Method	Thrombosis Incidence*	Systemic heparin	Flush stumps & prime grafts with heparinized saline	Graft Types	Surgeon experience	
						Microsurgery training?	Prior experience with model
1-15	A	High	N	N	Espun PGS-PLGA^{Intact} Espun PGS-PLGA^{Removed} PCL^{Sheath}	N	N
16-24	B	High	Y	N	Espun PGS-PLGA^{Intact} Espun PGS-PLGA^{Removed} Espun PGS-PLGA^{Removed} PCL^{Sheath}	N	N
25-32	C	Low-Moderate	Y	Y	Espun PGS-PLGA^{Intact} Espun PGS-PLGA^{Removed} PCL^{Sheath}	N	N
33-43	D	None	N	N	Espun PGS-PVA^{Removed} PCL^{Sheath}	Y	Y

* Estimated. For many grafts, thrombosis was not definitively confirmed, but strongly suspected

3.3 RESULTS

3.3.1 Microfiber formation and PGS cross-linking

PCL, PLGA, PET, and PVA carriers all yielded microfibers from electrospinning, although fiber quality varied with carrier polymer (**Figure 29**). Espun pPGS-PCL^{Intact} fibers were the most challenging to electrospin and produced the most fusion between fibers, and thus were not studied in future experiments. Espun pPGS-PVA^{Intact} fibers showed the least fiber fusion, but fiber quality after thermal crosslinking depended on the time and temperature used. Espun PGS-PLGA^{Intact} fibers and Espun pPGS-PET fibers also demonstrated limited fiber fusion after thermal cross-linking. The amount of PGS in Espun PGS-PLGA$^{Intact\ or\ Removed}$ blends was

maximized to reduce the difference in graft composition from the original SCPL PGS design, as some Espun PGS-PLGA^{Intact} grafts were to be implanted without removing PLGA. The maximum pPGS:PLGA ratio that yielded minimal fiber fusion was 7:3 (**Figure 30**).

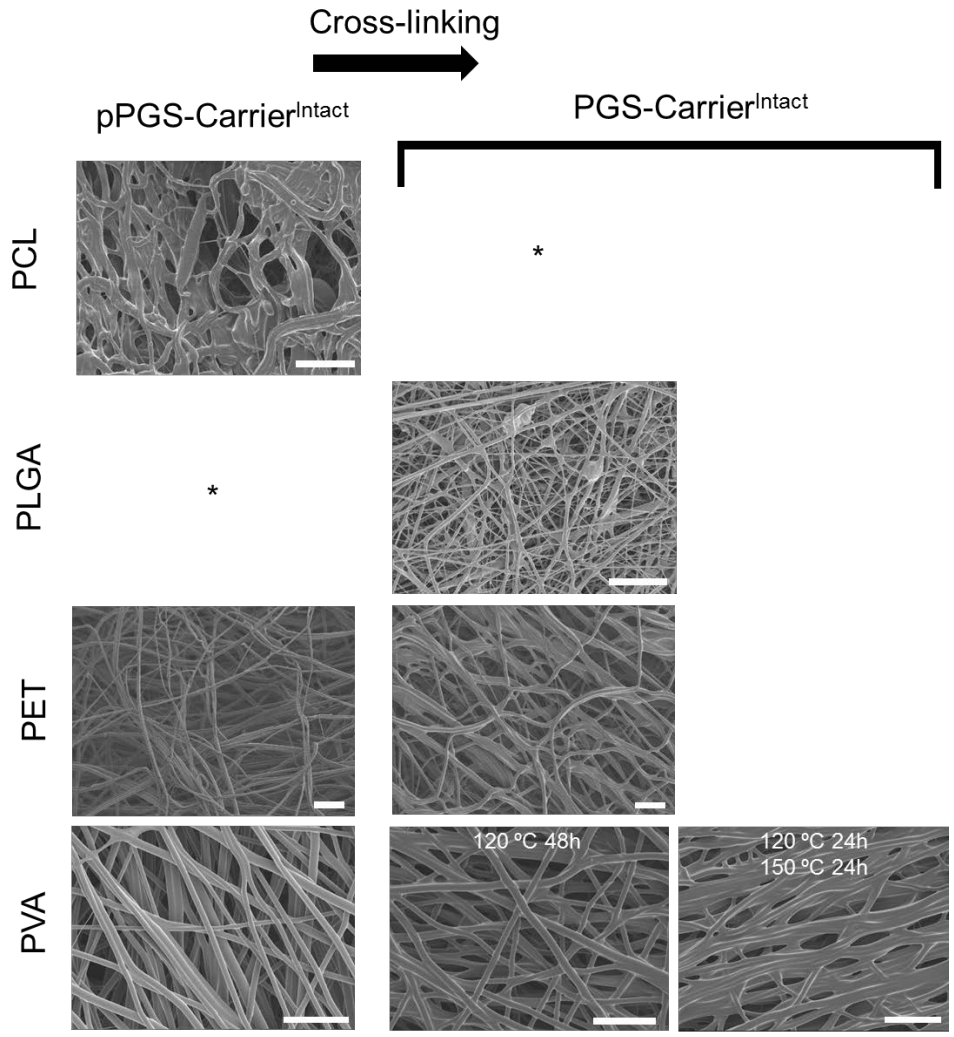

Figure 29. Microfiber formation and PGS crosslinking in Espun pPGS and PGS grafts
SEM of microfiber blends before and after cross-linking. All scale bars 25 µm (note not all magnifications are the same). For PGS-PVA blends, the degree of fiber fusion depends on thermal cross-linking conditions (overlaid white text). * indicates not measured. pPGS-PCL^{Intact} blends were not combined with chemical crosslinker, as further study of the blend was de-incentivized by its low fabrication efficiency and poor fiber quality. For PGS-PLGA^{Intact} blends, fibers already cross-link during and after electrospinning, as the blend already contains chemical cross-linker LTI. Images for PGS-PVA^{Intact} blends collected by Eric Jeffries and adapted from [169].

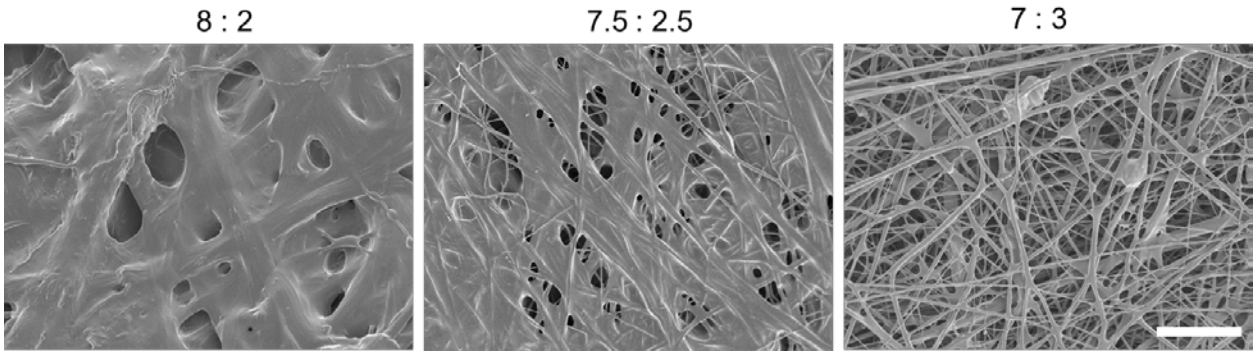

Figure 30. Maximization of PGS content in Espun pPGS-PVA^{intact} grafts
SEM of microfiber blends with varying pPGS:PLGA ratios. The maximum content of pPGS which sufficiently limited fiber fusion was 70% by mass (right). Scale bar 25 μm.

3.3.2 Removal of carrier polymer

Solvent washes removed varying amounts of carrier polymer from PGS microfibers. Solvent washing of Espun PGS-PLGA^{Intact} grafts reduced the mass by more than the total mass of PLGA added, suggesting that the vast majority of PLGA was removed in Espun PGS-PLGA^{Removed} grafts. The exact amount of PLGA residue is unknown, as it is unknown what the mass of unreacted pPGS monomer and oligomers was before and after solvent washing. Substantial residues of PET are suspected to remain after solvent washing of Espun PGS-PET^{Intact} grafts, as resultant Espun PGS-PET^{Removed} grafts demonstrated tearing failures at the same strains as PET-only microfibers. Consequently, mass measurement was not performed. Removal of PVA from Espun PGS-PVA^{Intact} grafts or sheets was characterized in detail by Jeffries et al [169]. Assuming the same mass of unreacted pPGS monomers and oligomers leaches out of Espun PGS-PVA^{Intact} fibers as does from nonporous PGS films, Espun PGS-PVA^{Removed} fibers can contain up to 14 % or 31% residual PVA for thermal crosslinking conditions 120 ºC at 48h and 120 ºC 24h + 150 ºC 24h, respectively.

The fiber structure for Espun PGS-Carrier^{Removed} grafts varied depending on the carrier polymer and thermal cross-linking conditions (**Figure 31**). Espun PGS-PVA^{Removed} fibers showed the least amount of fiber fusion. Espun PGS-PET^{Removed} fibers also showed resistance to fiber fusion. Transverse cross-sections of Espun PGS-Carrier^{Removed} tubes or sheets showed more fusion of fibers than did views of construct outer surface, suggesting that winding of successive layers of fibers may cause compression-induced fiber fusion within the construct wall.

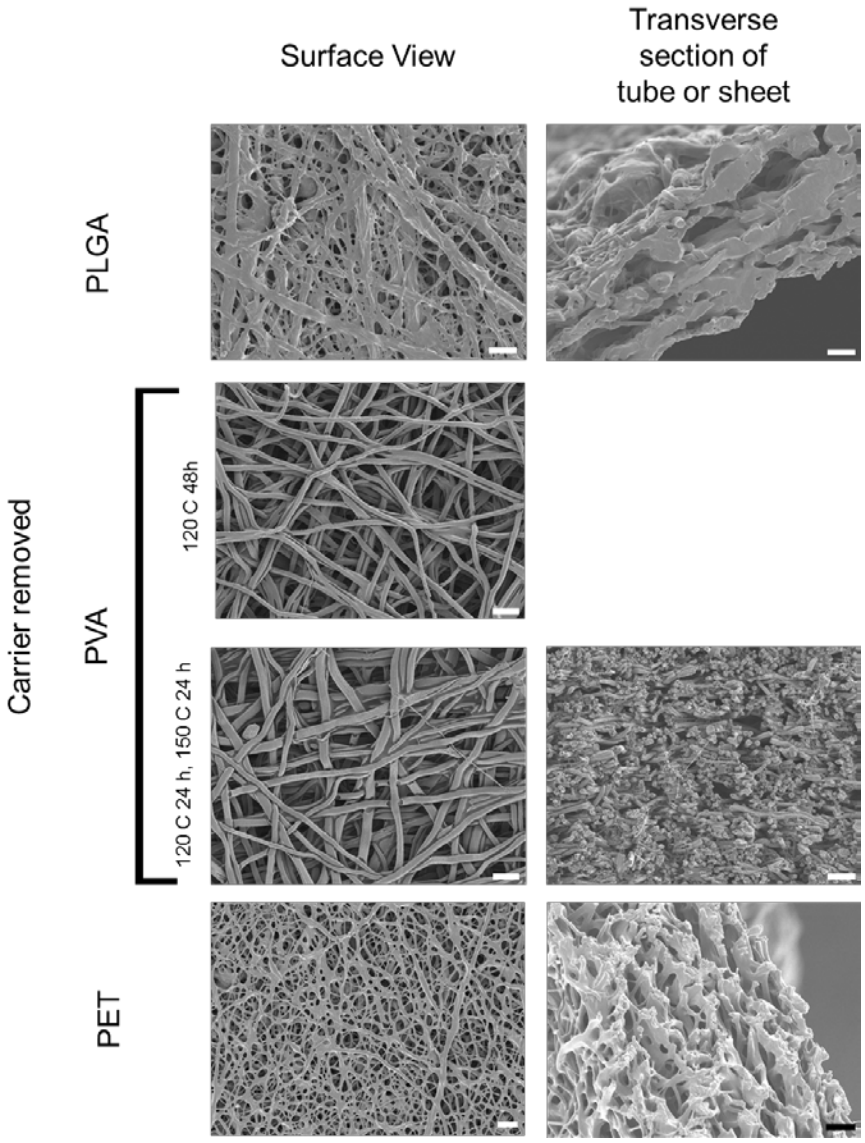

Figure 31. Fiber morphology of Espun PGS-Carrier^{Removed} blends
SEM images of PGS microfibers after removing carrier polymer. Left column shows surface view of sheets or tubes. Right column shows transverse sections of tubes or sheets. All scale bars 10 μm.

3.3.3 Application of PCL sheath, & finished composite grafts.

Implant-grade Espun PGS cores were prepared using both PLGA and PVA carrier polymers. PCL sheaths were applied to some groups of these PGS microfiber grafts (**Figure 32**). Espun PGS-PVA^{removed} PCL^{sheath} grafts, the luminal surface showed superficial fusion in some regions, but frequent gaps in fusion provide access to the space within the PGS core. Unsheathed grafts were also prepared for implantations.

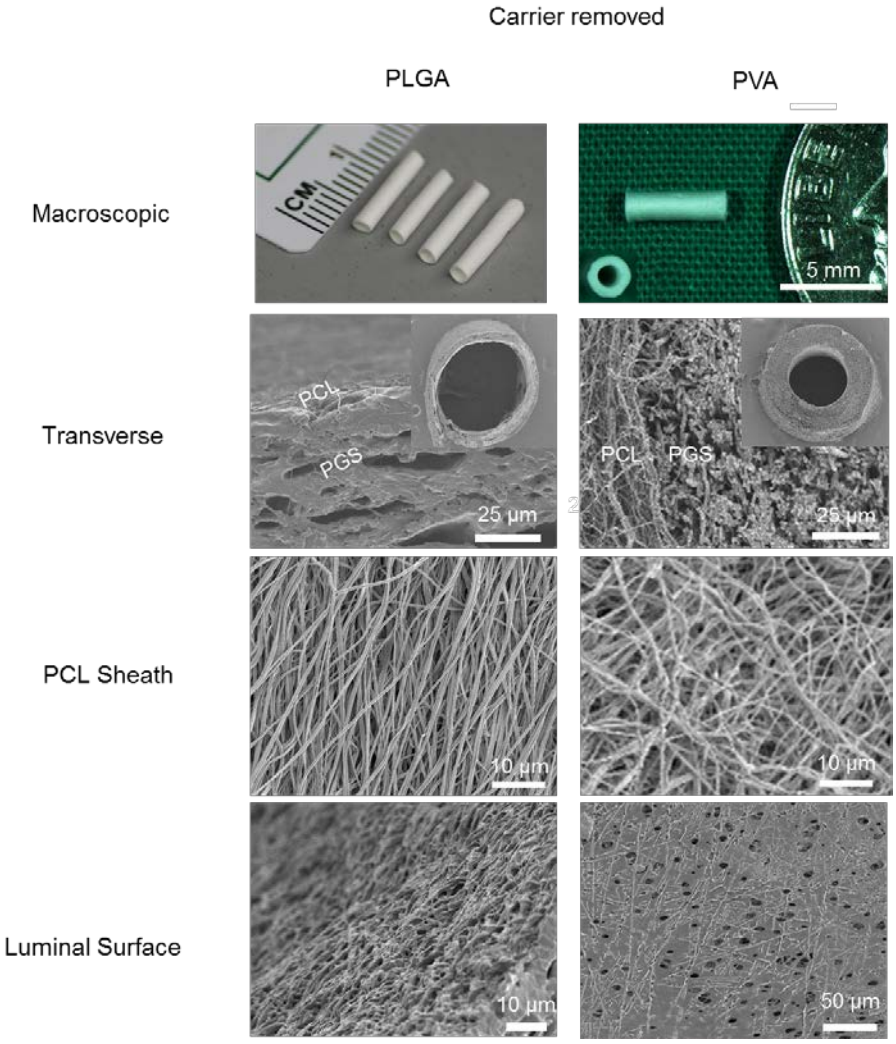

Figure 32. Structure of Espun PGS-Carrier^{Removed} PCL^{Sheath} grafts
Structure of Espun PGS-Carrier^{Removed} PCL^{Sheath} grafts, fabricated from PLGA (left column) or PVA (right column) carriers. *Macroscopic*. Camera or dissecting scope pictures of implant-ready grafts. Note that PLGA-derived grafts are designed for rat abdominal aorta interposition grafting, whereas PVA-derived grafts are designed at different dimensions for mouse abdominal aorta interposition grafting (described further in Chapter 4). *Transverse*. Transverse cross-sections of grafts show thin PCL sheath and PGS core regions, labeled with overlaid white text. Insets show low magnification of grafts. *PCL Sheath.* View of abluminal surface of graft shows coverage with PCL micro- and nano-fibers. *Luminal Surface.* View of blood-contacting surface of the graft. In PGS-PVA^{Removed} microfibers, fused fibers create a smooth surface in some regions, but frequent gaps in fusion provide access to the space within the core.

3.3.4 Pre-implant characterization of Espun PGS-PVA^{Removed} PCL^{sheath} grafts

Espun PGS-PVA^{Removed} PCL^{sheath} grafts were characterized in physical properties, geometry, and resorption rate *in vitro*. These grafts are comprised of an electrospun microfibrous PGS core and a PCL sheath (**Figure 32**, right). SEM shows that microfibers comprise the PGS core (~1.5 μm; **Table 5**), with space between some fibers and limited fusion between others. The luminal surface of the graft demonstrates some regions of superficial fiber fusion, but frequent gaps in fusion provide access to the space within the PGS core. The sheath consists of PCL micro- and nano-fibers and accounts for less than 5% of the total graft thickness (**Table 6**).

These Espun PGS-PVA^{Removed} PCL^{sheath} grafts vascular grafts showed some differences in physical properties and geometry from the SCPL PGS-PCL composite grafts described in Chapter 2 [118]. **Table 5** compares the physical properties of the PGS cores of both grafts. Espun PGS-PVA^{Removed} PCL^{sheath} grafts demonstrated reduced porosity and pore size, and 3-fold larger Young's Modulus compared with SCPL PGS. Espun grafts were designed for interpositional implantation into a mouse rather than rat infrarenal abdominal aorta, and thus are implanted at shorter length and reduced wall thickness (**Table 6**). Espun PGS-PVA^{Removed} fibers may contain some nontoxic residues of poly(vinyl alcohol) (PVA) not present in SCPL PGS [169]. Despite graft differences, both designs share a similar rate of hydrolytic degradation *in vitro* (**Figure 33**, **Table 5**).

Table 5. Physical properties of PGS core

	Symbol	Units	Espun PGS-PVA^{Removed} Microfibers	SCPL PGS Foam [118]
Pore Size	η^p	µm	1.87 ± 0.23	21.2 ± 0.79
Porosity	ω^p	%	47.1 ± 4.2	81.1± 0.7
Fiber Diameter	d^p	µm	1.45 ± 0.6	N/A
Degradation rate (mass loss at pH 11.75)	k_q^p	% h^{-1}	1.34	1.33
Young's Modulus	E^p	MPa	0.67 – 0.87 [169]	0.243 ± 0.072

Table 6. Graft geometry and implantation

	Espun PGS-PVA^{Removed} PCL^{Sheath}	SCPL PGS-PCL [118]
Animal Model	Mouse	Rat
Implantation site	Infrarenal Abdominal Aorta	Infrarenal Abdominal Aorta
Length (mm)	3 - 5	8 - 10
Inner diameter (µm)	718.9 ± 19.2	723 ± 1.33
Outer diameter (µm)	1164 ± 35.6	1313 ± 7.50
PGS core thickness (µm)	222.5 ± 21.1	264 ± 10.3
PCL sheath thickness (µm)	10.8 ± 2.88	15.7 ± 6.11

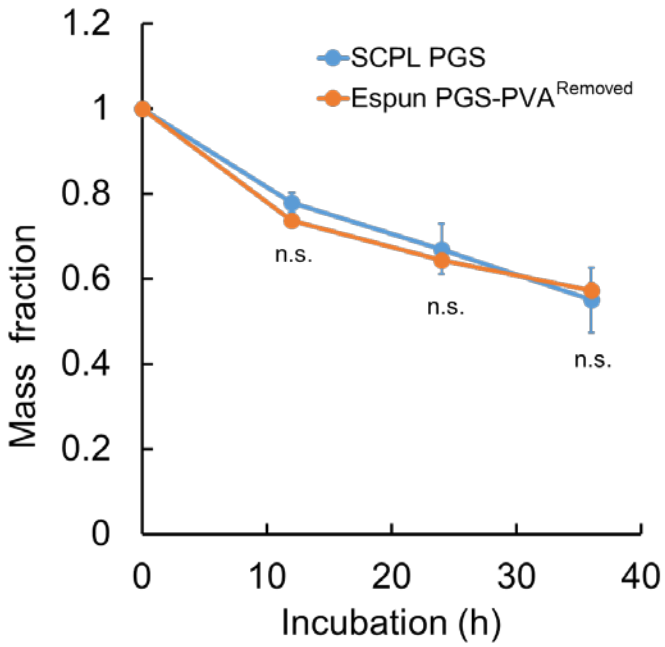

Figure 33. Hydrolytic degradation of Espun PGS-PVA^{Removed} and SCPL PGS in basic conditions
Fraction of mass remaining (mass fraction) vs. incubation time for the improved design (Espun PGS-PVA^{Removed} cores, orange) and the original design (SCPL PGS cores, blue). Disks of graft cores were incubated in pH 11.75 buffer at 37 °C with agitation to accelerate hydrolysis *in vitro*. n.s. – no statistically significant difference between mass fraction of SCPL PGS and Espun PGS ($P > 0.05$).

3.3.5 Translational potential of fabrication strategies

All strategies for fabricating Espun PGS cores showed translatability advantages in lead time, duration of skilled labor, and the number of steps requiring skilled labor (**Figure 34**). Of all the microfiber strategies, the only which required more fabrication steps than SCPL PGS was Espun PGS-PLGA^{Removed}. The increase in fabrication steps was due to additional purification steps necessitated by the need for thorough purification, as the electrospinning solution contains toxic LiBr salt and lysine triisocyanate cross-linker.

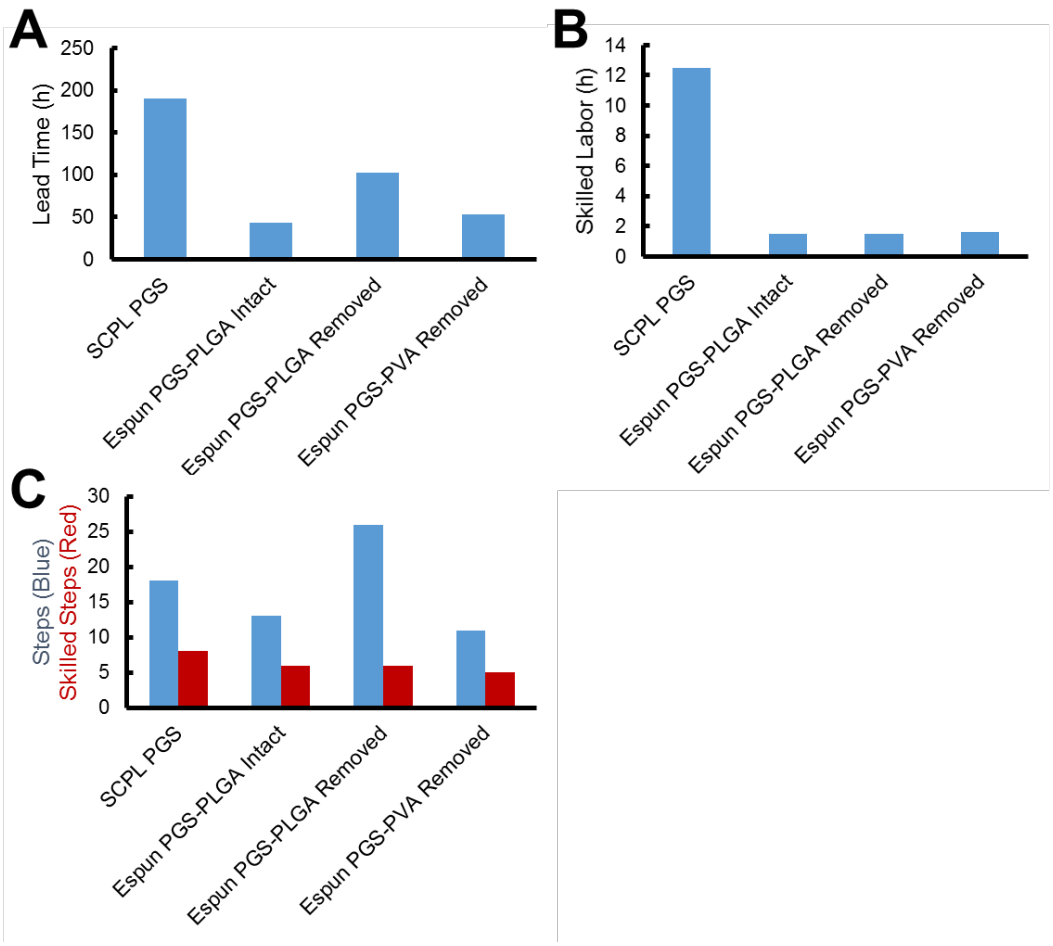

Figure 34. Translational potential for fabrication strategies of Espun PGS
Lead time (**A**), skilled labor required (**B**), and number of steps required (**C**) to produce the PGS cores for five usable, implant-grade grafts. PCL sheathing requires an additional 6 hours lead time, 2 hours skilled labor, 2 steps, and 1 skilled step (not pictured). **A.** Lead time (h), for each core fabrication strategy. All electrospun (Espun) fabrication methods require less time to fabricate than SCPL PGS. **B.** Skilled labor required (h). All Espun fabrication methods require less time of skilled manual labor than SCPL PGS. **C.** Total number of steps (blue) and number of steps requiring skilled labor (red). All µfiber fabrication methods used fewer steps requiring skilled labor than SCPL PGS. The total number of steps was also less for Espun fabrication, except for Espun PGS-PLGA^{Removed} grafts.

3.3.6 Mechanical characterizations

All microfiber cores measured demonstrated superior suture retention strength than SCPL PGS. PGS-PLGA microfiber cores demonstrated ~2-fold greater suture retention than compared with SCPL-PCL composite grafts (**Figure 35 A**). PGS-only microfibers derived from PVA blends demonstrated far-superior suture retention strength to SPCL PGS, which failed to achieve any measurable load before failing by tearing (**Figure 35 B**; collected by Eric Jeffries and reported in [169]).

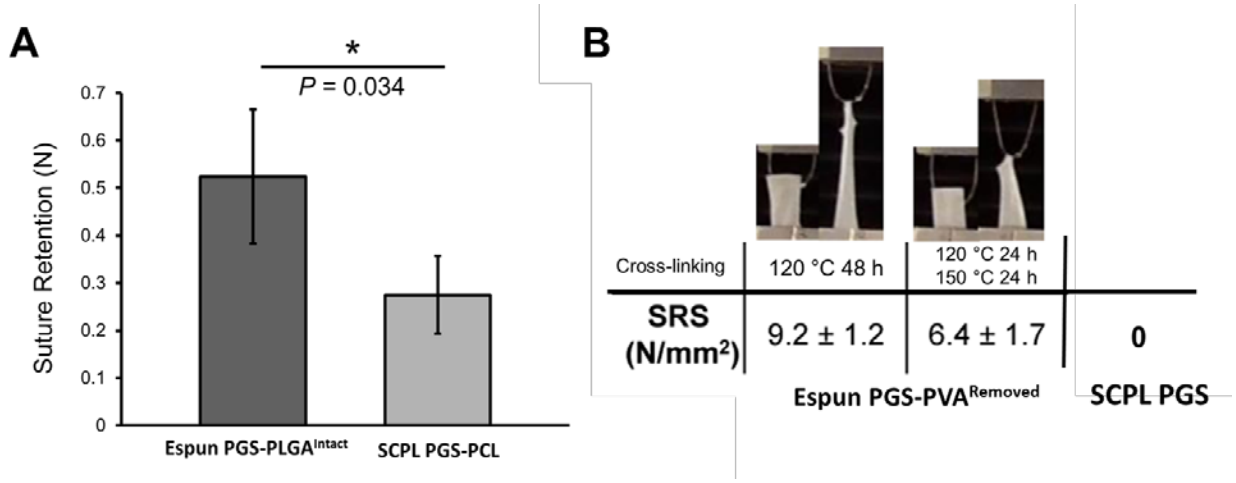

Figure 35. Suture retention strength of Espun cores
A. Suture retention comparison of Espun PGS-PLGA^{Intact} grafts and composites of SCPL PGS and PCL fibers (SCPL PGS-PCL). Espun PGS-PLGA^{Intact} (dark gray) showed significantly greater suture retention strength than SCPL PGS-PCL (light gray). Suture retention strength is reported as load at which constructs yielded or tore. * $P < 0.05$. **B.** Suture retention comparison of Espun PGS-PVA^{Removed} blends and SCPL PGS foams (SCPL PGS). Espun PGS at both thermal cross-linking conditions tested substantially exceed the suture retention strength of SCPL PGS, which failed to withstand any measurable load at the testing conditions used by Jeffries et al. Here, suture retention strength is normalized to sample thickness and suture diameter. **B** is adapted from [169].

Assessment of the circumferential wall stresses of graft cores showed that all Espun PGS-Carrier^{Removed} grafts had Young's moduli within 1 order of magnitude of rat native aortas (**Figure 36**). Espun PGS-PLGA^{Intact} grafts were substantially stiffer than native aortas by 3 orders of magnitude. Espun PGS-PLGA^{Intact} blends showed superior strength to SCPL PGS composites along the longitudinal axis, suggesting improved resistance to tearing during implantation (**Figure 37**).

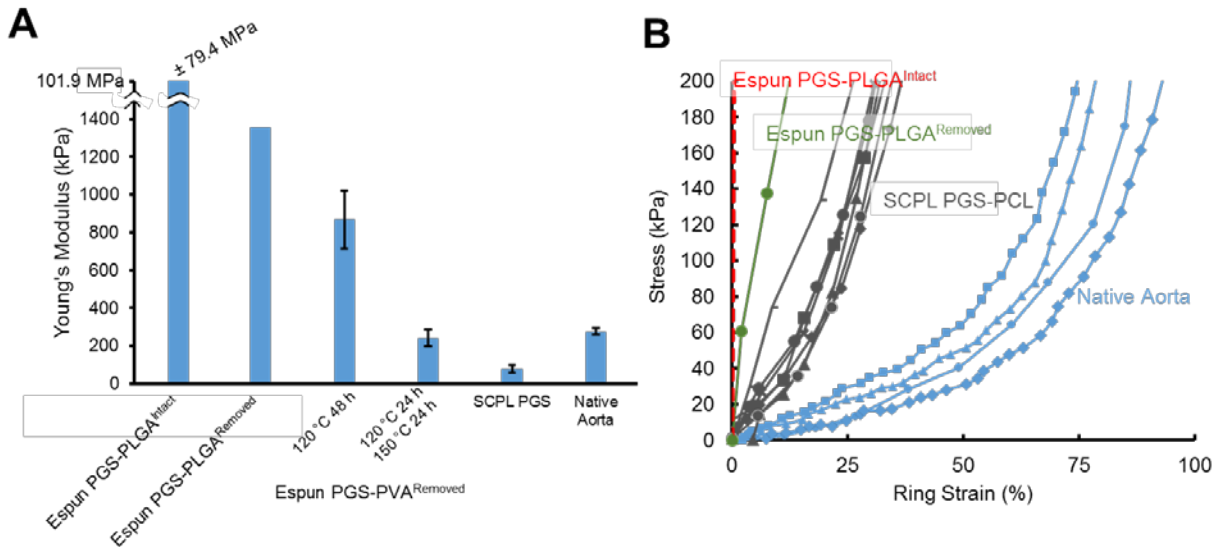

Figure 36. Mechanical properties of core materials in the circumferential direction
A. Young's moduli of ring sections of tubular cores. All Espun PGS and SCPL PGS cores are within 1 order of magnitude of the modulus of native rat abdominal aorta. Espun PGS-PLGA^{Intact} grafts (left) were three orders of magnitude stiffer than native tissue. Moduli taken from stress-strain data at wall stresses between 20 kPa and 200 kPa (shown in **B**), which we determined empirically to be the range of wall stresses at physiologic conditions.

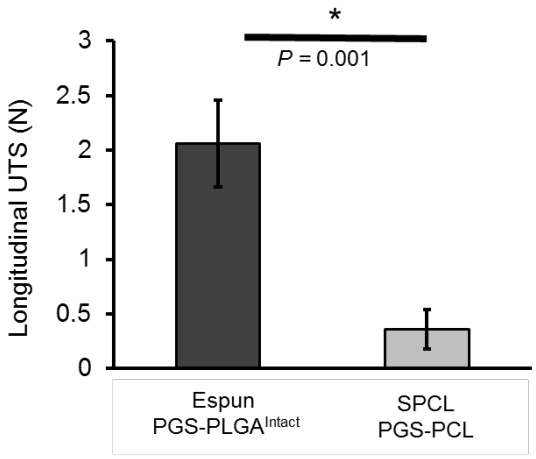

Figure 37. Longitudinal ultimate tensile strength
Espun PGS-PLGA^{Intact} grafts (dark gray, left) demonstrate significantly larger longitudinal ultimate tensile strength (UTS) than SCPL PGS-PCL grafts (light gray, right). * $P < 0.05$.

3.3.7 Surgical handling

We performed a total of 41 implants to assess surgical handling and *in vivo* performance. Espun grafts comprised of PGS-PLGA^{Intact}, PGS-PLGA^{Removed}, or PGS-PLGA^{Removed} PCL^{Sheath}; all were implanted with 100% success and demonstrated superior surgical handling to SCPL PGS-PCL when handled by a pediatric cardiothoracic surgeon lacking prior experience with the animal model (**Table 7**). Espun PGS-PVA^{Removed} PCL^{Sheath} grafts were also implanted with 100% success, but their handling was not compared to SCPL PGS-PCL as they were implanted by a separate team from the Research Institute of Nationwide Children's Hospital who had not handled SCPL PGS-PCL. However, the team did describe the surgical handling qualitatively as "good." Taken together, this data suggests that microfiber fabrication improved surgical handling compared with SCPL PGS-PCL.

Table 7. Surgical handling of implanted grafts

	Total implanted	Implant without damage	Tear but repaired	Unsuccessful	% Success	Surgeon Training	Experience with animal model
Espun PGS-PLGA^{Intact}	19	19	0	0	100	Pediatric Cardiothoracic	No
Espun PGS-PLGA^{Removed}	4	1	3	0	100	Pediatric Cardiothoracic	No
Espun PGS-PLGA^{Removed} PCL^{Sheath}	7	7	0	0	100	Pediatric Cardiothoracic	No
SCPL PGS-PCL	2	0	0	2	0	Pediatric Cardiothoracic	No
Espun PGS-PVA^{Removed} PCL^{Sheath}	9	9	0	0	100	Microsurgery	Yes

3.4 DISCUSSION

This chapter summarizes years of effort to improve the translational potential of fast-remodeling bio-inductive vascular grafts. Our strategy was to develop novel methods for fabricating grafts or graft cores from microfibers comprised of or containing cross-linked PGS. While clearly useful for vascular graft design, developing a fabrication technique for PGS microfibers would also be a far-reaching advance in tissue engineering and regenerative medicine, with relevance to any medical application requiring tensile loading and/or suture anchoring of resorbable materials. PGS is a unique and desirable material for engineering of soft tissues, as its elastic modulus can be tuned to match that of various tissues [169], and it resorbs rapidly *in vivo* with minimal inflammation [120]. To realize the potential of implantable PGS, various groups have pursued strategies to electrospin PGS ([169] for review). Though promising, the limitations of these

strategies motivated us to develop our own improved methods. For example, previously developed Espun pPGS–PCL^{Intact} blends exhibit mechanical properties more similar to PCL than PGS [176], and noncrosslinked pPGS may have a cytotoxic effect if pPGS is not removed from the scaffold [177]. Gelatin has been used as a carrier but it requires crosslinking methods that use glutaraldehyde, acrylate-ultraviolet (UV), or EDC-NHS, which may alter PGS structure and properties and trigger inflammation and calcification [178] [179] [180]. Coaxial electrospun pPGS–PLLA tolerated both thermal crosslinking and dissolution of the PLLA sheath without substantial fiber fusion [181]. However, the dichloromethane used to dissolve PLLA is toxic and a suspect carcinogen, requiring stringent and complete removal before biomedical applications. Two of the Espun PGS microfiber methods we developed in this chapter demonstrate advantages over these prior approaches. Espun PGS-PLGA^{Removed} microfibers can be spun with traditional electrospinning equipment rather than a core-shell setup, thereby simplifying the fabrication process and reducing costs. Espun PGS-PVA^{Removed} microfibers fabricate with more simplicity and shorter lead times than all other methods and circumvent the need for toxic solvent washes. We have recently published this method [169], and believe it will be adopted by others for its advantages in fabrication and biocompatibility.

In the present study, our primary objective was to improve the translatability of SCPL PGS-PCL composite grafts by developing PGS-based Espun microfiber grafts. Consequently, we employed a range of carrier polymers, including some blends previously reported by others. We began our experiments using PCL as a carrier simply because our laboratory has prior experience in elecrospinning PCL and had sufficient quantities on hand for initial exploration. Shortly thereafter, we began trying blends with PLGA because it is faster-resorbing than PCL, and thus residues left over after removing the bulk of PLGA should still resorb *in vivo* in a timely manner.

Additionally, PLGA removal could be foregone altogether, and the graft may still demonstrate fast-remodeling capability.

In later experiments, we began employing thermostable polymers, which enable thermal cross-linking of PGS, thereby circumventing the toxicity concerns of using chemical cross-linkers as required for PCL and PLGA blending. We chose PET as the first thermostable carrier because (1) it is clinically accepted as a vascular graft material with reasonable hemocompatibility and long-term biocompatibility, and (2) it is exceptionally low-cost, as one of the most common polyesters used in industry. However, the stiffness and non-degradability of PET are major limitations, and residues not removed by solvent washing could contribute to neointimal hyperlasia and long-term inflammation in the graft. We considered leaving PET in to serve as a non-resorbable backbone promoting continued graft strength during PGS resorption, but the distribution of PET within fibers is unknown, and small fragments of PET might be freed during PGS degradation. These nondegradable fragments could cause embolism formation and/or accumulate in the liver and kidneys, all potential causes of morbidity.

PVA shares PET's advantage of thermostability, but without the disadvantage of non-degradability. PVA is a common FDA-approved additive in food and drugs, alleviating biocompatibility concerns. It is also water-soluble, enabling facile removal from PGS-PVA blends without requiring washes with toxic organic solvents. Clearly, PVA has theoretical advantages as a carrier for PGS electrospinning compared to the previously listed polymers. However, PGS-PVA blends were used in our vascular grafts last, as the ideal PVA formulation and optimized electrospinning parameters were not determined until after Espun PGS-PLGA microfiber grafts were thoroughly investigated. Espun PGS-PVA^{Removed} blends have been thoroughly characterized by Jeffries et al. in [169].

In choosing an electrospinning method for improved translatability of bio-inductive grafts, microfiber quality was the first selection criterion. Ideally, microfibers must resist fusion into nonporous sheets, which are prone to failure by tearing and resorb slowly due to low surface area and impermeability to cell infiltration. We ruled PCL out as a carrier early in our investigation, as fibers demonstrated substantial fusion even at a 1:1 ratio of pPGS:PCL. We were surprised to find substantial fiber fusion using the same electrospinning conditions reported by Sant et al. [176] for similar blends, in which fusion was not reported as a problem. PLGA carrier blends were the first to demonstrate distinct fibers at relevant wall thickness, though fusion still occurred, especially within the wall. Consequently, most early work on Espun PGS-based grafts focused on PLGA blends. PET blends were the first to demonstrate minimal fiber fusion, and for those fibers to survive thermal cross-linking. However, PVA blends demonstrated comparable fiber quality with thermal cross-linking. This equivalence, when coupled with the theoretical advantages of PVA as a carrier, drove us to focus further development efforts on PVA blends over PET blends. We initially selected thermal cross-linking conditions of 120 °C for 24 h and 150 °C for an additional 24 h because we expected the 150 °C cure temperature to yield PGS with high tensile strength, which we believed would be advantageous in vascular surgery. Consequently, all of the implanted Espun PGS-PVA^{Removed} grafts were cured at this temperature. However, we later found that softer PGS microfibers have superior surgical handling, as they can be strained substantially farther without failing [169], thereby reducing the likelihood of suture pull-out during surgery. Thus we began constructing Espun PGS-PVA^{Removed} grafts using 120 °C for 48 h, which we characterized *in vitro* but have not yet implanted.

We removed the carrier polymer in some of our microfiber grafts in order to match the composition of core material as closely as possible to that of our original SCPL PGS design.

However, we also left PLGA carrier in the microfibers of some grafts, as Espun PGS-PLGA^{Intact} microfibers might also fit the criteria for a fast-remodeling bio-inductive vascular graft. Removing PLGA from PGS blends requires the use of organic solvents. We employed additional steps to swell and contract the construct to maximize removal of impurities, as these blends require substantial quantities of toxic cross-linker lysine triisocyante and toxic LiBr salt. Purification yielded Espun PGS-PLGA^{Removed} microfibers in which the majority of PLGA is removed, but fiber fusion increased compared with prior to solvent washing. Despite requiring lengthy purification steps and having the potential for residual toxicity, Espun PGS-PLGA^{Removed} grafts were among the first suturable vascular grafts developed by our laboratory, and thus were fabricated and implanted in substantial number. Our second attempt in removing carrier polymer was with PET blends. Washing PET blends in HFIP did change their mechanical properties, but substantial PET residues seemed to remain, as resultant microfibers retain a propensity for tearing failure at tensions lower than expected for surgery. Consequently, we discontinued further work with PET blends.

PVA removal from Espun PGS-PVA blends was the simplest process with minimal toxicity risk, as only water and ethanol washes were required. However, a substantial amount of PVA carrier likely remains after washing. Residual PVA may be cross-linked into polymer chains by polycondensation with pPGS, entrapped between PGS polymer chains, or rendered insoluble from heat curing [169]. The presence of PVA residues might not source undesired effects. PVA showed no significant cytotoxicity *in vitro*. It is possible that PVA may affect protein adsorption or material degradation rate.

All Espun microfiber grafts demonstrated advantages in fabrication and surgical handling compared to SCPL grafts, thereby validating our hypothesis that microfiber fabrication would

improve graft translational potential. Espun PGS-PVA^{Removed} PCL^{Sheath} grafts showed the greatest advantages in translational potential, and consequently are the focus of the next chapter. These blends demonstrated the simplest fabrication with the shortest lead times, and were implanted with 100% success. Espun PGS-PLGA^{Intact} grafts were implanted without mechanical failure, but these grafts might retain cytotoxic residues of chemical cross-linker lysine triisocyanate and LiBr salt. Espun PGS-PLGA^{Removed} grafts required substantially larger lead times and more steps than PVA strategies. Their surgical handling was limited by a 75% incidence of repairable tearing during implant surgery, although this was still superior to SCPL PGS-PCL grafts which all tore irreparably when handled by the same surgeon.

3.5 LIMITATIONS AND FUTURE DIRECTIONS

Future work will address the limitations of this investigation. An ideal fabrication method should produce a range of structures with tunable properties. At present, the tunability of graft structural and physical properties remains to be further explored. Consequently, ongoing work by others in our laboratory focuses on determining the effects of tunable electrospinning parameters such as infusion rate, voltage difference, spinneret-collector distance, and mandrel rotational speed. Such work will empower our laboratory to implement design changes warranted from *in vivo* results of our implantations, which are further detailed in Chapter 4. The electrospinning processes we developed are clearly more translatable than SCPL techniques, but at present they are still manual processes requiring skilled labor. Skilled labor tends to increase costs and challenge quality control, as it adds human error to variability within and between batches. The present processes require a human operator to periodically adjust voltage and/or move the collecting

mandrel or rod to ensure even fiber deposition. Human operators were also needed to assess whether fibers were being formed efficiently, which varies with humidity, temperature, and air flow rate. Automating these adjustments or eliminating the need for them could remove the human element from the process. To approach automation, our laboratory is building a custom electrospinning enclosure with tighter environmental control and a programmable moving stage.

Even with automation, electrospinning is still less reproducible and less cost-effective than traditional polymer spinning techniques used by the medical textiles industry. Enabling PGS prepolymer to be melt spun and drawn would even further improve the translational potential of graft fabrication. Unfortunately, the low Tg of PGS prepolymer complicates these methods similarly to in electrospinning, as pPGS fibers flow and fuse during thermal cross-linking. Efforts to increase the Tg of pPGS, or modifications to enable cross-linking without heat or chemical cross-linkers, might realize the translational advantages of textiles industry techniques.

3.6 CONCLUSION

Here we developed several novel methods for fabricating vascular grafts from microfibers comprised from or containing PGS. Espun PGS-PVA^{Removed} PCL^{Sheath} grafts demonstrated the simplest and fastest fabrication, but all Espun fabrication methods demonstrated advantages over SCPL PGS-PCL grafts in surgical handling, lead time, and fabrication simplicity. These findings validate our hypothesis that fabricating graft cores from microfibers improve the translational potential of fast-remodeling bio-inductive vascular grafts. These methods may positively impact the broader field of tissue engineering and regenerative medicine, as they yield suturable PGS implants which could prove useful in a range of soft-tissue applications. Improving graft strength

and fabrication simplicity improves the translational potential of bio-inductive grafts, but only if they retain their previously demonstrated long-term performance. Consequently, we investigated graft performance *in vivo* in Chapter 4.

4.0 PERFORMANCE TESTING OF IMPROVED DESIGN

In Chapter 3 we improved graft surgical handling and simplified fabrication by constructing tubular graft cores from electrospun microfibers. This process substantially improves the feasibility of applying bio-inductive grafts in a clinical setting. However, to potentially improve patient care, the new design must retain the excellent long-term performance demonstrated by the original design in Chapter 2. In Chapter 4 we report performance testing of our newly developed microfibrous grafts.

4.1 INTRODUCTION

The potential translational advantages of microfibrous grafts may only be realized if they retain the favorable long-term performance demonstrated by the original SCPL design. Consequently, we implanted the most promising graft designs from the previous chapter in rodent models. Performance testing of implants requires reproducible surgical technique. The majority of our pilot implantation studies in Chapter 3 were complicated by uncertainty in surgical technique, as they occurred early in the learning curve for a surgeon who was not trained in microsurgery or the animal model. Grafts implanted with methods A through C (**Table 4**) realized high rates of acute thrombosis independent of graft composition. Consequently, graft propensity for thrombosis could not be evaluated, and graft remodeling was only assessed in the few patent

grafts. Surgical technique became reproducible through collaboration with Christopher Breuer's laboratory at the Research Institute of Nationwide Children's Hospital. Their team of microsurgeons have extensive experience in an even more technically challenging mouse model for interpositional arterial vascular grafts. This team's expertise enabled our laboratory to evaluate the time course of microfiber graft performance and remodeling *in vivo*.

The objective of this chapter's investigation is to assess the long-term performance of our most promising bio-inductive vascular graft designs from Chapter 3. We hypothesized that these grafts would approach the long-term performance of the original microporous PGS-PCL composite design despite the reduced pore size. Our rationale is that even nonporous PGS resorbs rapidly *in vitro* [119, 120, 174], and nonporous fast-remodeling vascular grafts have previously formed neoarteries *in situ* [114, 136, 139]. To test our hypothesis, we assessed the in-host remodeling of 3 graft designs: (1) Espun PGS-PLGA^{Intact} (2) Espun PGS-PLGA^{Removed}, and (3) Espun PGS-PVA^{Removed} PCL^{Sheath}. In the latter group, favorable patency enabled us to observed remodeling over a time course of 3 months, 6 months, and 1 year. Within this group, to understand the graft remodeling processes in both dilating and undilated grafts, we selectively sacrificed animals based on diameter change observed from non-invasive Doppler ultrasound. At explant, we characterized grafts in complication incidence, tissue architecture, and mechanical properties.

Importantly, this study also contributes to a larger body of work. Our laboratory is collaborating with both Jay Humphrey's team at Yale University and Christopher Breuer's team at the Research Institute of Nationwide Children's Hospital to develop a framework for rationally designing bio-inductive vascular grafts. This framework uses *in vivo* observations to inform a computational model of graft remodeling, which will simulate further experiments *in*

silico to determine the optimal states for graft structure, mechanical properties, and resorption kinetics. Consequent to the collaborative nature of this work, a substantial portion of the study design, data collection, and analysis was performed outside of the University of Pittsburgh. Collaborators include Ramak Khosravi, Cameron A. Best, Yong-Ung Lee, Tai Yi, Matthew R. Bersi, Toshiharu Shinoka, Jay D. Humphrey, and Christopher K. Breuer. We identify each collaborator's contribution in the methods and results section of this chapter. Currently our cross-institutional team is preparing a manuscript which presents this data in the context of developing a framework for rational design of bio-inductive vascular grafts [182]. However, such context is outside the scope of this dissertation. Herein we report graft performance in the context of assessing translational potential of the current design.

4.2 METHODS

4.2.1 Graft implantation

Grafts were implanted as described in **3.2.9.**

4.2.2 Ultrasound Monitoring

Ultrasound monitoring was provided by Christopher Breuer's team at The Research Institute at Nationwide Children's Hospital. Implants were monitored longitudinally until explant with high frequency Doppler ultrasonography (Vevo® 2100, VisualSonics Inc, Toronto, Canada). After induction of anesthesia (1.5% inhaled isoflurane vaporized with oxygen at 1 L/min, Baxter) the

ventral abdomen was chemically depilated and ultrasound gel applied (Aquasonic Clear®). Body temperature was maintained at 38°C for the duration of ultrasound interrogation. Long axis images were acquired in B-mode, pulse wave, and color Doppler. Image J (NIH, Bethesda, MD) was used to quantify TEVG and adjacent artery lumen diameters. TEVG lumen diameters are reported as the mean ± SD of three measurements (proximal anastomosis, mid-graft, distal anastomosis) and are normalized to the mean lumen diameter of the adjacent artery.

4.2.3 Graft Harvest

For grafts implanted using methods A-C of Chapter 3: All animals were cared for in accordance with IACUC-approved protocols at the University of Pittsburgh and the Research Institute of Nationwide Children's Hospital. Animals were euthanized at predetermined time points, or pre-emptively if grafts occlusion was suspected by Doppler ultrasound or if the animal was exhibiting distress. Euthanasia methods included CO_2 asphyxiation, or anesthetized surgical exsanguination during harvest. The latter method was used in some sacrifices, as it allows patency to be examined. Patency was checked in those grafts by clamping the aorta distal to the graft, then transecting the native aorta between the clamp and the graft. Pulsatile leakage of blood confirmed graft patency.

For grafts implanted using method D of Chapter 3: Grafts were harvested by Christopher Breuer's team at 3, 6, and 12 months (n=3/time point). At the appropriate endpoint, animals were euthanized by intraperitoneal injection of ketamine (300 mg/kg) and xylazine (30 mg/kg) overdose cocktail followed by induction of pneumothorax. Mice were then systemically perfused with cold 1x PBS. A continuous vascular segment comprised of the TEVG and a 1-2 mm portion of native infrarenal abdominal aorta distal and proximal to the sites of anastomosis

was harvested and placed in 1x HBSS until biaxial mechanical testing. In order to ensure adequate pressurization during mechanical testing, branching vessels were also identified and ligated. Prior to explant, small sutures were placed at multiple locations along the TEVG, proximal IAA, and distal IAA and photographs were taken to record their positions both *in vivo* and following excision. Distances between these suture markers were measured using ImageJ software and used to determine the *in vivo* axial stretches (the ratio between the loaded and unloaded axial length of each segment).

4.2.4 Histology and Immunohistochemistry

For grafts implanted using methods A-C of Chapter 3: Explants were fixed in 2% paraformaldehyde for 2 h at room temperature, then frozen in OCT with liquid nitrogen and stored at -80 °C until use. Sections were cut to 8 μm thickness using a cryomicrotome (HM525, Thermo Scientific, Waltham MA), mounted on glass slides, and stored at -80°C until staining.

For grafts implanted using method D of Chapter 3: Christopher Breuer's team planned and performed histology and immunohistochemistry on neoarteries. After biaxial mechanical testing, samples were fixed in 10% NBF at 4°C for 24hrs, dehydrated, paraffin embedded, and serially sectioned (4 μm thick sections). Representative sections were analyzed at 5 regions of interest: proximal aorta, proximal anastomosis, TEVG, distal anastomosis, and distal aorta. Histological analysis included: hematoxylin and eosin (HE), Masson's trichrome (TRI), Picrosirius Red (PSR), Hart's, and von Kossa (VK) stainings. For immunohistochemical analysis, slides were rehydrated and blocked for endogenous peroxidase activity (0.3% H_2O_2 in MeOH) and nonspecific background staining (Background Sniper, BioCare Medical). Antigens were retrieved with citrate buffer (pH 6.0, 90°C, 15:00 min). Slides were incubated overnight at

4°C with the following primary antibodies: rabbit anti-collagen I (1:250, Abcam), rabbit anti-collagen III (1:250, Abcam), anti-human smooth muscle actin (cross reacts with mouse, 1:500, Dako), rabbit anti-calponin (1:200, Abcam) and rat anti-F4/80 (1:1000, AbD Serotec). Primary antibody binding was detected by incubation with species appropriate biotinylated secondary antibodies (Vector) followed by binding of horseradish peroxidase streptavidin and subsequent chromogenic development with 3,3-diaminobenzidine (Vector). Finally, nuclei were counterstained with Gill's hematoxylin, and slides were dehydrated and coverslipped.

4.2.5 Imaging and quantification of histology/IHC sections

For grafts implanted using methods A-C of Chapter 3: Slides were stained with hematoxalin and eosin (H&E) and von Kossa according to standard protocols, and imaged using a Nikon Eclipse Ti inverted microscope with Nikon Elements software (Melville, NY). Tissue sections were examined for elastin autofluroescence using an Olympus Fluoview FV1000-MPE Multiphoton microscope with a 1.12 NA 25x MPE water immersion objective. [134] Excitation was set to 870 nm, and the emission range was set to 525-575 nm for elastin.

For grafts implanted using method D of Chapter 3: Christopher Breuer's and Jay Humphrey's teams imaged and quantified images of neoartery sections. Slides were imaged using an Olympus BX/51 microscope and associated Olympus DP70 digital camera, with PSR images taken under polarized light. Analysis of the digital images was performed using a custom MATLAB script that converts the original red, green, blue (RGB) images to the hue, saturation, lightness (HSL) color space to enable additional pixel-specific thresholding and delineation of individual constituents of interest, as previously described. For Picosirius red (PSR)-stained sections, area fractions of red, orange, yellow, and green pixels were quantified to identify the

relative distribution of large and small collagen fibers and differences in fibrillar collagen packing at each time point and throughout the 5 regions of interest. IHC images were first inverted, and the inverted RGB images were then converted to HSL color space, with HSL parameters chosen to isolate light blue pixels (H=160°-210°, S=0.1-1.0, L=0.47-1.0). Associated area fractions were calculated based on the total number of pixels that satisfied the HSL thresholding requirements for each constituent, divided by the total number of pixels identified as having any HSL parameter values other than those for the color black (the uniform background color, as established by an initial global thresholding).

4.2.6 Statistical Analysis

All data are presented as mean ± standard error of the mean (SEM). Differences between groups were analyzed using a one-way analysis of variance (ANOVA), and Bonferroni corrections were used to account for multiple statistical comparisons. Statistical significance was indicated by p values < 0.05.

4.3 RESULTS

4.3.1 Patency

Graft patency appeared to correlate with implantation technique (**Table 8**). The exception is Espun PGS-PLGA^{Removed} PCL^{Sheath} grafts. Those grafts were prone to thrombosis secondary to PGS core buckling from the compressive force of PCL, as we had not yet implemented the salt-

hardening step which reduces graft compression. Implantation methods A and B showed poor patency rates, while method C showed substantial improvement, and D yielded 100% patency. Thrombosis was the cause or suspected cause of occlusion in all closed grafts. 100% patency in Espun PGS-PVA^{Removed} PCL^{Sheath} grafts implanted by method D suggests favorable hemocompatibility of that design. However, further conclusions are difficult to draw, as graft blood-compatibility for other designs could not be de-coupled from any thromobgenicity inherent in implantation methods A-C and the surgeon's lack of prior experience with those methods.

Table 8. Patency rates for implanted grafts

Implant Method	Graft	Occlusion Risk	Patency (%; Minimum Estimate)	No. of patent grafts	Time point (days)	Observations *in vivo*
A	Espun PGS-PLGA^{Intact}	Thrombosis	0%	0		
	Espun PGS-PLGA^{Removed} PCL^{Sheath}	Thrombosis	0%	0		
	SCPL PGS-PCL	Tearing	N/A (Implant Failure)	0		
B	Espun PGS-PLGA^{Intact}	Thrombosis	0%	0		
	Espun PGS-PLGA^{Removed}	Thrombosis, Tearing	25%	1	90 n=1	Dilation
	Espun PGS-PLGA^{Removed} PCL^{Sheath}	Thrombosis, graft buckling	0%	0		
C	Espun PGS-PLGA^{Intact}	Thrombosis	75%	3	70 n=3	Dilation, calcification
	Espun PGS-PLGA^{Removed} PCL^{Sheath}	Thrombosis, graft buckling	0%	0		
D	Espun PGS-PVA^{Removed} PCL^{Sheath}	N/A	100%	9	90 n=3; 180 n=3; 365 n=3	Slowed material degradation, elastin deposition, dilation, calcification

4.3.1 Remodeling of Espun PGS-PLGA microfibers with or without PLGA removal

The patent grafts from implantation methods A-C offer some insight into the remodeling potential of vascular grafts made using Espun PGS-PLGA with or without PLGA removed. Graft numbers, explant time points, and findings are summarized in **Table 8** (columns 5-7). Both Espun designs lacking PCL sheaths demonstrated substantial resorption of graft material and neotissue formation, but remodeled tissues were prone to dilation (**Figure 38**). These neoarteries contained regions with gross similarity to neointimal hyperplasia, largely acellular regions of dense matrix, and regions of chronic inflammation likely due to residual polymer. Elastin was not seen in neoarteries, as they were negative for elastin autofluorescence. Mineralization was observed in the aneurysmal regions of grafts (**Figure 39**).

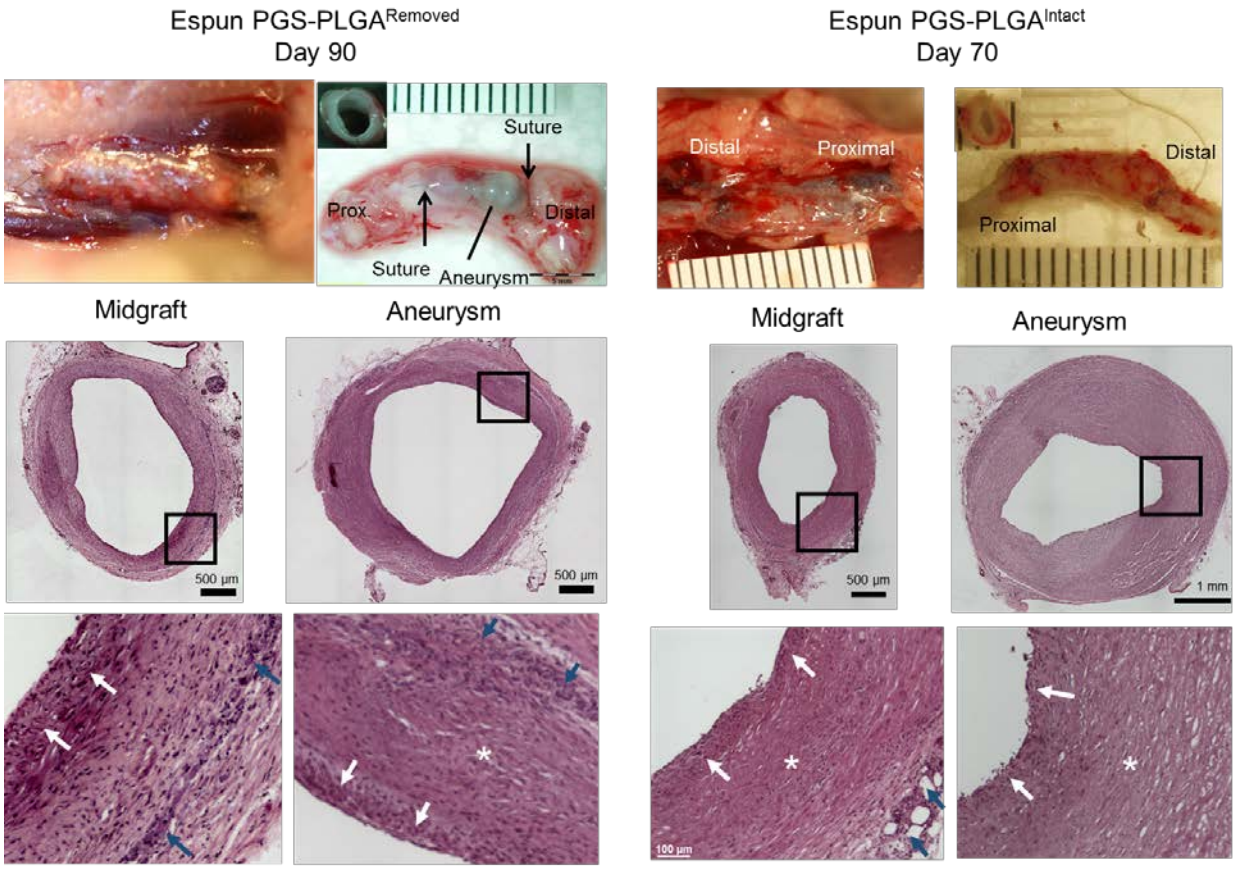

Figure 38. Gross morphology and histology of Espun PGS-PLGA grafts
Morphology and histology of Espun PGS-PLGA^{Removed} (left two columns) and Espun PGS-PLGA^{Intact} microfiber grafts (right two columns). Neither design includes a PCL sheath. *Top row*: *in situ* and explant gross morphology. Inset shows midgraft transverse section. *Bottom rows:* H&E staining of midgraft and aneurysmal portions of explants. Boxed region indicates region of higher magnification shown below. White arrows denote regions of putative neointimal hyperplasia. Blue arrows denote putative residual graft material and associated inflammation. * indicates cell-poor regions comprised primarily of dense extracellular matrix.

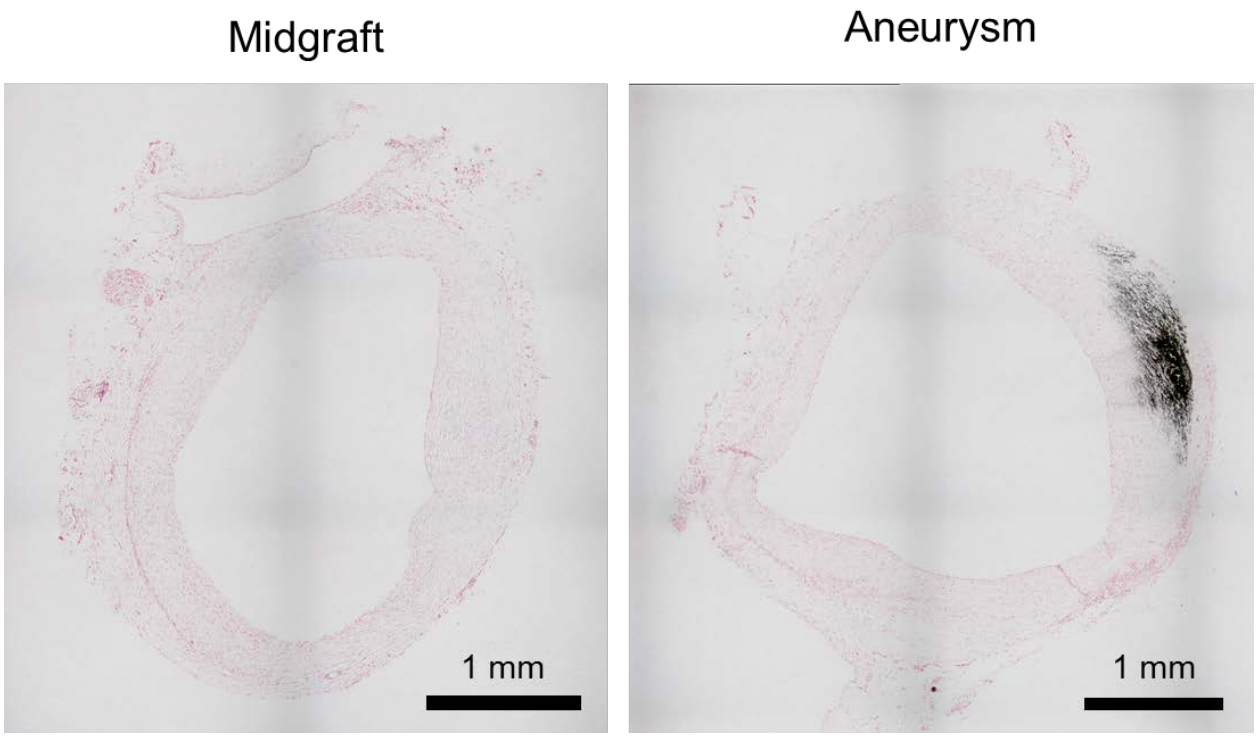

Figure 39. von Kossa staining of Espun PGS-PLGA^{Removed} grafts at day 90
von Kossa staining of midgraft (left) and aneurysm (right) shows mineralization (black) in aneurysmal sections.

4.3.2 Dilation in Espun PGS-PVA^{Removed} PCL^{Sheath} grafts

Espun PGS-PVA^{Removed} PCL^{Sheath} grafts were implanted by a surgical team at the Research Institute at Nationwide Children's hospital. This team achieved 100% patency in their model. Neoarteries from these grafts demonstrated elastic fiber formation but also showed slower resorption of graft material, and experienced dilation in most cases (**Figure 40 A**). These grafts showed no evidence of thrombosis in the absence of systemic heparinization, suggesting favorable hemocompatibility in small diameter, high flow arterial circulation. Dilation was a prevalent complication. Dilation incidence over time is shown in **Figure 40**. At 3 months post-

implant, 78% (7/9) of implanted grafts demonstrated dilation of over 25% the initial graft inner diameter. At the 6 month time point, 83% of remaining grafts were dilated (5/6). By 1 year post-implant, 100% (3/3) of the remaining grafts were dilated.

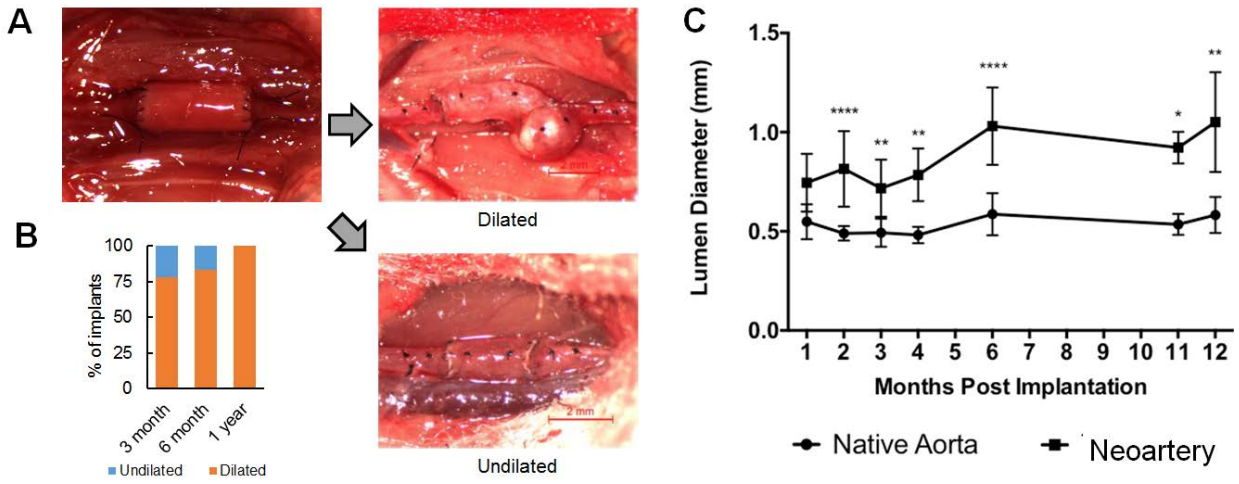

Figure 40. Dilation in Espun PGS-PVA^{Removed} PCL^{Sheath} grafts
A. *In situ* images of graft remodeling from day 0 (left) to 6 months post-implant (right column) show dilation in most grafts (top), with one graft remaining undilated (bottom). Red scale bar in right column images is 2 mm. Images taken by Tai Yi and Yong Ung-Lee. **B.** Incidence of graft dilation at each time point. Grafts demonstrating more than 25% increase in initial inner diameter ("dilated"; orange) increased proportionally at each time point, with 100% of grafts dilated at 1 year post-implant. **C.** Luminal diameter of neoarteries (square) and adjacent aorta (circle) over the time course of the study. Diameter was measured by non-invasive ultrasound at 1, 2, 3, 4, 6, 11, and 12 months post-implant. *'s indicate significant difference compared with the native aorta at that time point.

4.3.3 Espun PGS-PVA^{Removed} PCL^{Sheath} grafts limit cell infiltration and material resorption

Neotissue formed primarily on the luminal and abluminal surfaces of graft material, which partially resorbed over the course of 1 year (**Figure 41**). By 3 months post-implant, substantial neotissue formed on the luminal surface of grafts, but the graft material was largely retained

except in one graft. By 6 months post-implant, much graft material resorbed, but much persisted, and calcification was suspected in one animal. Material residues were still present at 1 year post-implant, with neotissue thickness varying both between and within explants. Grafts with larger dilations showed non-uniform wall thickness of residual graft material at 3 months.

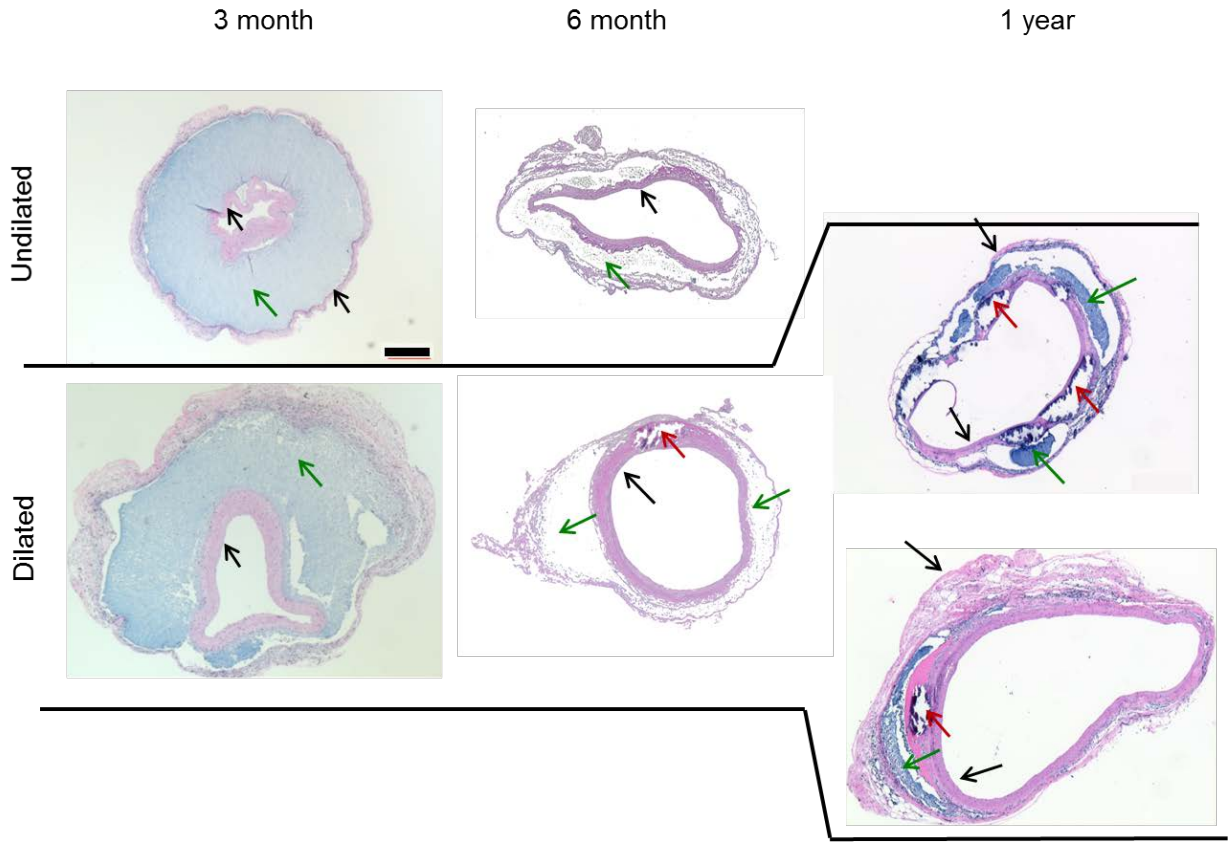

Figure 41. Neotissue formation and material residues in Espun PGS-PVA^{Removed} PCL^{Sheath} grafts
H&E staining of midgraft region of neoarteries at 3 months, 6 months and 1 year. Images are arranged according to their maximum level of dilation at any location in the neoartery. All images are set to the same scale (scale bar 200 µm). *At 3 months*, neotissue (black arrows) forms primarily on the luminal and abluminal surfaces of most grafts, and substantial quantities of graft material (green arrows) remain present. Graft remodeling is observed as nearly complete in only one animal, though some residues are still present. *At 6 months*, partial degradation of material is observed. White spaces represent the putative location of residual graft material, which likely fell out of sections during cutting. Calcification was suspected in some neoarteries (red arrow). *At 1 year*, some graft residues still remain, and putative calcification occurred at a higher frequency (red arrows).

4.3.4 Matrix architecture of neoarteries and adjacent aortas remodels over time

Matrix architecture in neoarteries and native aortas varied over the time course of the study, including between 6 months and 1 year. At 3 months post-implant, elastic fibers deposited in neoarteries in multiple layers with structural similarity to native arteries. However, elastic fiber organization regressed at 6 months and 1 year post-implant (**Figure 42**). Collagen deposition in neotissues was evident starting at 3 months post-implant, with no significant change in the ratio of densely packed vs. loosely packed collagen fibers over time. However, collagen composition of the adjacent abdominal aorta varied over the study time course. The ratio of densely packed collagen to looser collagen increased between 3 months and 6 months, then returned toward original values by 1 year post-implant (**Figure 43**).

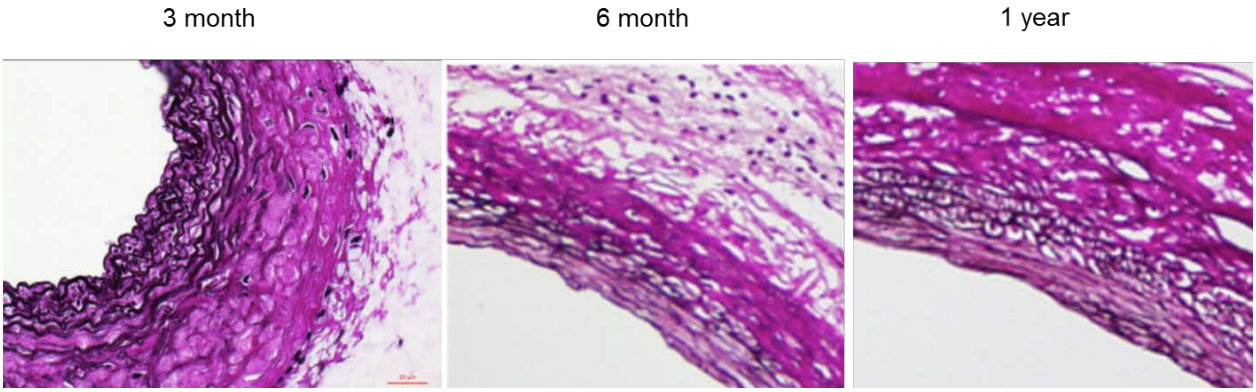

Figure 42. Elastic fiber organization in neotissues of Espun PGS-PVA^{Removed} PCL^{Sheath} grafts
Hart's staining of luminal neotissue in neoarteries at 3 months, 6 months, and 1 year post-implant. Elastic fibers stain dark purple. Modified from figure created by Cameron Best, Yong-Ung Lee, Tai Yi, and Ramak Khosravi; in preparation for [182].

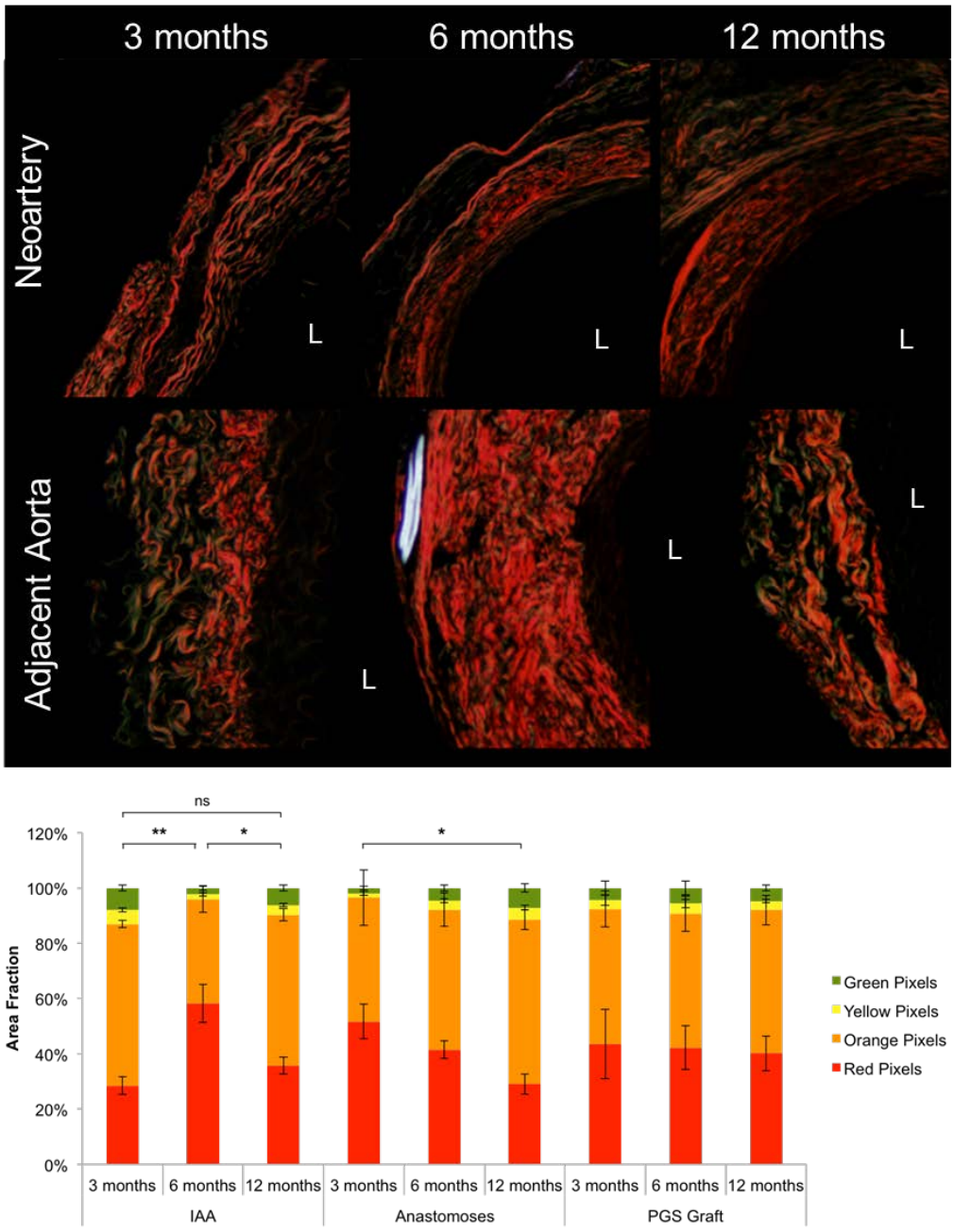

Figure 43. Collagen fiber density of neotissues in Espun PGS-PVA^{Removed} PCL^{Sheath} grafts
A. Picosirius Red (PSR) staining of neoarteries and adjacent infrarenal abdominal aortas at each time point. Under polarized light, stained collagen fibers appear as green, yellow, orange, or red; listed in order of increasing packing density. Images taken at 20x magnification. *L* indicates neoartery lumen. **B.** Quantification of the area fraction of each collagen fiber color in adjacent infrarenal aorta (IAA), neoartery at the anastomosis, and the midgraft region of the neoartery (PGS graft). In adjacent aorta (IAA), the area fraction of denser collagen fibers (orange and red) increased at 6 months, but then reverted to 3-month levels at 1 year. Neoartery collagen fibers retained 3-month densities over the course of 1 year. Values are mean ± SEM. *$p < 0.05$, **$p < 0.005$, ns indicates not significant. Modified from figure created by Ramak Khosravi and Cameron Best in preparation for [182].

4.3.5 Cell distribution, inflammation, and graft mineralization

Figure 44 summarizes the distribution of myofibroblasts (alpha-SMA$^+$, calponin$^-$, SM-MHC$^-$), contractile smooth muscle (alpha-SMA$^+$, calponin$^-$, SM-MHC$^+$), and macrophages (F4/80$^+$) in neoarteries. Graft luminal surface neotissue was rich in alpha-SMA positive cells and calponin positive cells at 3 months post-implant. Few of these cells were also positive for smooth muscle myosin heavy chain (SM-MHC), suggesting the majority are myofibroblasts or synthetic smooth muscle cells rather than contractile smooth muscle cells. The number of contractile smooth muscle cells increased from 3 to 6 months. By 12 months, SM-MHC-positive cells had re-organized into a densely packed layer near the luminal surface of the neoartery. Macrophages were sparsely distributed in neoarteries at 3 and 6 months post-implant, but dramatically increased in number by 1 year, and localized most densely in regions surrounding putative graft material residues. Mineralization also tended to co-localize in regions adjacent to putative graft materials. Mineralized regions positive for von Kossa stain were found in all 1-year neoarteries (3/3), with the majority of stain found at the periphery of white spaces likely to be graft residues which were lost during sectioning (**Figure 45**). Mineralization was also found in 1/3 grafts at 3 months and 6 months.

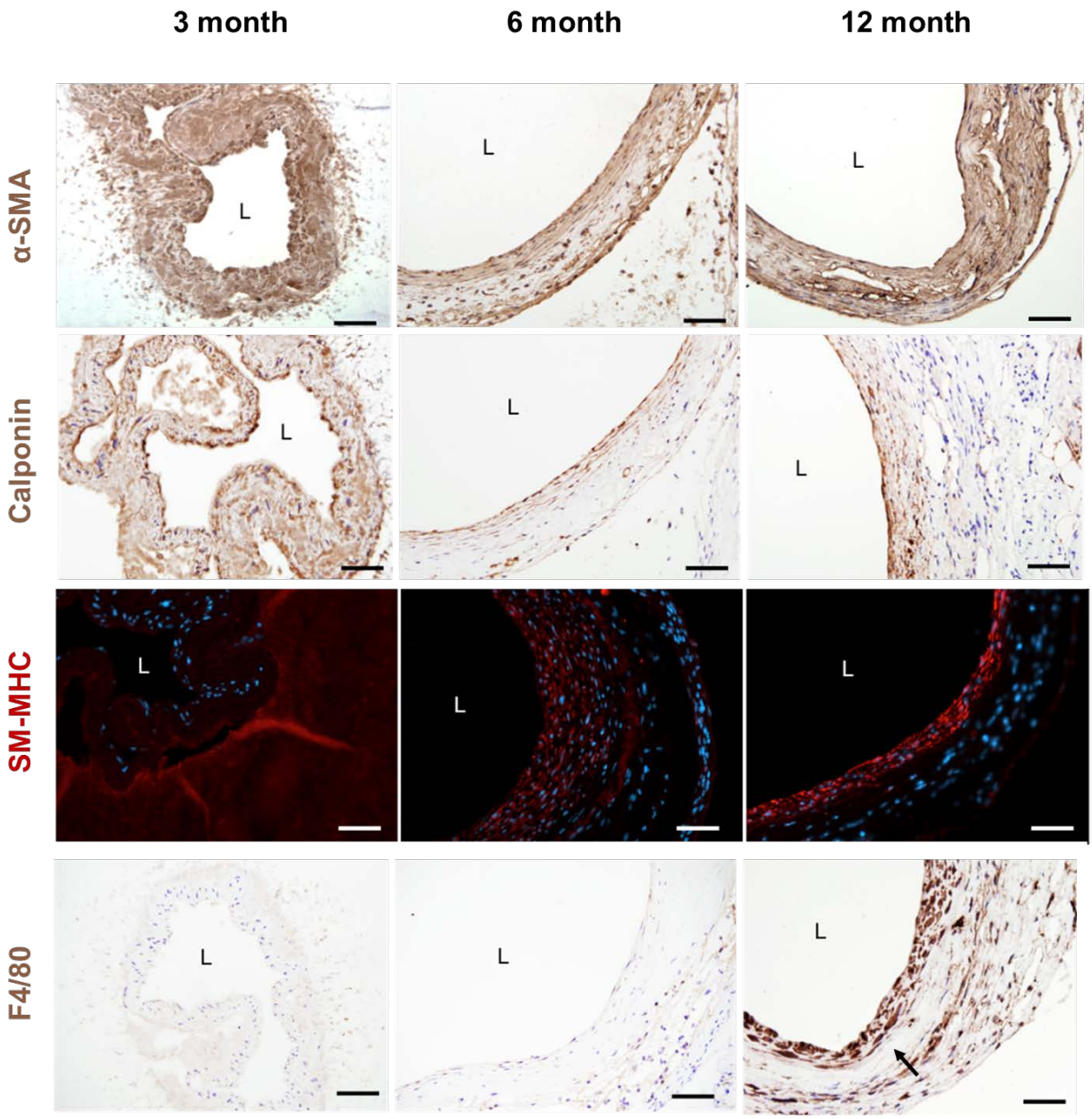

Figure 44. Cellular distribution in neotissues of Espun PGS-PVA^{Removed} PCL^{Sheath} grafts
Immunohistochemical and immunofluorescent staining of neoarteries for alpha-smooth muscle actin (α-SMA; brown), calponin (brown), smooth muscle myosin heavy chain (SM-MHC; red), and F4/80 (brown). *Top row*: α-SMA is present in the luminal surface of neotissues throughout the time course. *Second row*: calponin stains many cells in the luminal surface of neotissues, though it does not co-localize with all α-SMA^{+} cells. *Third row*: SM-MHC is sparse at 3 months post-implant, but is more common at 6 months, and becomes concentrated into several dense cellular layers by 1 year post-implant. *Bottom row*: F4/80 staining marks macrophages, which are sparse at 3 months and 6 months, but densely populate neoarteries at 1 year post-implant. F4/80 is most concentrated at the periphery of regions devoid of any stain (arrow), which are likely to be residual graft material which was lost during sectioning. L indicates vessel lumen.

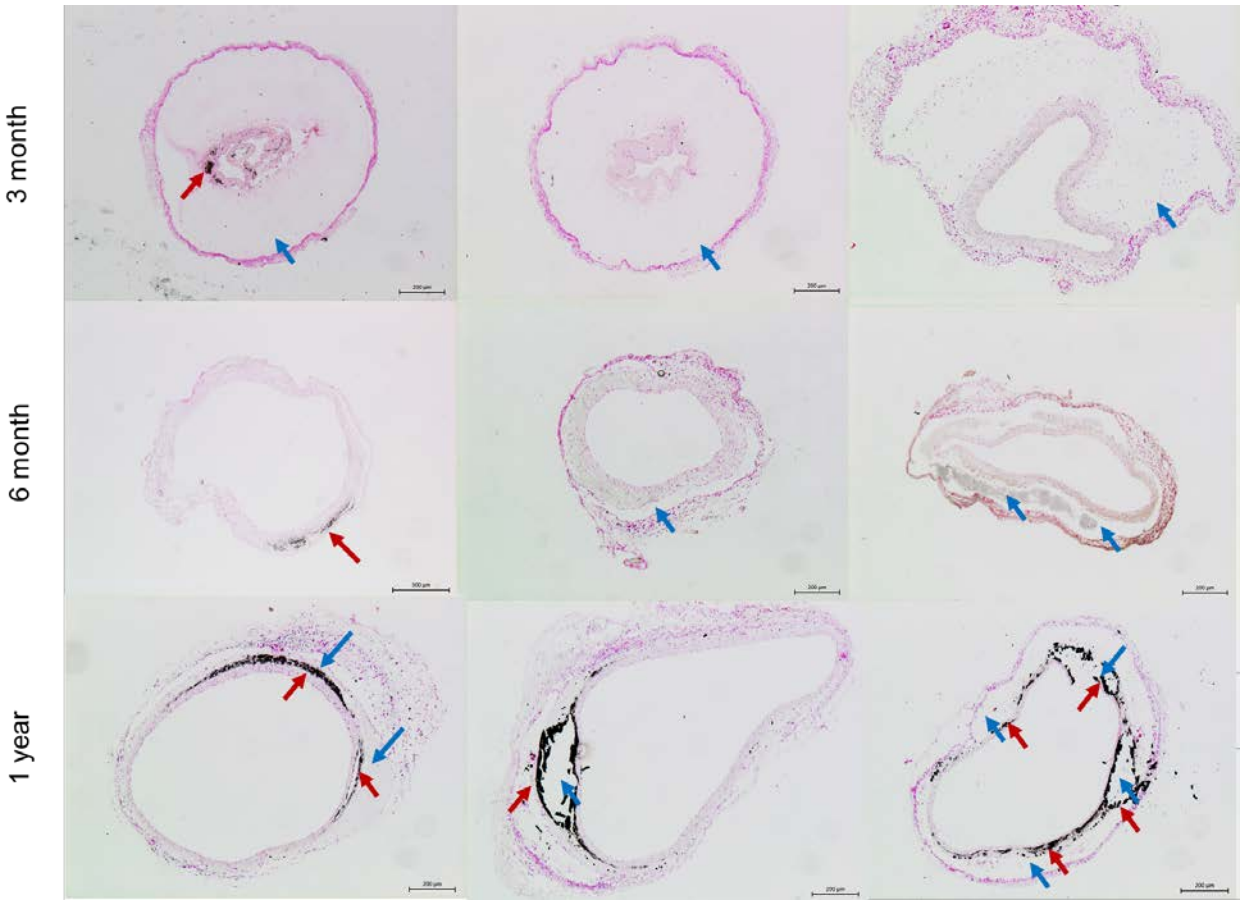

Figure 45. Mineralization in neotissues of Espun PGS-PVA^{Removed} PCL^{Sheath} grafts
von Kossa staining shows mineralization (black stain indicated by red arrows) in 5/9 neoarteries. Blue arrows denote the likely location of graft residual material. At 1 year post-implant (bottom row), all neoarteries show mineralization, with the majority co-localized with the edges of putative graft residues (blue arrows). Scale bars 200 µm, except for the 6 month neoartery with calcification, for which the scale is 500 µm. Modified from figure created by Cameron Best, Yong-Ung Lee, Tai Yi, and Ramak Khosravi; in preparation for [182].

4.4 DISCUSSION

This chapter summarizes our efforts to assess the *in vivo* performance of our electrospun designs for bio-inductive vascular grafts. Despite the advantages of electrospinning as a fabrication technique for vascular grafts, relatively few research groups have investigated such designs *in vivo* ([163] for review). We identified that the majority of materials used were slow-resorbing polymers. Some teams have also electrospun natural materials such as collagen and soluble elastin [183], or proteins which simulate their properties [184], in order to better stimulate the mechanical and biological properties of native arteries. Our design departs from the others tested in that it is made primarily from a fast-resorbing elastomer. Further, our material has already demonstrated *in vivo* hemocompatibility and fast-remodeling, as described in [118] and Chapter 2. Consequently, we expected our electrospun microfiber grafts to match or exceed the patency and remodeling potential of previously reported electrospun vascular grafts.

Low patency rates were seen in the first 32 implants, likely resultant from our surgeon's lack of microsurgery training or prior experience in the animal model. Consequently, we were unable to assess patency as a function of graft design in those implants. Further, in-host remodeling could only be assessed in the few patent grafts, which included only four samples split between two groups (Espun PGS-PLGA^{Intact} [n = 3 at 70 days], and Espun PGS-PLGA^{Removed} [n = 1 at 90 days]).

Espun PGS-PLGA^{Intact} and PGS-PLGA^{Removed} grafts extensively remodeled into neotissues with few material residues by 90 days post-implant. The mechanism of remodeling likely differs from that of SCPL PGS-PCL. Due to small pore size and fusion between fibers,

Espun PGS-PLGA^{Intact} and PGS-PLGA^{Removed} grafts likely limit the deposition of provisional matrix and initial myeloid cell infiltrate to the luminal and abluminal surfaces of the graft. Consequently, the total amount of provisional matrix and initial cellular infiltrate in the acute phase should be less in Espun PGS-PLGA$^{Intact\ or\ Removed}$ grafts than in SCPL PGS-PCL grafts. In turn, the capacity of Espun PGS-PLGA$^{Intact\ or\ Removed}$ grafts to recruit macrophages, synthetic cells, and stem/progenitor cells should be reduced. The result of lower early macrophage recruitment would likely be less subsequent recruitment of synthetic cells and other macrophages, and slower degradation of the graft material, which would be further slowed by the inability of recruited macrophages to infiltrate beneath the graft's outer surface until more surface erosion takes place. Fewer synthetic cells could reduce the rate of matrix deposition within the graft. The net result may be a slower graft remodeling process in Espun PGS-PLGA$^{Intact\ or\ Removed}$ than in SCPL PGS-PCL. Despite the likely slower remodeling process, Espun PGS-PLGA$^{Intact\ or\ Removed}$ grafts generated neovessels with few material residues remaining within 70 days. This result corroborates previous findings that nonporous but fast-resorbing vascular grafts can form neoarteries [113, 114, 139].

A slower remodeling process in Espun PGS-PLGA grafts may explain differences in resultant neoarteries compared to those formed from SCPL PGS-PCL grafts. The discrepancies included dilation, absence of elastin, and regions of dense matrix with few cells. Dilation could be a result of slower matrix deposition in Espun PGS-PLGA neoarteries. Slower material degradation may further limit matrix deposition; both espun PGS-PLGA^{Intact} and PGS-PLGA^{Removed} grafts are stiffer than SCPL PGS-PCL grafts, thereby shielding synthetic cells from physiological cyclic strains known to promote matrix deposition [26, 27] including insoluble elastin [28]. PGS has previously promoted elastin deposition *in vitro* [121, 185] and *in vivo* [118,

135], which is thought to be due to its similarity to arterial mechanical properties [185]. Stiffer PGS might not produce the same effect. In support of this hypothesis, we did detect elastin deposition in Espun PGS-PVA^{Removed} PCL^{Sheath} grafts, which are the closest to arteries in mechanical properties out of the electrospun grafts we implanted. However, these grafts were also implanted into a mouse rather than rat model, so direct comparisons to the other grafts should be made with caution. Alternatively, the absence of neoartery elastin in some electrospun grafts could also be due to differences in the ability of PGS-based microfibers to adsorb tropoelastin compared with SCPL PGS. This is an active area of investigation in the Weiss laboratory in collaboration with our own. Regions of dense matrix could be caused by several features of Espun PGS-PLGA-based grafts. Longer residence time of macrophages in the slow degrading graft could promote the formation of dense collagen-rich matrix seen in traditional foreign body responses [142]. Dense matrix deposition and reduction in cell density in the neomedia could also be secondary to aneurysmal dilatation, as both occur in the natural pathohistology of aortic aneurysms [186]. Toxicity from residual lysine triisocyante cross-linker or LiBr salt could have also contributed to cell death in these matrix-dense regions.

We applied PCL fiber sheaths to some microfiber grafts primarily to improve surgical handling by improving suture retention strength. Prior to conducting implantations, we also acknowledged that the PCL sheath may serve the additional function of providing mechanical support while the graft remodels. This structural safety net could protect grafts from dilation or aneurysm if the neotissue is unable to sustainably bear load as the graft core resorbs. However, our team had never tested this theory. Our previous use of SCPL PGS constrained our grafts to require PCL sheaths to render them suturable. By developing PGS microfibers with adequate surgical handling, we were able to implant some grafts without PCL sheaths for the first time.

Espun PGS-PLGA^{Intact} grafts demonstrated adequate surgical handling without a PCL sheath, and remodeled into neotissues with minimal graft residues remaining at 70 days post-implant. However, all PGS-PLGA^{Intact} neoarteries demonstrated substantial dilation. Similarly, the Espun PGS-PLGA^{Removed} graft also remodeled, but it dilated and formed an aneurysm at the distal anastomosis. Our tentative conclusion was that a PCL sheath is needed required prevent graft dilation in fast-remodeling bio-inductive grafts. Our initial attempts to apply a PCL sheath to Espun PGS-PLGA^{Removed} grafts compressed the PGS cores, causing buckling of the lumen during surgical manipulation. To reduce propensity buckling failure, we temporarily impregnated PGS cores with NaCl crystals prior to applying the PCL sheath, as described in **3.2.5**. This technique appeared to prevent buckling failure in Espun PGS-PVA^{Removed} PCL^{Sheath} grafts, which we selected for more extensive study.

Multiple time points and thorough histological characterization are required to understand the time course of graft inflammatory response, cell infiltration, and matrix deposition. For grafts 1 through 32, low patency rates prevented our team from attaining the sample sizes required to sacrifice at multiple times. In rodent interpositional vascular grafting, patency is largely a function of surgical technique. To improve patency rates, we began collaborating with a team of experienced microsurgeons in the Breuer laboratory at the Research Institute of Nationwide Children's Hospital. We provided the team with Espun PGS-PVA^{Removed} PCL^{Sheath} grafts, which was our most translatable graft design at the time. The team successfully implanted these grafts at 100% implant success and patency. This collaboration enabled graft patency and remodeling time course to be adequately assessed.

Espun PGS-PVA$^{\text{Removed}}$ PCL$^{\text{Sheath}}$ grafts formed artery-like neotissues on the luminal surface of grafts, which retained the majority of graft material at 3 months post-implant. The remodeling process was likely similar to that of Espun PGS-PLGA$^{\text{Intact or Removed}}$ grafts, except for three differences: (1) Graft material degradation was likely limited to the luminal surface, because the slow degrading PCL sheath likely limits phagocyte-mediated graft degradation on the abluminal surface of the graft; (2) The graft core material is substantially closer in Young's modulus to that of native arteries; and (3) There is minimal risk of toxicity from graft residues, as Espun PGS-PVA$^{\text{Removed}}$ PCL$^{\text{Sheath}}$ grafts contain no chemical cross-linkers or toxic salts, and are purified using water and ethanol.

Neotissue formation in Espun PGS-PVA$^{\text{Removed}}$ PCL$^{\text{Sheath}}$ grafts reflects these differences in the remodeling process from Espun PGS-PLGA$^{\text{Intact or Removed}}$ grafts. At 3 months, these neotissues contained elastic fibers, likely due to closer mechanical matching between graft material and native arteries. Neotissues in Espun PGS-PVA$^{\text{Removed}}$ PCL$^{\text{Sheath}}$ contained substantial quantities of α-SMA^{+} cells at 3 months post-implant, which are likely responsible for this elastic fiber production. α-SMA^{+} cells at 3 months likely include a combination of myofibroblasts (α-SMA^{+}, Calponin^{-}, SM-MHC^{-}) [187] and synthetic vascular smooth muscle cells (α-SMA^{+}, Calponin^{-}, SM-MHC^{-}) [188], with few contractile cells present (SM-MHC^{+}). [188]. Adult synthetic vascular smooth muscle cells have been shown to produce tropoelastin, the bulk component of elastin, as well as and fibrillin-1 *in vitro* [121]. Myofibroblasts may also produce elastic fiber components [189]. While elastic fiber formation at 3 months was encouraging, elastic fibers appeared less organized at 6 months and 12 months post-implant. Slowed material degradation may have contributed to fiber degeneration by prolonging the presence of macrophages. Macrophages can secrete MMP's and reactive oxygen species which

damage elastic fibers. [190, 191] At 1 year post-implant, macrophages ($F4/80^{+}$) dramatically increased in population, consistent with this theory.

At 1 year post-implant, many of the remaining α-SMA^{+} cells were also SM-MHC^{+}, suggesting their differentiation toward, or replacement with, contractile smooth muscle cells. Contractile smooth muscle produces negligible components of elastic fibers and is unlikely to sufficiently repair the damaged elastic network. The presence of contractile smooth muscle is encouraging from the perspective of avoiding stenosis by neointimal hyperplasia, as it is instead the synthetic phenotype that is responsible for proliferating and migrating into the neointima [188]. However, the presence of large quantities of macrophages at 1 year post-implant poses a risk for de-differentiation of contractile smooth muscle back toward synthetic phenotypes. In atherosclerosis, macrophages secrete PDGF which promotes smooth muscle migration and proliferation [191].

Dilation occurred at high incidence in Espun PGS-$PVA^{Removed}$ PCL^{Sheath} grafts. Dilation is a potentially serious complication, as in some cases dilation can lead to graft rupture or other aneurysmal pathologies. We were surprised to observe dilation at such high incidence, as we applied a slow-resorbing PCL sheath to the Espun PGS-$PVA^{Removed}$ core to prevent dilation. However, dilation of the graft's luminal neotissue could still occur in the presence of a non-dilating outer sheath. The cause of dilation was likely the gradual erosion of the luminal surface of the PGS-$PVA^{Removed}$ core, which subsequently allowed the neotissue on the graft's luminal surface to dilate. In this model, the graft's neotissue would continue to dilate until reaching the PCL sheath. Indeed, the dilation of neoartery inner diameter rarely exceeded the diameter of the PCL sheaths of the grafts (1.16 mm). Aneurysmal dilatation was observed in some grafts, which could be due to retraction of the PCL sheath at the anastomoses during surgical handling. To

prevent dilation in future designs, grafts could be constructed with reduced wall thickness of the core, thereby setting the PCL sheath to a diameter closer to the desired final diameter of the neoartery. Aneurysm at the anastomoses could be avoided by preventing delamination of the PCL sheath from the PGS core using biodegradable adhesive.

Despite the prevalence of graft dilation, most Espun PGS-PVA^{Removed} PCL^{Sheath} grafts demonstrated elastin-rich neotissues on their luminal surfaces at 3 months post-implant. Elastic fibers protect healthy arteries by conferring elastic recoil to arteries, thereby preventing dynamic tissue creep from arterial pressurization [192]. It is likely that despite its presence, the elastin was not mechanically functional. Indeed, in the case of nonfunctional elastin, neoarteries would be prone to dilation by collagen fatigue [193]. Residual PGS graft material is also prone to creep in this graft design, as we found Espun PGS-PVA^{Removed} cores to deform plastically at the thermal cross-linking conditions used in this study [169].

Calcification was observed in all Espun PGS-PVA^{Removed} PCL^{Sheath} grafts, and was most prevalent at 1 year post-implant. Calcification was most prevalent along the surface of residual graft material, co-localized with both F4/80^{+} macrophages and α-SMA^{+} myofibroblasts and smooth muscle cells. One potential mechanism is smooth muscle cell transdifferentiation into chondrocytes, as observed in atherosclerosis and by de Valence et al in electrospun PCL vascular grafts [138]. The co-localized macrophages may be driving the process by mediating smooth muscle apoptosis and transdifferentiation into osteoblast-like cells, as occurs in atherosclerosis [194, 195].

We originally hypothesized that electrospun microfibrous vascular grafts made with PGS would retain the excellent long-term performance observed by the SCPL PGS-PCL design. Taken together, our results refute this hypothesis. However, the findings do not necessarily refute

our central hypothesis that grafts must remodel rapidly to form functional neoarteries rather than a traditional foreign body response. Rather, these results clarify that pore size likely determines the rate at which grafts can remodel. Thus the central hypothesis can be refined to state that in order for a vascular graft to remodel rapidly, it must (1) be comprised of a material with the capacity to degrade rapidly *in vivo*, and (2) it must possess pores large enough for phagocytic cells to infiltrate in sufficient number to realize such rapid degradation.

4.5 LIMITATIONS AND FUTURE DIRECTIONS

Future work will address the limitations of this study. The rate of graft remodeling was likely limited in all microfiber grafts by small pore size. Increasing pore size would increase the number of cells captured by the graft, thereby improving the rate at which neotissue forms and graft material resorbs [163]. Restoring pore size to that of SCPL PGS-PCL grafts (21 μm diameter) would likely restore the rate and quality of graft remodeling. Efforts are currently underway to increase pore size by altering electrospinning parameters. In new unimplanted second generation designs, we have already demonstrated that pore size can be doubled by tuning electrospinning parameters (**Figure 46**). PGS microfibers made from PVA blends resorbed substantially slower than those made from PLGA blends. PVA blends had the simplest and most rapid fabrication with the least potential for cytotoxicity, so efforts to accelerate their *in vivo* degradation could yield the most translatable graft. In addition to increasing pore size, reducing the curing temperature can also accelerate hydrolytic degradation rate (**Figure 47**). Consequently, we are constructing our second generation PVA-based microfiber grafts using

thermal crosslinking at 120 ºC for 48 h. Fibers made at this curing condition also have the added benefit of elastic deformation [169], thus providing additional resistance to aneurysmal dilatation.

Early stage graft remodeling is unknown, as the present study did not investigate the graft remodeling process earlier than 70 days post-implant. Assessing graft remodeling within this window could provide crucial insights into the mechanics of neotissue formation. The role of inflammatory cells in particular should be analyzed, as work by the Breuer laboratory has suggested that infiltrating macrophages promote neotissue formation and improve patency by releasing cytokines and growth factors [158]. The origin and retention of cells populating the neoartery is also unclear in the present study. Methods such as bone marrow labeling could track the proportion of cells that come from circulation, as well as their long-term retention. Lastly, the true *in vivo* performance of Espun PGS-PLGA$^{\text{Intact or Remodeled}}$ grafts is unknown, as the surgeon who performed those implantations used a technique with high complication rates. Providing this graft design to the Nationwide Children's Hospital team could elucidate *in vivo* performance, but we chose to forego such testing because PLGA blends are limited in translational potential by their lengthy fabrication method and potential for cytotoxicity.

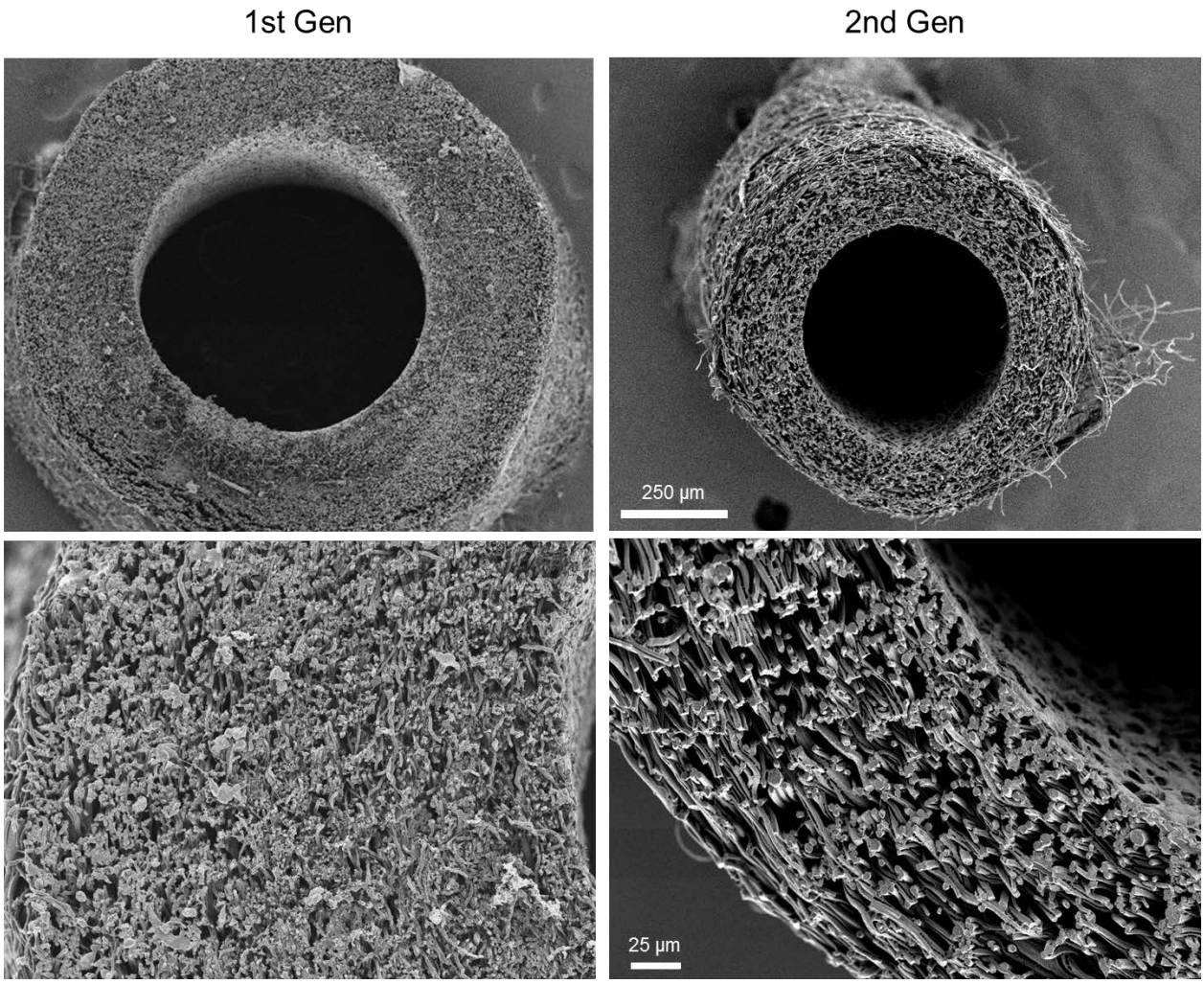

Figure 46. Comparison of 1st and 2nd generation Espun PGS-PVA^{Removed} grafts
SEM images compare the structure of first generation electrospun grafts (1st gen; left) with a second generation design (2nd gen; right) optimized for remodeling potential and surgical handling. Magnification is identical in each row, allowing for side-by-side comparison of geometry. Second generation grafts demonstrate substantially increased pore size to enhance cell infiltration, and have reduced inner diameter and wall thickness to better match the native mouse aorta. Scale bar 250 µm for first row, and 25 µm for second row.

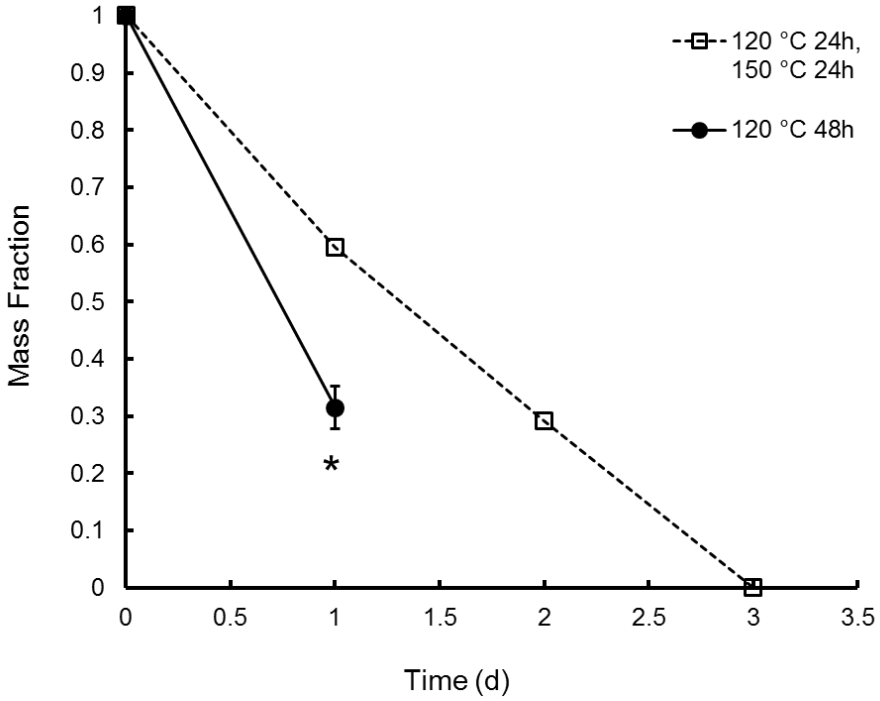

Figure 47. Effect of curing conditions on hydrolytic degradation of Espun PGS-PVA^{Removed} microfibers
Fraction of mass remaining (mass fraction) vs. incubation time for Espun PGS-PVA^{Removed} microfibers thermally cross-linked under first generation conditions (120 ºC 24h, 150 ºC 24h; square with dotted line) and second generation conditions (120 ºC 48h; circle with solid line). Disks of graft cores were incubated in pH 11.75 buffer at 37 °C with agitation to accelerate hydrolysis *in vitro*. 2nd gen microfibers resorbed at twice the rate of 1st gen microfibers in these conditions. Error bars represent standard deviation. Error bars are not shown for 1st gen grafts, as they are smaller than the markers used. *$P < 0.01$.

4.6 CONCLUSION

This chapter investigated the *in vivo* performance of the electrospun PGS grafts developed in Chapter 3. Electrospun grafts demonstrated substantial *in-host* remodeling, but did not replicate the likeness to native arteries realized by the SCPL PGS-PCL design. Small pore size likely prevented cell infiltration in all microfiber designs, and may explain the persistence of graft residues in Espun PGS-PVA^{Removed} PCL^{Sheath} microfiber designs. Increasing pore size and

adjusting thermal crosslinking conditions might restore the fast-remodeling potential of these grafts. Preventing PCL sheath disruption at the anastamoses could also protect grafts from aneurysmal dilatation. These future directions are areas of active investigation by our laboratory. Their successful implementation could restore the fast-remodeling potential of the grafts, thereby empowering us to leverage the potential translational advantages that microfiber grafts hold over SCPL vascular grafts.

5.0 OUTLOOK AND FINAL SUMMARY

The long-term objective of this body of work is to improve the clinical performance of vascular grafts. To achieve this objective, we employed next generation materials to revitalize a strategy developed by a previous generation: fast-remodeling bio-inductive vascular grafts. After proving the concept in 2012, our short term objective became to investigate the translational potential of our fast-remodeling bio-inductive design. To this end we began an iterative process of performance testing and redesign, with usability and fabrication throughput as new design criteria.

The work described in this dissertation represents 1.5 cycles of the iterative design and validation process. Herein we tested the long-term performance of our initial prototype (Chapter 2), adjusted the design for enhanced usability and fabrication throughput (Chapter 3), and repeated performance testing (Chapter 4). We succeeded in improving surgical handling and fabrication throughput, but at the cost of *in vivo* performance. Further iterations are required to concurrently realize favorable performance, usability, and ease of fabrication. This dissertation represents an important first step in design optimization which critically informs the next set of experiments. Importantly, our findings should also constructively influence others pursuing bio-inductive vascular graft designs, as well as impact the broader fields of tissue engineering and regenerative medicine.

5.1 SCPL PGS COMPOSITES - IMPACT AND OUTLOOK

We previously demonstrated that fast-resorbing bio-inductive vascular grafts made with SCPL PGS remodel into neoarteries with few material residues retained within 3 months [118]. In this dissertation, we further demonstrated that neoartery remodeling continues between 3 months and 1 year, despite the presence of elastin, mechanical compliance, and the absence of most graft materials. This key cautionary finding should influence others in the field to extend the duration of their *in vivo* experiments, as it suggests that neoarteries continue to remodel long after the majority of material residues resorb. The difference in short-term and long-term results may be even more pronounced in patients with cardiovascular disease, whose native arteries remodel pathologically without insult.

Despite favorable performance, the translational potential of SCPL PGS is low. We quantified the limitations of SCPL fabrication in Chapter 2 (**Figure 34**). While SCPL PGS may have limited translational potential, it has virtually unlimited research potential. In the hands of an experienced microsurgeon, composite vascular grafts containing SCPL achieve near-ideal *in situ* remodeling in small animals. Understanding this process could empower the field to reproduce or improve it in more translatable graft designs. Determining the identity, origin, and role of each participating cell type would enable rational design of strategies to induce or enhance these processes in translatable grafts.

To ensure that findings in SCPL grafts are relevant to the clinical situation, future studies should supplement the rat abdominal aorta interposition model with more clinically relevant animal models. Aged animals with cardiovascular disease, diabetes, and/or renal dysfunction should be used to simulate various clinical situations, and are likely to demonstrate altered *in situ* remodeling processes. Large animal models also better simulate human hemodynamics and

healing potential, although there is debate about which best represents the clinical situation. Also critical to simulate is clinically relevant vascular graft lengths, which are on the order of many inches to feet. Long grafts are difficult to fabricate with SCPL PGS, as crack-like defects form at a rate that scales with length and thickness. To simulate remodeling in the central region of long grafts, shorter SCPL grafts could be implanted in a novel rat model. The model anastomoses a loop of ePTFE graft to each aortic stump, then bridges the gap between ePTFE grafts with the test graft. The ePTFE loops prevent host cells at the native aorta anastomoses from migrating into the graft, thereby simulating the clinical situation presented at the central region of long vascular graft [196]. This model could provide crucial *in vivo* insights, but is no substitute for implanting long grafts in a large animal. Our impending need to produce longer grafts was a major driver for our pursuit of more versatile graft fabrication methods.

5.2 ESPUN PGS MICROFIBER COMPOSITE - IMPACT AND OUTLOOK

In Chapter 3 we demonstrated that electrospinning microfiber fabrication improves the surgical handling, fabrication throughput, and reproducibility of microfibrous PGS vascular grafts. This achievement enabled us to develop and implant novel vascular graft designs with handling and fabrication advantages over SCPL composite grafts, as described in Chapter 4. Importantly, electrospinning also enables us to fabricate larger and longer vascular grafts for large animal studies, which are substantially more challenging to construct from SCPL structures. More broadly, facile construction of electrospun PGS microfibers could profoundly impact the fields of biomaterials, tissue engineering, and regenerative medicine. To our knowledge, this technique is the first to yield PGS scaffolds capable of withstanding the suture anchoring and tensile

loading required of most *in vivo* applications [169]. PGS has long been considered a desirable biomaterial for soft tissue applications due to its soft and elastic mechanical properties, rapid resorption *in vivo* by surface erosion, biocompatibile degradation products, and muted inflammatory response [162]. Facile implantation of PGS microfibers will empower the scientific community to apply PGS toward solving a range of medical problems.

Our *in vivo* performance study in Chapter 4 demonstrated both constructive and pathological remodeling in microfibrous PGS grafts. This is clearly a reduction in performance compared with the original SCPL design. The key difference in graft properties between electrospun PGS and SCPL PGS is reduced porosity (47.1 vs. 81.1%) and pore size (1.87 vs. 21.2 μm), which likely inhibited cell infiltration and thereby slowed material resorption and induced chronic inflammation in microfibrous PGS. By demonstrating the importance of pore size even in fast-resorbing materials, this work should inform the design of other fast-resorbing bio-inductive implants. In light of the limited neotissue formation of electrospun PGS-based grafts, the SCPL PGS-PCL composite graft developed in Aim 1 remains the best-performing graft of all those developed in this dissertation work. However, we expect that with increased pore size, microfibrous PGS grafts can supersede SCPL PGS-PCL grafts in translational potential. Increasing pore size in electrospun PGS grafts should enhance cell infiltration, thereby enabling graft remodeling to approach or match that seen in SCPL PGS-PCL grafts, whilst retaining the advantages of electrospinning fabrication. **Table 9** summarizes the advantages and limitations of each graft developed in this work, and includes recommended strategies for overcoming each limitation. Our team is already applying our learnings to the next graft design. At present we are leveraging the versatility of electrospinning to increase porosity and pore size,

which could improve the in-host remodeling in the electrospun PGS-PVA^{Removed}-PCL grafts (**Figure 46**).

Table 9. Summary of graft designs

Graft*	Core	Sheath	Advantages	Limitations	Mitigation Strategies
SCPL PGS-PCL	SCPL PGS	Electrospun PCL micro- and nano-fibers	Cell infiltration	Requires gentle surgical handling	Thicken PCL sheath
			Rapid material clearance	High rate of fabrication defects	Process development for SCPL technique
			Constructive graft remodeling	Fabrication requires manual labor	Process development and quality control strategies for SCPL technique
				Neoartery compliance and tissue architecture differs from native	Modulate cell infiltration and matrix deposition with local protein delivery
Electrospun PGS-PVA^{Removed}-PCL	Electrospun PGS with PVA carrier removed	Electrospun PCL micro- and nano-fibers	Surgical handling	Cell infiltration	Increase pore size
				Slow material degradation	Increase phagocyte infiltration – by increasing pore size
			Simplest fabrication	Dilation	Increase matrix deposition – by increasing synthetic cell infiltration – by increasing pore size
					Reduce wall thickness of core
				Calcification at 1 year post-implant	Ensure material resorption by 1 year - by increasing synthetic cell infiltration – by increasing pore size
Electrospun PGS-PLGA^{Intact}	Electrospun PGS with PLGA carrier intact	None	Simpler fabrication than SCPL PGS-PCL	Thrombosis (blood compatibility unknown)	Blood compatibility testing
					Antithrombogenic surface modification
				Compliance mismatch	Remove PLGA
				Cytotoxicity (isocyanate and LiBr)	Additional water and ethanol washes to quench isocyanate and remove leachables
				Limited cell infiltration	Increase pore size
					Reduce fiber fusion – by increasing ratio of PLGA to PGS in blend
				Dilation	Increase matrix deposition – by increasing synthetic cell infiltration – by increasing pore size
					Reduce wall thickness of core
Electrospun PGS-PLGA^{Removed}	Electrospun PGS with PLGA carrier removed	None	Simpler fabrication than SCPL PGS-PCL	Suture pull-through during implantation	Apply PCL sheath
				Limited cell infiltration	Increase pore size
					Reduce fiber fusion – by increasing ratio of PLGA to PGS in blend
				Dilation	Increase matrix deposition – by increasing synthetic cell infiltration – by increasing pore size
					Reduce wall thickness of core
				Thrombosis (blood compatibility unknown)	Blood compatibility testing
					Antithrombogenic surface modification

*Listed in descending order of potential for clinical translation

5.3 FINAL SUMMARY

The ideal vascular graft should be readily available at low cost, yet perform as well as a living artery. A cell-free, fast-remodeling bio-inductive vascular graft could fit these criteria and profoundly improve upon current graft performance. First-generation designs of fast-resorbing vascular grafts are already in human clinical trials, indicating that a range of stakeholders embrace the clinical promise of a bio-inductive design. The work in this dissertation represents an important step forward in our efforts to understand and improve the translational potential of a PGS-based bio-inductive vascular graft. Insights from this work will help our team and others to improve designs for vascular grafts and other implants. Our team has already begun applying our learnings toward a next generation electrospun design which could realize the performance, usability, and fabrication criteria required for clinical translation. Though further design iterations are undoubtedly required, this dissertation work brings the research community closer to delivering an impactful solution to a major clinical problem.

BIBLIOGRAPHY

1. Conte MS. The ideal small arterial substitute: a search for the Holy Grail? FASEB J 1998;12:43-5.

2. Go AS, Mozaffarian D, Roger VL, Benjamin EJ, Berry JD, Blaha MJ, et al. Heart disease and stroke statistics--2014 update: a report from the American Heart Association. Circulation 2014;129:e28-e292.

3. Rowe VL, Lee W, Weaver FA, Etzioni D. Patterns of treatment for peripheral arterial disease in the United States: 1996-2005. J Vasc Surg 2009;49:910-7.

4. Roy-Chaudhury P, Sukhatme VP, Cheung AK. Hemodialysis vascular access dysfunction: a cellular and molecular viewpoint. J Am Soc Nephrol 2006;17:1112-27.

5. Archie JP, Jr. Femoropopliteal bypass with either adequate ipsilateral reversed saphenous vein or obligatory polytetrafluoroethylene. Ann Vasc Surg 1994;8:475-84.

6. Nicoloff AD, Taylor LM, Jr., McLafferty RB, Moneta GL, Porter JM. Patient recovery after infrainguinal bypass grafting for limb salvage. J Vasc Surg 1998;27:256-63; discussion 64-6.

7. Norgren L, Hiatt WR, Dormandy JA, Nehler MR, Harris KA, Fowkes FG, et al. Inter-Society Consensus for the Management of Peripheral Arterial Disease (TASC II). Eur J Vasc Endovasc Surg 2007;33 Suppl 1:S1-75.

8. Goldman S, Zadina K, Moritz T, Ovitt T, Sethi G, Copeland JG, et al. Long-term patency of saphenous vein and left internal mammary artery grafts after coronary artery bypass surgery: results from a Department of Veterans Affairs Cooperative Study. J Am Coll Cardiol 2004;44:2149-56.

9. Desai M, Seifalian AM, Hamilton G. Role of prosthetic conduits in coronary artery bypass grafting. Eur J Cardiothorac Surg 2011;40:394-8.

10. Suckow BD, Kraiss LW, Stone DH, Schanzer A, Bertges DJ, Baril DT, et al. Comparison of graft patency, limb salvage, and antithrombotic therapy between prosthetic and autogenous below-knee bypass for critical limb ischemia. Ann Vasc Surg 2013;27:1134-45.

11. Faries PL, Logerfo FW, Arora S, Hook S, Pulling MC, Akbari CM, et al. A comparative study of alternative conduits for lower extremity revascularization: all-autogenous conduit versus prosthetic grafts. J Vasc Surg 2000;32:1080-90.

12. Kapadia MR, Popowich DA, Kibbe MR. Modified prosthetic vascular conduits. Circulation 2008;117:1873-82.

13. Writing Group M, Lloyd-Jones D, Adams RJ, Brown TM, Carnethon M, Dai S, et al. Heart disease and stroke statistics--2010 update: a report from the American Heart Association. Circulation 2010;121:e46-e215.

14. Shinoka T, Breuer C. Tissue-engineered blood vessels in pediatric cardiac surgery. Yale J Biol Med 2008;81:161-6.

15. Petrossian E, Reddy VM, Collins KK, Culbertson CB, MacDonald MJ, Lamberti JJ, et al. The extracardiac conduit Fontan operation using minimal approach extracorporeal circulation: early and midterm outcomes. J Thorac Cardiovasc Surg 2006;132:1054-63.

16. Huynh TT, Pham M, Griffin LW, Villa MA, Przybyla JA, Torres RH, et al. Management of distal femoral and popliteal arterial injuries: an update. Am J Surg 2006;192:773-8.

17. Fox CJ, Gillespie DL, O'Donnell SD, Rasmussen TE, Goff JM, Johnson CA, et al. Contemporary management of wartime vascular trauma. J Vasc Surg 2005;41:638-44.

18. Da Lio AL, Jones NF. New concepts and materials in microvascular grafting: prosthetic graft endothelial cell seeding and gene therapy. Microsurgery 1998;18:263-6.

19. Bassiouny HS, White S, Glagov S, Choi E, Giddens DP, Zarins CK. Anastomotic intimal hyperplasia: mechanical injury or flow induced. J Vasc Surg 1992;15:708-16; discussion 16-7.

20. Bergamini TM, Bandyk DF, Govostis D, Kaebnick HW, Towne JB. Infection of vascular prostheses caused by bacterial biofilms. J Vasc Surg 1988;7:21-30.

21. Sabik JF, 3rd. Understanding saphenous vein graft patency. Circulation 2011;124:273-5.

22. Ramcharan KS, Lip GY, Stonelake PS, Blann AD. The endotheliome: a new concept in vascular biology. Thromb Res 2011;128:1-7.

23. Weinberg CB, Bell E. A blood vessel model constructed from collagen and cultured vascular cells. Science 1986;231:397-400.

24. Girton TS, Oegema TR, Tranquillo RT. Exploiting glycation to stiffen and strengthen tissue equivalents for tissue engineering. J Biomed Mater Res 1999;46:87-92.

25. Ogle BM, Mooradian DL. Manipulation of remodeling pathways to enhance the mechanical properties of a tissue engineered blood vessel. J Biomech Eng 2002;124:724-33.

26. Seliktar D, Black RA, Vito RP, Nerem RM. Dynamic mechanical conditioning of collagen-gel blood vessel constructs induces remodeling in vitro. Ann Biomed Eng 2000;28:351-62.

27. Seliktar D, Nerem RM, Galis ZS. Mechanical strain-stimulated remodeling of tissue-engineered blood vessel constructs. Tissue Eng 2003;9:657-66.

28. Isenberg BC, Tranquillo RT. Long-term cyclic distention enhances the mechanical properties of collagen-based media-equivalents. Ann Biomed Eng 2003;31:937-49.

29. Berglund JD, Mohseni MM, Nerem RM, Sambanis A. A biological hybrid model for collagen-based tissue engineered vascular constructs. Biomaterials 2003;24:1241-54.

30. Matsuda T, He H. Newly designed compliant hierarchic hybrid vascular grafts wrapped with a microprocessed elastomeric film--I: Fabrication procedure and compliance matching. Cell Transplant 2002;11:67-74.

31. Hirai J, Kanda K, Oka T, Matsuda T. Highly oriented, tubular hybrid vascular tissue for a low pressure circulatory system. ASAIO J 1994;40:M383-8.

32. He H, Matsuda T. Newly designed compliant hierarchic hybrid vascular graft wrapped with microprocessed elastomeric film--II: Morphogenesis and compliance change upon implantation. Cell Transplant 2002;11:75-87.

33. Grassl ED, Oegema TR, Tranquillo RT. A fibrin-based arterial media equivalent. J Biomed Mater Res A 2003;66:550-61.

34. Long JL, Tranquillo RT. Elastic fiber production in cardiovascular tissue-equivalents. Matrix Biol 2003;22:339-50.

35. Ahmann KA, Weinbaum JS, Johnson SL, Tranquillo RT. Fibrin degradation enhances vascular smooth muscle cell proliferation and matrix deposition in fibrin-based tissue constructs fabricated in vitro. Tissue Eng Part A 2010;16:3261-70.

36. Syedain ZH, Tranquillo RT. TGF-beta1 diminishes collagen production during long-term cyclic stretching of engineered connective tissue: implication of decreased ERK signaling. J Biomech 2011;44:848-55.

37. Isenberg BC, Williams C, Tranquillo RT. Endothelialization and flow conditioning of fibrin-based media-equivalents. Ann Biomed Eng 2006;34:971-85.

38. Syedain ZH, Meier LA, Bjork JW, Lee A, Tranquillo RT. Implantable arterial grafts from human fibroblasts and fibrin using a multi-graft pulsed flow-stretch bioreactor with noninvasive strength monitoring. Biomaterials 2011;32:714-22.

39. Syedain ZH, Weinberg JS, Tranquillo RT. Cyclic distension of fibrin-based tissue constructs: evidence of adaptation during growth of engineered connective tissue. Proc Natl Acad Sci U S A 2008;105:6537-42.

40. Swartz DD, Russell JA, Andreadis ST. Engineering of fibrin-based functional and implantable small-diameter blood vessels. Am J Physiol Heart Circ Physiol 2005;288:H1451-60.

41. Tschoeke B, Flanagan TC, Koch S, Harwoko MS, Deichmann T, Ella V, et al. Tissue-engineered small-caliber vascular graft based on a novel biodegradable composite fibrin-polylactide scaffold. Tissue Eng Part A 2009;15:1909-18.

42. Koch S, Flanagan TC, Sachweh JS, Tanios F, Schnoering H, Deichmann T, et al. Fibrin-polylactide-based tissue-engineered vascular graft in the arterial circulation. Biomaterials 2010;31:4731-9.

43. Syedain ZH, Meier LA, Lahti MT, Johnson SL, Tranquillo RT. Implantation of completely biological engineered grafts following decellularization into the sheep femoral artery. Tissue engineering Part A 2014;20:1726-34.

44. Meier LA, Syedain ZH, Lahti MT, Johnson SS, Chen MH, Hebbel RP, et al. Blood outgrowth endothelial cells alter remodeling of completely biological engineered grafts implanted into the sheep femoral artery. J Cardiovasc Transl Res 2014;7:242-9.

45. Remuzzi A, Mantero S, Colombo M, Morigi M, Binda E, Camozzi D, et al. Vascular smooth muscle cells on hyaluronic acid: culture and mechanical characterization of an engineered vascular construct. Tissue Eng 2004;10:699-710.

46. Soffer L, Wang X, Zhang X, Kluge J, Dorfmann L, Kaplan DL, et al. Silk-based electrospun tubular scaffolds for tissue-engineered vascular grafts. J Biomater Sci Polym Ed 2008;19:653-64.

47. Zhang X, Wang X, Keshav V, Johanas JT, Leisk GG, Kaplan DL. Dynamic culture conditions to generate silk-based tissue-engineered vascular grafts. Biomaterials 2009;30:3213-23.

48. Lovett M, Eng G, Kluge JA, Cannizzaro C, Vunjak-Novakovic G, Kaplan DL. Tubular silk scaffolds for small diameter vascular grafts. Organogenesis 2010;6:217-24.

49. Yang D, Guo T, Nie C, Morris SF. Tissue-engineered blood vessel graft produced by self-derived cells and allogenic acellular matrix: a functional performance and histologic study. Ann Plast Surg 2009;62:297-303.

50. Neff LP, Tillman BW, Yazdani SK, Machingal MA, Yoo JJ, Soker S, et al. Vascular smooth muscle enhances functionality of tissue-engineered blood vessels in vivo. J Vasc Surg 2011;53:426-34.

51. Niklason LE, Gao J, Abbott WM, Hirschi KK, Houser S, Marini R, et al. Functional arteries grown in vitro. Science 1999;284:489-93.

52. Quint C, Kondo Y, Manson RJ, Lawson JH, Dardik A, Niklason LE. Decellularized tissue-engineered blood vessel as an arterial conduit. Proc Natl Acad Sci U S A 2011;108:9214-9.

53. Dahl SL, Kypson AP, Lawson JH, Blum JL, Strader JT, Li Y, et al. Readily available tissue-engineered vascular grafts. Sci Transl Med 2011;3:68ra9.

54. ClinicalTrials.gov. Evaluation of the Safety and Efficacy of a Vascular Prosthesis as an Above-Knee Bypass Graft in Patients With Peripheral Arterial Disease: National Library of Medicine, National Institutes of Health; 2015 [cited 2015 May 24, 2015]. Available from: https://clinicaltrials.gov/ct2/show/NCT01872208.

55. ClinicalTrials.gov. Evaluation of the Safety and Efficacy of a Vascular Prosthesis for Hemodialysis Access in Patients With ESRD 2015 [cited 2005 May 24]. Available from: https://clinicaltrials.gov/ct2/show/NCT01744418.

56. ClinicalTrials.gov. Safety and Efficacy of a Vascular Prosthesis for Hemodialysis Access in Patients With End-Stage Renal Disease 2015 [May 24, 2015]. Available from: https://clinicaltrials.gov/ct2/show/NCT01840956.

57. Hoerstrup SP, Cummings Mrcs I, Lachat M, Schoen FJ, Jenni R, Leschka S, et al. Functional growth in tissue-engineered living, vascular grafts: follow-up at 100 weeks in a large animal model. Circulation 2006;114:I159-66.

58. Kelm JM, Emmert MY, Zurcher A, Schmidt D, Begus Nahrmann Y, Rudolph KL, et al. Functionality, growth and accelerated aging of tissue engineered living autologous vascular grafts. Biomaterials 2012;33:8277-85.

59. Shinoka T, Shum-Tim D, Ma PX, Tanel RE, Isogai N, Langer R, et al. Creation of viable pulmonary artery autografts through tissue engineering. J Thorac Cardiovasc Surg 1998;115:536-45; discussion 45-6.

60. Shin'oka T, Imai Y, Ikada Y. Transplantation of a tissue-engineered pulmonary artery. N Engl J Med 2001;344:532-3.

61. Watanabe M, Shin'oka T, Tohyama S, Hibino N, Konuma T, Matsumura G, et al. Tissue-engineered vascular autograft: inferior vena cava replacement in a dog model. Tissue Eng 2001;7:429-39.

62. Mirensky TL, Nelson GN, Brennan MP, Roh JD, Hibino N, Yi T, et al. Tissue-engineered arterial grafts: long-term results after implantation in a small animal model. J Pediatr Surg 2009;44:1127-32; discussion 32-3.

63. Nelson GN, Mirensky T, Brennan MP, Roh JD, Yi T, Wang Y, et al. Functional small-diameter human tissue-engineered arterial grafts in an immunodeficient mouse model: preliminary findings. Arch Surg 2008;143:488-94.

64. Cho SW, Lim SH, Kim IK, Hong YS, Kim SS, Yoo KJ, et al. Small-diameter blood vessels engineered with bone marrow-derived cells. Ann Surg 2005;241:506-15.

65. Zhao Y, Zhang S, Zhou J, Wang J, Zhen M, Liu Y, et al. The development of a tissue-engineered artery using decellularized scaffold and autologous ovine mesenchymal stem cells. Biomaterials 2010;31:296-307.

66. Krawiec JT, Vorp DA. Adult stem cell-based tissue engineered blood vessels: a review. Biomaterials 2012;33:3388-400.

67. Brennan MP, Dardik A, Hibino N, Roh JD, Nelson GN, Papademitris X, et al. Tissue-engineered vascular grafts demonstrate evidence of growth and development when implanted in a juvenile animal model. Ann Surg 2008;248:370-7.

68. Mirensky TL, Hibino N, Sawh-Martinez RF, Yi T, Villalona G, Shinoka T, et al. Tissue-engineered vascular grafts: does cell seeding matter? J Pediatr Surg 2010;45:1299-305.

69. Roh JD, Sawh-Martinez R, Brennan MP, Jay SM, Devine L, Rao DA, et al. Tissue-engineered vascular grafts transform into mature blood vessels via an inflammation-mediated process of vascular remodeling. Proc Natl Acad Sci U S A 2010;107:4669-74.

70. Hibino N, McGillicuddy E, Matsumura G, Ichihara Y, Naito Y, Breuer C, et al. Late-term results of tissue-engineered vascular grafts in humans. J Thorac Cardiovasc Surg 2010;139:431-6, 6 e1-2.

71. Patterson JT, Gilliland T, Maxfield MW, Church S, Naito Y, Shinoka T, et al. Tissue-engineered vascular grafts for use in the treatment of congenital heart disease: from the bench to the clinic and back again. Regen Med 2012;7:409-19.

72. ClinicalTrials.gov. A Pilot Study Investigating the Clinical Use of Tissue Engineered Vascular Grafts in Congenital Heart Surgery 2015 [cited 2015 May 24, 2015]. Available from: https://clinicaltrials.gov/ct2/show/NCT01034007.

73. Hashi CK, Zhu Y, Yang GY, Young WL, Hsiao BS, Wang K, et al. Antithrombogenic property of bone marrow mesenchymal stem cells in nanofibrous vascular grafts. Proc Natl Acad Sci U S A 2007;104:11915-20.

74. Nieponice A, Soletti L, Guan J, Hong Y, Gharaibeh B, Maul TM, et al. In vivo assessment of a tissue-engineered vascular graft combining a biodegradable elastomeric scaffold and muscle-derived stem cells in a rat model. Tissue engineering Part A 2010;16:1215-23.

75. He W, Nieponice A, Soletti L, Hong Y, Gharaibeh B, Crisan M, et al. Pericyte-based human tissue engineered vascular grafts. Biomaterials 2010;31:8235-44.

76. Soletti L, Nieponice A, Guan J, Stankus JJ, Wagner WR, Vorp DA. A seeding device for tissue engineered tubular structures. Biomaterials 2006;27:4863-70.

77. Zhou M, Liu Z, Liu C, Jiang X, Wei Z, Qiao W, et al. Tissue engineering of small-diameter vascular grafts by endothelial progenitor cells seeding heparin-coated decellularized scaffolds. J Biomed Mater Res B Appl Biomater 2012;100:111-20.

78. Tillman BW, Yazdani SK, Neff LP, Corriere MA, Christ GJ, Soker S, et al. Bioengineered vascular access maintains structural integrity in response to arteriovenous flow and repeated needle puncture. J Vasc Surg 2012;56:783-93.

79. Krawiec JT, Weinbaum JS, St Croix CM, Phillippi JA, Watkins SC, Rubin JP, et al. A cautionary tale for autologous vascular tissue engineering: impact of human demographics on the ability of adipose-derived mesenchymal stem cells to recruit and differentiate into smooth muscle cells. Tissue engineering Part A 2015;21:426-37.

80. L'Heureux N, Paquet S, Labbe R, Germain L, Auger FA. A completely biological tissue-engineered human blood vessel. FASEB J 1998;12:47-56.

81. L'Heureux N, Dusserre N, Konig G, Victor B, Keire P, Wight TN, et al. Human tissue-engineered blood vessels for adult arterial revascularization. Nat Med 2006;12:361-5.

82. McAllister TN, Maruszewski M, Garrido SA, Wystrychowski W, Dusserre N, Marini A, et al. Effectiveness of haemodialysis access with an autologous tissue-engineered vascular graft: a multicentre cohort study. Lancet 2009;373:1440-6.

83. Wystrychowski W, Cierpka L, Zagalski K, Garrido S, Dusserre N, Radochonski S, et al. Case study: first implantation of a frozen, devitalized tissue-engineered vascular graft for urgent hemodialysis access. J Vasc Access 2011;12:67-70.

84. Wystrychowski W, McAllister TN, Zagalski K, Dusserre N, Cierpka L, L'Heureux N. First human use of an allogeneic tissue-engineered vascular graft for hemodialysis access. J Vasc Surg 2014;60:1353-7.

85. Norotte C, Marga FS, Niklason LE, Forgacs G. Scaffold-free vascular tissue engineering using bioprinting. Biomaterials 2009;30:5910-7.

86. Skardal A, Zhang J, Prestwich GD. Bioprinting vessel-like constructs using hyaluronan hydrogels crosslinked with tetrahedral polyethylene glycol tetracrylates. Biomaterials 2010;31:6173-81.

87. Schilling JA, Shurley HM, Joel W, White BN, Bradford RH. Abdominal Aortic Grafts: Use of in Vivo Structured Autologous and Homologous Fibrocollagenous Tubes. Ann Surg 1964;159:819-28.

88. Sparks CH. Die-grown reinforced arterial grafts: observations on long-term animal grafts and clinical experience. Ann Surg 1970;172:787-94.

89. Sparks CH. Silicone mandril method for growing reinforced autogenous femoro-popliteal artery grafts in situ. Ann Surg 1973;177:293-300.

90. Campbell JH, Efendy JL, Campbell GR. Novel vascular graft grown within recipient's own peritoneal cavity. Circ Res 1999;85:1173-8.

91. Chue WL, Campbell GR, Caplice N, Muhammed A, Berry CL, Thomas AC, et al. Dog peritoneal and pleural cavities as bioreactors to grow autologous vascular grafts. J Vasc Surg 2004;39:859-67.

92. Bowald S, Busch C, Eriksson I. Arterial regeneration following polyglactin 910 suture mesh grafting. Surgery 1979;86:722-9.

93. Bowald S, Busch C, Eriksson I. Absorbable material in vascular prostheses: a new device. Acta Chir Scand 1980;146:391-5.

94. Greisler HP. Arterial regeneration over absorbable prostheses. Arch Surg 1982;117:1425-31.

95. Greisler HP, Kim DU, Price JB, Voorhees AB, Jr. Arterial regenerative activity after prosthetic implantation. Arch Surg 1985;120:315-23.

96. Greisler HP, Ellinger J, Schwarcz TH, Golan J, Raymond RM, Kim DU. Arterial regeneration over polydioxanone prostheses in the rabbit. Arch Surg 1987;122:715-21.

97. Gogolewski S, Galletti G, Ussia G. Polyurethane vascular prostheses in pigs. Colloid & Polymer Science 1987;265:774-8.

98. Galletti G, Gogolewski S, Ussia G, Farruggia F. Long-term patency of regenerated neoaortic wall following the implant of a fully biodegradable polyurethane prosthesis: experimental lipid diet model in pigs. Ann Vasc Surg 1989;3:236-43.

99. Audell L, Bowald S, Busch C, Eriksson I. Polyglactin mesh grafting of the pig aorta. The two-year follow-up in an experimental animal. Acta Chir Scand 1980;146:97-9.

100. Greisler HP, Kim DU, Dennis JW, Klosak JJ, Widerborg KA, Endean ED, et al. Compound polyglactin 910/polypropylene small vessel prostheses. J Vasc Surg 1987;5:572-83.

101. Roh JD, Nelson GN, Brennan MP, Mirensky TL, Yi T, Hazlett TF, et al. Small-diameter biodegradable scaffolds for functional vascular tissue engineering in the mouse model. Biomaterials 2008;29:1454-63.

102. Lantz GC, Badylak SF, Coffey AC, Geddes LA, Blevins WE. Small intestinal submucosa as a small-diameter arterial graft in the dog. J Invest Surg 1990;3:217-27.

103. Sandusky GE, Lantz GC, Badylak SF. Healing comparison of small intestine submucosa and ePTFE grafts in the canine carotid artery. J Surg Res 1995;58:415-20.

104. Sandusky GE, Jr., Badylak SF, Morff RJ, Johnson WD, Lantz G. Histologic findings after in vivo placement of small intestine submucosal vascular grafts and saphenous vein grafts in the carotid artery in dogs. Am J Pathol 1992;140:317-24.

105. Prevel CD, Eppley BL, McCarty M, Jackson JR, Voytik SL, Hiles MC, et al. Experimental evaluation of small intestinal submucosa as a microvascular graft material. Microsurgery 1994;15:586-91; discussion 92-3.

106. Huynh T, Abraham G, Murray J, Brockbank K, Hagen PO, Sullivan S. Remodeling of an acellular collagen graft into a physiologically responsive neovessel. Nat Biotechnol 1999;17:1083-6.

107. Yokota T, Ichikawa H, Matsumiya G, Kuratani T, Sakaguchi T, Iwai S, et al. In situ tissue regeneration using a novel tissue-engineered, small-caliber vascular graft without cell seeding. J Thorac Cardiovasc Surg 2008;136:900-7.

108. Hashi CK, Derugin N, Janairo RR, Lee R, Schultz D, Lotz J, et al. Antithrombogenic modification of small-diameter microfibrous vascular grafts. Arterioscler Thromb Vasc Biol 2010;30:1621-7.

109. Kurobe H, Maxfield MW, Tara S, Rocco KA, Bagi PS, Yi T, et al. Development of small diameter nanofiber tissue engineered arterial grafts. PLoS One 2015;10:e0120328.

110. Tara S, Kurobe H, Rocco KA, Maxfield MW, Best CA, Yi T, et al. Well-organized neointima of large-pore poly(L-lactic acid) vascular graft coated with poly(L-lactic-co-epsilon-caprolactone) prevents calcific deposition compared to small-pore electrospun poly(L-lactic acid) graft in a mouse aortic implantation model. Atherosclerosis 2014;237:684-91.

111. Soletti L, Nieponice A, Hong Y, Ye SH, Stankus JJ, Wagner WR, et al. In vivo performance of a phospholipid-coated bioerodable elastomeric graft for small-diameter vascular applications. J Biomed Mater Res A 2011;96:436-48.

112. Bergmeister H, Seyidova N, Schreiber C, Strobl M, Grasl C, Walter I, et al. Biodegradable, thermoplastic polyurethane grafts for small diameter vascular replacements. Acta Biomater 2015;11:104-13.

113. Lepidi S, Abatangelo G, Vindigni V, Deriu G, Zavan B, Tonello C, et al. In vivo regeneration of small-diameter (2 mm) arteries using a polymer scaffold. FASEB journal : official publication of the Federation of American Societies for Experimental Biology 2006;20:103-5.

114. Lepidi S, Grego F, Vindigni V, Zavan B, Tonello C, Deriu GP, et al. Hyaluronan biodegradable scaffold for small-caliber artery grafting: preliminary results in an animal model. Eur J Vasc Endovasc Surg 2006;32:411-7.

115. Zavan B, Vindigni V, Lepidi S, Iacopetti I, Avruscio G, Abatangelo G, et al. Neoarteries grown in vivo using a tissue-engineered hyaluronan-based scaffold. FASEB journal : official publication of the Federation of American Societies for Experimental Biology 2008;22:2853-61.

116. Duncan DR, Chen PY, Patterson JT, Lee YU, Hibino N, Cleary M, et al. TGFbetaR1 inhibition blocks the formation of stenosis in tissue-engineered vascular grafts. J Am Coll Cardiol 2015;65:512-4.

117. Safety and Performance of the COR-VG-001 Conduit in Pediatric Patients for Extracardiac Total Cavopulmonary Connection (EC-TCPC 2015 [cited 2015 May 24, 2015]. Available from: https://clinicaltrials.gov/ct2/show/NCT02377674.

118. Wu W, Allen RA, Wang Y. Fast-degrading elastomer enables rapid remodeling of a cell-free synthetic graft into a neoartery. Nat Med 2012;18:1148-53.

119. Wang Y, Kim YM, Langer R. In vivo degradation characteristics of poly(glycerol sebacate). J Biomed Mater Res A 2003;66:192-7.

120. Wang Y, Ameer G, Sheppard B, Langer R. A tough biodegradable elastomer. Nature Biotechnology 2002;20:602-6.

121. Lee KW, Stolz DB, Wang Y. Substantial expression of mature elastin in arterial constructs. Proc Natl Acad Sci U S A 2011;108:2705-10.

122. Crapo PM, Gao J, Wang Y. Seamless tubular poly(glycerol sebacate) scaffolds: high-yield fabrication and potential applications. J Biomed Mater Res A 2008;86:354-63.

123. Kapadia MR, Aalami OO, Najjar SF, Jiang Q, Murar J, Lyle B, et al. A reproducible porcine ePTFE arterial bypass model for neointimal hyperplasia. J Surg Res 2008;148:230-7.

124. Veith FJ, Gupta SK, Ascer E, White-Flores S, Samson RH, Scher LA, et al. Six-year prospective multicenter randomized comparison of autologous saphenous vein and expanded polytetrafluoroethylene grafts in infrainguinal arterial reconstructions. J Vasc Surg 1986;3:104-14.

125. Zetrenne E, McIntosh BC, McRae MH, Gusberg R, Evans GR, Narayan D. Prosthetic vascular graft infection: a multi-center review of surgical management. Yale J Biol Med 2007;80:113-21.

126. Butterly DW, Schwab SJ. Dialysis access infections. Curr Opin Nephrol Hypertens 2000;9:631-5.

127. Sartore S, Chiavegato A, Faggin E, Franch R, Puato M, Ausoni S, et al. Contribution of adventitial fibroblasts to neointima formation and vascular remodeling: from innocent bystander to active participant. Circ Res 2001;89:1111-21.

128. Li L, Terry CM, Shiu YT, Cheung AK. Neointimal hyperplasia associated with synthetic hemodialysis grafts. Kidney Int 2008;74:1247-61.

129. Zilla P, Bezuidenhout D, Human P. Prosthetic vascular grafts: wrong models, wrong questions and no healing. Biomaterials 2007;28:5009-27.

130. An YH, Friedman RJ. Concise review of mechanisms of bacterial adhesion to biomaterial surfaces. J Biomed Mater Res 1998;43:338-48.

131. Nataf P, Lansac E. Dilation of the thoracic aorta: medical and surgical management. Heart 2006;92:1345-52.

132. Gao J, Crapo PM, Wang Y. Macroporous elastomeric scaffolds with extensive micropores for soft tissue engineering. Tissue Eng 2006;12:917-25.

133. Bauer EM, Qin Y, Miller TW, Bandle RW, Csanyi G, Pagano PJ, et al. Thrombospondin-1 supports blood pressure by limiting eNOS activation and endothelial-dependent vasorelaxation. Cardiovasc Res 2010;88:471-81.

134. Hill MR, Duan X, Gibson GA, Watkins S, Robertson AM. A theoretical and non-destructive experimental approach for direct inclusion of measured collagen orientation and recruitment into mechanical models of the artery wall. J Biomech 2012;45:762-71.

135. Allen RA, Wu W, Yao M, Dutta D, Duan X, Bachman TN, et al. Nerve regeneration and elastin formation within poly(glycerol sebacate)-based synthetic arterial grafts one-year post-implantation in a rat model. Biomaterials 2014;35:165-73.

136. Lepidi S, Abatangelo G, Vindigni V, Deriu GP, Zavan B, Tonello C, et al. In vivo regeneration of small-diameter (2 mm) arteries using a polymer scaffold. FASEB J 2006;20:103-5.

137. Enomoto S, Sumi M, Kajimoto K, Nakazawa Y, Takahashi R, Takabayashi C, et al. Long-term patency of small-diameter vascular graft made from fibroin, a silk-based biodegradable material. Journal of vascular surgery 2010;51:155-64.

138. de Valence S, Tille JC, Mugnai D, Mrowczynski W, Gurny R, Moller M, et al. Long term performance of polycaprolactone vascular grafts in a rat abdominal aorta replacement model. Biomaterials 2012;33:38-47.

139. Zavan B, Vindigni V, Lepidi S, Iacopetti I, Avruscio G, Abatangelo G, et al. Neoarteries grown in vivo using a tissue-engineered hyaluronan-based scaffold. FASEB J 2008;22:2853-61.

140. Mendelson K, Schoen F. Heart valve tissue engineering: concepts, approaches, progress, and challenges. Annals of biomedical engineering 2006;34:1799-819.

141. Torikai K, Ichikawa H, Hirakawa K, Matsumiya G, Kuratani T, Iwai S, et al. A self-renewing, tissue-engineered vascular graft for arterial reconstruction. J Thorac Cardiovasc Surg 2008;136:37-45, e1.

142. Anderson JM, Rodriguez A, Chang DT. Foreign body reaction to biomaterials. Semin Immunol 2008;20:86-100.

143. Major MR, Wong VW, Nelson ER, Longaker MT, Gurtner GC. The foreign body response: at the interface of surgery and bioengineering. Plast Reconstr Surg 2015;135:1489-98.

144. Hellstrom M, Kalen M, Lindahl P, Abramsson A, Betsholtz C. Role of PDGF-B and PDGFR-beta in recruitment of vascular smooth muscle cells and pericytes during embryonic blood vessel formation in the mouse. Development 1999;126:3047-55.

145. Shi Y, O'Brien JE, Jr., Fard A, Zalewski A. Transforming growth factor-beta 1 expression and myofibroblast formation during arterial repair. Arterioscler Thromb Vasc Biol 1996;16:1298-305.

146. Hinz B, Phan SH, Thannickal VJ, Galli A, Bochaton-Piallat ML, Gabbiani G. The myofibroblast: one function, multiple origins. Am J Pathol 2007;170:1807-16.

147. Yoshida T, Owens GK. Molecular determinants of vascular smooth muscle cell diversity. Circ Res 2005;96:280-91.

148. Lin S, Sandig M, Mequanint K. Three-dimensional topography of synthetic scaffolds induces elastin synthesis by human coronary artery smooth muscle cells. Tissue engineering Part A 2011;17:1561-71.

149. Abe R, Donnelly SC, Peng T, Bucala R, Metz CN. Peripheral blood fibrocytes: differentiation pathway and migration to wound sites. J Immunol 2001;166:7556-62.

150. Byrne AM, Bouchier-Hayes DJ, Harmey JH. Angiogenic and cell survival functions of vascular endothelial growth factor (VEGF). J Cell Mol Med 2005;9:777-94.

151. Gnecchi M, Zhang Z, Ni A, Dzau VJ. Paracrine mechanisms in adult stem cell signaling and therapy. Circ Res 2008;103:1204-19.

152. Valle-Prieto A, Conget PA. Human mesenchymal stem cells efficiently manage oxidative stress. Stem Cells Dev 2010;19:1885-93.

153. Matsumura G, Miyagawa-Tomita S, Shin'oka T, Ikada Y, Kurosawa H. First evidence that bone marrow cells contribute to the construction of tissue-engineered vascular autografts in vivo. Circulation 2003;108:1729-34.

154. Hibino N, Villalona G, Pietris N, Duncan DR, Schoffner A, Roh JD, et al. Tissue-engineered vascular grafts form neovessels that arise from regeneration of the adjacent blood vessel. FASEB J 2011;25:2731-9.

155. Spiller KL, Anfang RR, Spiller KJ, Ng J, Nakazawa KR, Daulton JW, et al. The role of macrophage phenotype in vascularization of tissue engineering scaffolds. Biomaterials 2014;35:4477-88.

156. Plate KH, Breier G, Weich HA, Risau W. Vascular endothelial growth factor is a potential tumour angiogenesis factor in human gliomas in vivo. Nature 1992;359:845-8.

157. Stratman AN, Schwindt AE, Malotte KM, Davis GE. Endothelial-derived PDGF-BB and HB-EGF coordinately regulate pericyte recruitment during vasculogenic tube assembly and stabilization. Blood 2010;116:4720-30.

158. Hibino N, Yi T, Duncan DR, Rathore A, Dean E, Naito Y, et al. A critical role for macrophages in neovessel formation and the development of stenosis in tissue-engineered vascular grafts. FASEB J 2011;25:4253-63.

159. Brown BN, Ratner BD, Goodman SB, Amar S, Badylak SF. Macrophage polarization: an opportunity for improved outcomes in biomaterials and regenerative medicine. Biomaterials 2012;33:3792-802.

160. Sussman EM, Halpin MC, Muster J, Moon RT, Ratner BD. Porous implants modulate healing and induce shifts in local macrophage polarization in the foreign body reaction. Ann Biomed Eng 2014;42:1508-16.

161. Jones EA, le Noble F, Eichmann A. What determines blood vessel structure? Genetic prespecification vs. hemodynamics. Physiology 2006;21:388-95.

162. Gabriele PD, Harris J. Regenerating the Future of Biomaterials in Orthopedics. Medical Design Briefs.

163. Rocco KA, Maxfield MW, Best CA, Dean EW, Breuer CK. In vivo applications of electrospun tissue-engineered vascular grafts: a review. Tissue Eng Part B Rev 2014;20:628-40.

164. Bull DA, Hunter GC, Holubec H, Aguirre ML, Rappaport WD, Putnam CW. Cellular origin and rate of endothelial cell coverage of PTFE grafts. J Surg Res 1995;58:58-68.

165. Zern BJ, Chu H, Wang Y. Control growth factor release using a self-assembled [polycation:heparin] complex. PLoS One 2010;5:e11017.

166. Shing Y, Folkman J, Sullivan R, Butterfield C, Murray J, Klagsbrun M. Heparin affinity: purification of a tumor-derived capillary endothelial cell growth factor. Science 1984;223:1296-9.

167. Cross MJ, Claesson-Welsh L. FGF and VEGF function in angiogenesis: signalling pathways, biological responses and therapeutic inhibition. Trends Pharmacol Sci 2001;22:201-7.

168. Lee KW, Johnson NR, Gao J, Wang Y. Human progenitor cell recruitment via SDF-1alpha coacervate-laden PGS vascular grafts. Biomaterials 2013;34:9877-85.

169. Jeffries EM, Allen RA, Gao J, Pesce M, Wang Y. Highly elastic and suturable electrospun poly(glycerol sebacate) fibrous scaffolds. Acta Biomater 2015;18:30-9.

170. Sill TJ, von Recum HA. Electrospinning: applications in drug delivery and tissue engineering. Biomaterials 2008;29:1989-2006.

171. Finne-Wistrand A, Albertsson AC, Kwon OH, Kawazoe N, Chen G, Kang IK, et al. Resorbable scaffolds from three different techniques: electrospun fabrics, salt-leaching porous films, and smooth flat surfaces. Macromol Biosci 2008;8:951-9.

172. Bettinger CJ. Biodegradable elastomers for tissue engineering and cell-biomaterial interactions. Macromol Biosci 2011;11:467-82.

173. Jeffries EM, Allen RA, Wang Y, inventorsMethods of electrospinning and compositions made therefrom. PCT application2013 December 20, 2013.

174. Pomerantseva I, Krebs N, Hart A, Neville CM, Huang AY, Sundback CA. Degradation behavior of poly(glycerol sebacate). J Biomed Mater Res A 2009;91:1038-47.

175. Hong Y, Takanari K, Amoroso NJ, Hashizume R, Brennan-Pierce EP, Freund JM, et al. An elastomeric patch electrospun from a blended solution of dermal extracellular matrix and biodegradable polyurethane for rat abdominal wall repair. Tissue Eng Part C Methods 2012;18:122-32.

176. Sant S, Hwang CM, Lee SH, Khademhosseini A. Hybrid PGS-PCL microfibrous scaffolds with improved mechanical and biological properties. J Tissue Eng Regen Med 2011;5:283-91.

177. Li Y, Cook W, D.,, Moorhoff C, Huang W, C.,, Chen Q, Z. Synthesis, characterization and properties of biocompatible poly(glycerol sebacate) pre-polymer and gel. Polymer International 2012;64:534-47.

178. Ifkovits JL, Devlin JJ, Eng G, Martens TP, Vunjak-Novakovic G, Burdick JA. Biodegradable fibrous scaffolds with tunable properties formed from photo-cross-linkable poly(glycerol sebacate). ACS Appl Mater Interfaces 2009;1:1878-86.

179. Ravichandran R, Venugopal JR, Sundarrajan S, Mukherjee S, Ramakrishna S. Poly(Glycerol sebacate)/gelatin core/shell fibrous structure for regeneration of myocardial infarction. Tissue engineering Part A 2011;17:1363-73.

180. Liu T, Teng WK, Chan BP, Chew SY. Photochemical crosslinked electrospun collagen nanofibers: synthesis, characterization and neural stem cell interactions. J Biomed Mater Res A 2010;95:276-82.

181. Yi F, LaVan DA. Poly(glycerol sebacate) nanofiber scaffolds by core/shell electrospinning. Macromol Biosci 2008;8:803-6.

182. Khosravi R, Best CA, Allen RA, Stowell CET, Zhuang JJ, Lee YU, et al. Evaluation of the long-term functional efficacy of a novel electrospun poly(glycerol sebacate) based vascular graft in mice In Preparation 2015.

183. McClure MJ, Sell SA, Simpson DG, Walpoth BH, Bowlin GL. A three-layered electrospun matrix to mimic native arterial architecture using polycaprolactone, elastin, and collagen: a preliminary study. Acta Biomater 2010;6:2422-33.

184. Kumar VA, Caves JM, Haller CA, Dai E, Liu L, Grainger S, et al. Acellular vascular grafts generated from collagen and elastin analogs. Acta Biomater 2013;9:8067-74.

185. Crapo PM, Wang Y. Physiologic compliance in engineered small-diameter arterial constructs based on an elastomeric substrate. Biomaterials 2010;31:1626-35.

186. Jones GT. The Pathohistology of Abdominal Aortic Aneurysm, Diagnosis, Screening and Treatment of Abdominal, Thoracoabdominal and Thoracic Aortic Aneurysms. InTech 2011.

187. Frangogiannis NG, Michael LH, Entman ML. Myofibroblasts in reperfused myocardial infarcts express the embryonic form of smooth muscle myosin heavy chain (SMemb). Cardiovasc Res 2000;48:89-100.

188. Campbell JH, Campbell GR. Smooth muscle phenotypic modulation--a personal experience. Arterioscler Thromb Vasc Biol 2012;32:1784-9.

189. Klingberg F, Hinz B, White ES. The myofibroblast matrix: implications for tissue repair and fibrosis. J Pathol 2013;229:298-309.

190. Sherratt MJ. Tissue elasticity and the ageing elastic fibre. Age (Dordr) 2009;31:305-25.

191. Koga J, Aikawa M. Crosstalk between macrophages and smooth muscle cells in atherosclerotic vascular diseases. Vascul Pharmacol 2012;57:24-8.

192. Patel A, Fine B, Sandig M, Mequanint K. Elastin biosynthesis: The missing link in tissue-engineered blood vessels. Cardiovasc Res 2006;71:40-9.

193. Mironov V, Kasyanov V. Emergence of clinical vascular tissue engineering. Lancet 2009;373:1402-4.

194. Aikawa E, Nahrendorf M, Figueiredo JL, Swirski FK, Shtatland T, Kohler RH, et al. Osteogenesis associates with inflammation in early-stage atherosclerosis evaluated by molecular imaging in vivo. Circulation 2007;116:2841-50.

195. Tara S, Kurobe H, Maxfield MW, Rocco KA, Yi T, Naito Y, et al. Evaluation of remodeling process in small-diameter cell-free tissue-engineered arterial graft. J Vasc Surg 2014.

196. Pennel T, Zilla P, Bezuidenhout D. Differentiating transmural from transanastomotic prosthetic graft endothelialization through an isolation loop-graft model. J Vasc Surg 2013;58:1053-61.